

**Studies on Biochemical Modifications and
Membrane Organization of VDAC: A Biophysical
Approach**

DOCTOR OF PHILOSOPHY

By

Naveen Kumar Bhatraju



Department of Animal Sciences
School of Life Sciences
University of Hyderabad
Hyderabad-500 046, India-

June 2011



University of Hyderabad
School of Life Sciences
Department of Animal Sciences
Hyderabad-500 046

DECLARATION

I, Naveen Kumar Bhatraju, hereby declare that this thesis entitled "**Studies on Biochemical Modifications and Membrane Organization of VDAC: A Biophysical Approach**" submitted by me under the guidance and supervision of Dr. Subhendu Ghosh & Prof. Aparna Dutta Gupta is an original and independent research work. I also declare that it has not been submitted previously in part or in full to this University or any other University or Institution for the award of any degree or diploma.

Date: 30 -6-2011

Name: Naveen Kumar Bhatraju

Signature: *B. Naveen Bhatraju*

Enrollment No.: 05LAPH02



University of Hyderabad
School of Life Sciences
Department of Animal Sciences
Hyderabad-500 046

CERTIFICATE

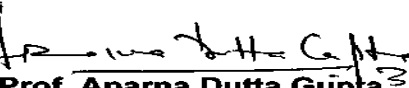
This is to certify that this thesis entitled "**Studies on Biochemical Modifications and Membrane Organization of VDAC: A Biophysical Approach**" is a record of bonafide work done by Mr. Naveen Kumar Bhatraju, a research scholar for Ph.D. programme in Department of Animal Sciences, University of Hyderabad under our guidance and supervision.

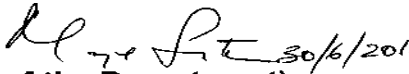
The thesis has not been submitted previously in part or full to this or any other University or Institution for the award of any degree or diploma.

Supervisors:

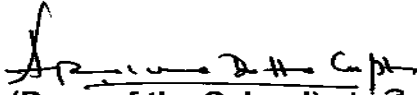

Dr. Subhendu Ghosh
Department of Biophysics
University of Delhi South
New Delhi, INDIA

Department of Biophysics
University of Delhi
South Campus
New Delhi-110021


Prof. Aparna Dutta Gupta 30/6/11
Department of Animal Sciences
School of Life Sciences,
University of Hyderabad, INDIA
PROF. APARNA DUTTA GUPTA
School of Life Sciences
University of Hyderabad
Hyderabad-500 046. INDIA


(Head of the Department) 30/6/2011

अध्यक्ष / HEAD
जंतु विज्ञान विभाग
Department of Animal Sciences
जैविक विज्ञान संकाय
School of Life Sciences
हैदराबाद विश्वविद्यालय
University of Hyderabad
हैदराबाद / Hyderabad-500 046.


(Dean of the School) 30/6/11
संकाय अध्यक्ष / Dean
जैविक विज्ञान संकाय
School of Life Sciences
हैदराबाद विश्वविद्यालय
UNIVERSITY OF HYDERABAD
हैदराबाद / HYDERABAD-500 046.

Acknowledgements

I would like to express my gratitude to my supervisor Dr. Subhendu Ghosh for his guidance during my PhD.

I would like to express my gratitude to my supervisor Prof. Aparna Dutta Gupta for her encouragement and constant support during the PhD tenure.

I would like to thank Prof. Manjula Sritharan and Prof. S. Dayananda, present and former Heads, Department of Animal Sciences for extending the departmental facilities.

I am grateful to Prof. M. Ramanadham and Prof. A.S. Raghavendra, present and former Deans, School of Life Sciences for extending the school facilities. Further, I must thank School and administration for allowing me to work at Delhi University during this tenure.

I would like to thank my doctoral committee members Prof. B. Senthilkumaran, Department of Animal Sciences and Dr. S. Bapi Raju, Department of MCIS for their constructive criticism and suggestions.

World is full of good people. I would like to mention a few whom I encountered during my PhD tenure: Prof. M.V. Rajam, UDSC, Prof. Indraneel Das Gupta, UDSC, Prof. Anjan Das Gupta, Univ. of Calcutta, Prof. Ivet Bahar, Univ. of Pittsburgh, Dr. Lee-Wei Yang, Tsing-Hua university, Prof. J. S. Murguía, Universidad Autonoma de San Luis potosi, Mexico, Prof. A. Arneodo, Dr. Benjamin Audit, Bordeaux university.

Dr. M. K. Das needs a special mention, without whose help, the theoretical part of this work would not have been possible.

I will be failing in my duties if I do not acknowledge the support I received from all my teachers at University of Hyderabad.

I would like to thank the entire faculty, FIDAS, UDSC for helping me in all possible ways.

I would like to thank all my friends, colleagues and all the Ph.D. students of School of Life Sciences.

I cannot forget Aravind, Mujahid, Girish, Suresh, Chaitanya, Sridevi, Sridhar, Dileep, Venkat, Naresh, Jacob, Nagesh, Tirupathaiah, Kishore, Debashish, Venu and Raghu for making me feel at home all through these years of my stay at University of Hyderabad.

I would like to acknowledge Chetan, Satish, Maneesh, Diwakar, Shaveta, Micheal, Tamilarasan, and Thenral- their constant support and encouragement has been indispensable during the Ph.D tenure.

I would also like to thank Chetan Malik, Rajeev Gupta and Satyajeet for their help and support.

I would like to acknowledge Dr. Amal Kanti Bera, Dr. Jyotirmoy Banerjee, Dr. Smarajit Manna and Anindita Bhattacharjee for their timely help.

I would like to thank Dr. Nirpendra Singh, Dr. Manish and Dr. Ujjaini (CIF, UDSC) for their constant support and help during my stay at UDSC.

I would like to thank administrative and non-teaching staff of School of Life Sciences for their timely support.

I would like to thank University grants commission for the fellowship during the PhD tenure.

My parents and my brother are always behind me in every achievement.

Naveen Kumar Bhatraju...

Dedicated to my parents...

Abbreviations

| | |
|-------------------------------|---|
| AD | - Alzheimer's disease |
| AIF | - Apoptosis inducing factor |
| ALS | - Amyotrophic lateral sclerosis |
| ATP | - Adenosine triphosphate |
| BSA | - Bovine serum albumin |
| Bp | - Base pairs |
| cDNA | - Complementary DNA |
| DDW | - Double distilled water |
| DNA | - Deoxyribonucleic acid |
| dNTP | - Deoxynucleoside triphosphates |
| DPhPC | - 1,2-diphytanoyl-5 α -glycero-3-phosphate |
| EDTA | - Ethylenediaminetetraacetic acid |
| <i>E.coli</i> | - <i>Escherichia coli</i> |
| FFT | - Fast fourier transform |
| FT | - Fourier transform |
| HCl | - Hydrochloric acid |
| H ₂ O ₂ | - Hydrogen peroxide |
| I | - Current |
| JNK | - cJun N-terminal kinase |
| KCl | - Potassium chloride |
| kDa | - Kilo Dalton |
| LB | - Luria-Bertani medium |
| LDAO | - Lauryldimethylamine-oxide |
| MALDI | - Matrix assisted LASER desorption ionization |
| MgCl ₂ | - Magnesium chloride |
| MnO ₂ | - Manganese dioxide |

| | |
|------------------------------|--|
| uCi | - Microcurie |
| | - Microgram |
| μl | - Microliter |
| mM | - Millimolar |
| ms | - Millisecond |
| mV | - Millivolt |
| MPT | - Mitochondrial permeability transition pore |
| MF-DFA | - Multifractal-detrended fluctuation analysis |
| N | - Normal |
| NaOH | - Sodium hydroxide |
| ng | - nanogram |
| NO | - Nitric oxide |
| NOS | - Nitric oxide synthase |
| OMM | - Outer mitochondrial membrane |
| ONOO [•] | - Peroxynitrite |
| O ₂ ^{•-} | - Superoxide radical |
| PD | - Parkinson's disease |
| PA | - pico ampere |
| PAGE | - Polyacrylamide gel electrophoresis |
| P _o | - Open probability |
| PTP | - Permeability transition pore |
| PVDF | - Polyvinylidene fluoride |
| RNA | - Ribonucleic acid |
| RNS | - Reactive nitrogen species |
| ROS | - Reactive oxygen species, |
| SDS | - Sodium dodecyl sulfate |
| Ser | - Serine |
| SMAC | - Second mitochondrial derived activator of caspases |

| | |
|---------------|----------------------------------|
| TEMED | - N N N' N'-Tetraethylenediamine |
| Thr | - Threonine |
| TOF | - Time of flight |
| Tyr | - Tyrosine |
| VDAC | Voltage dependent anion channel |
| w/v | weight/volume Hexa |
| 6X-His | histidine tag |

Table of Contents

| <u>Contents</u> | <u>Pages</u> |
|---|--------------|
| Chapter 1: General Introduction | 1-14 |
| 1.1 Mitochondrial Outer Membrane Ion Channels | |
| 1.2 Voltage dependent anion channel (VDAC) | |
| 1.3 Isoforms of VDAC | |
| 1.4 Channel activity of VDAC | |
| 1.5 Structure of VDAC | |
| 1.6 Voltage dependent gating of VDAC | |
| 1.7 Extra-mitochondrial localization of VDAC | |
| 1.8 Regulation of VDAC | |
| 1.9 VDAC, mitochondria mediated apoptosis and human diseases | |
| 1.10 Aims and Objectives | |
| Chapter 2: Role of Nitric Oxide in Biochemical and Biophysical modification of VDAC: Studies on Single Channel | 15-34 |
| 2.1 Review of literature | |
| 2.2 Materials and Methods | |
| 2.3 Results and Discussion | |
| Chapter 3: Phosphorylation of VDAC: Studies on structure-function relationship | 35-59 |
| 3.1 Review of literature | |
| 3.2 Materials and Methods | |
| 3.3 Results and Discussion | |
| Chapter 4: Dynamics of VDAC multichannels: Computational Analyses | 60-76 |
| 4.1 Review of literature | |
| 4.2 Materials and Methods | |
| 4.3 Results and Discussion | |

| | |
|-------------------------------|--------------|
| Chapter 5: Conclusions | 77-80 |
| Summary | 81-83 |
| Bibliography | 84-98 |
| Appendix-I | |
| Appendix-II | |

General Introduction

Chapter-1

1. General Introduction:

Mitochondria were thought to be important for the generation of cellular energy alone. This prevailing view has been extended by the research in the past two decades suggesting the major role played by the mitochondria in various other cellular processes including inter-organelle communication, cell signaling events, cell proliferation, cell death and diseases. Ion channels located on the outer and inner membranes play a key role in realizing the multiple functions of the mitochondria, making the organelle central to cellular physiology and pathology.

1.1. Mitochondrial outer membrane ion channels:

Mitochondria are believed to be evolved from the uptake of an endosymbiotic precursor bacterium from the α -proteobacterial subgroup into a eukaryotic precursor cell. Although the lipid composition of both the membranes changed during the course of evolution, some of the proteins specifically mitochondrial outer membrane ion channels are structurally conserved, providing a circumstantial evidence for the endosymbiotic theory (Zeth 2010).

Outer mitochondrial membrane (OMM) was initially thought to be a non-selective envelope covering the mitoplast. The identification and characterization of major ion channels present on the OMM revealed many interesting characteristics of OMM including its selective permeability and its role in cross-talk between mitochondrial sub-compartments and cytoplasm. Further, the OMM has been identified to serve as a venue for cell survival/death decisions. The major ion channels present on the OMM are voltage dependent anion channel (VDAC) and translocase of outer membrane (TOM) group of channels. While TOM group of channels play an important role in import of proteins into the mitochondrial internal compartments, VDAC is known to play an important role in mitochondrial bioenergetics and intrinsic cell death pathway.

1.2. Voltage dependent anion channel (VDAC):

Schein *et al.*, detected pore forming activity analogous to the bacterial porin in the mitochondrial extract of *Paramecium tetraurelia* (Schein, *et al.* 1976) constitutes the first ever report on VDAC, as it was later renamed (Colombini 1979). VDAC, also known as the mitochondrial porin (Benz 1985) is an integral protein of the outer mitochondrial membrane. The purification of VDAC from various tissues and organisms (De Pinto, *et al.* 1987a) and subsequent electrophysiological characterization in reconstituted bilayers revealed its highly conserved structural and functional features (Benz 1994). The observed structural conservation is at the level of secondary structure but not in the primary structure (Song and Colombini 1996). The alternating polar and non-polar residues in the primary structure, a characteristic of 'β-strands', is remarkably conserved even when the sequence similarity is below the level of statistical significance (Song and Colombini 1996).

VDAC is the most abundant protein in the OMM (Yamamoto, *et al.* 2006). It accounts for 0.4% of the total mitochondrial proteome. Single polypeptide of VDAC has 283 amino acid residues with a molecular weight of ~31 kDa, forms a voltage dependent pore in the OMM. The evidence for the monomeric nature of the channel came from the electron microscopic imaging of two dimensional crystals of *N. crassa* (Mannella 1987), genetic studies of *S.cerevesiae* VDAC (Peng, *et al.* 1992a) and hydrodynamic studies of detergent solubilized rat VDAC (Linden, *et al.* 1982). The electron microscopic imaging of VDAC crystals also demonstrated that VDAC molecules are arranged in hexagonal arrays (Mannella 1987, Parsons 1965). This typical arrangement of VDAC channels is further substantiated by high resolution atomic force microscopic imaging studies of OMM from yeast and potato tubers (Goncalves, *et al.* 2007, Hoogenboom, *et al.* 2007).

VDAC located on the OMM forms a main interface between the mitochondrial sub-compartments and cytoplasm. It forms a major gate regulating the entry/exit of the molecules between intermembrane space and cytoplasm (Benz 1994). It also allows the exchange of ATP/ADP, inorganic phosphate (P_i) in open state

(Rostovtseva and Colombini 1997). VDAC has been shown to transport calcium ions in closed state (Gincel, *et al.* 2001).

VDAC serves as a functional anchor point for many molecules that interact with mitochondria. No less than 55 interacting partners of VDAC were identified (Roman, *et al.* 2006b). The functional significance of most of these interacting partners is unknown and requires further investigation. The main interacting partners of VDAC whose role in modulating its activity and thus mitochondrial functioning include the pro/anti apoptotic Bcl-2 family proteins (Shimizu, *et al.* 1999), kinases (Mathupala, *et al.* 2006), cytochrome c (Shimizu, *et al.* 1999) and cytoskeletal proteins (Roman, *et al.* 2006b). All these proteins were shown to modulate the structure and conformational dynamics of VDAC [reviewed in (Shoshan-Barmatz, *et al.* 2010a)].

1.3. Isoforms of VDAC:

In chordates three different isoforms were found to be expressed from three individual genes *VDAC1*, *VDAC2* and *VDAC3*. Various groups studying VDAC consensually agree that VDAC3 could be considered as the oldest among the three isoforms. While VDAC3 and VDAC1/2 were diverged around 365 million years ago, the divergence between the VDAC1 and VDAC2 isoforms was estimated to occur approximately 289 million years ago (Saccone, *et al.* 2003). VDAC1 is the most successful and recent porin among all the three isoforms. In agreement with the preceding statement, VDAC1 is the most abundant isoform found in the OMM. Both immunological studies and real time PCR experiments suggest that VDAC1 is 10 times more abundant than VDAC2 and 100 times more abundant than VDAC3 isoforms (De Pinto, *et al.* 2010a). Thus, most information available was related to the VDAC1. VDAC2 has an extra 12 amino acid residues at the N-terminus.

Although the apparent molecular weight of the three VDAC isoforms was found to be ~31kDa, the electrophoretic mobilities of each of the isoforms were found to vary. Proteomic studies showed that VDAC1 has lower electrophoretic mobility. VDAC2 in spite of higher molecular weight has the same electrophoretic mobility as

that of VDAC1, while VDAC3 has the highest mobility in the SDS-PAGE. 2D electrophoresis of purified VDAC protein always resulted in multiple spots (Yamamoto, *et al.* 2006). These mobility patterns could be attributed to the post-translational modifications of VDAC isoforms.

1.4. Channel activity of VDAC:

The functional properties of VDAC have been mainly studied in reconstituted artificial membrane systems. Proteoliposomes or planar lipid bilayers (PLB) are the two main membrane systems used to study the pore-forming activity of VDACs. The swelling and shrinking of the proteoliposomes could be measured by the absorbance changes in solution. The swelling and shrinking are caused by the presence of the permeable and non-permeable solutes in the solution. Carbohydrates and polyethylene glycols (PEG) of different molecular weight were used as solutes in such experiments containing VDAC reconstituted proteoliposomes and suggested a molecular size cutoff of 6.8 kDa for the VDAC channel (Colombini 1980). From these results, the diameter of VDAC pore was calculated to be around 3-4 nm.

PLBs separating two aqueous compartments form a perfect biomimetic system for the characterization of reconstituted single channels. The channel activity allowing the flow of ions across the membrane is measured by changes in the current. For measuring the channel activity, VDAC can be reconstituted into a phospholipid bilayer by two different methods (Benz, *et al.* 1979, Mueller, *et al.* 1963). Both the methods were found to give similar results for reconstituted VDAC (Colombini 1979). Various studies suggest that the insertion of the first channel into the PLB is random and the subsequent insertions are directed by the previously inserted channels (Li and Colombini 2002). A VDAC channel existing on the PLB increase the insertion rate of other VDAC channels by 10 orders of magnitude when compared to the first insertion and this behavior was termed as auto-directed insertion (Zizi, *et al.* 1995). Furthermore, only the first channel inserts into the membrane in a random orientation and the rest of the channels inserted into PLB in the same orientation as that of the first channel (Marques, *et al.* 2004).

The most frequently observed single channel conductance values of reconstituted mitochondrial VDAC in 1M KCl range between 4 and 4.5 nS (Benz 1994, Colombini 1980). Apart from the main conductance state, different sub-states were also reported, indicating that VDAC can exist in different stable conformations. In the main conductance state, VDAC allows the passage of various small ions (e.g. Cl⁻, K⁺, Na⁺), also large anions such as glutamate (Gincel, *et al.* 2000) and ATP (Rostovtseva and Colombini 1997) and to large cations, such as acetylcholine, dopamine (Gincel, *et al.* 2000) and Tris (Benz 1990). As the name suggests the channel is slightly anion-selective ($P_{\text{anion}} / P_{\text{cation}} = 2:1$) for salts containing equally mobile anions and cations (e.g. KCl) (Gincel, *et al.* 2000). The analysis of three dimensional structure of VDAC reveals the prevalence of the positively charged residues in the pore walls, explaining the slightly anion selective nature (Ujwal, *et al.* 2008).

1.5. Structure of VDAC:

In 2008, simultaneously three groups solved the structure of VDAC at atomic resolution by three independent approaches. Bayrhuber *et al.*, and Hiller *et al.*, solved the structure of human VDAC1 (hVAC1) in parallel by a novel approach combining nuclear magnetic resonance spectroscopy (NMR) and X-ray crystallography (Bayrhuber, *et al.* 2008) or solution NMR alone (Hiller, *et al.* 2008). The crystal structure of murine VDAC1 (mVDAC1) in lipid bicelles was determined by X-ray crystallography (Ujwal, *et al.* 2008). All the three structures were almost identical with a 19 strand β -barrel and an N-terminal α -helix located inside the barrel (fig. 1.1). This structure is consistent with one of the earlier models based on the sequence analysis of yeast VDAC (Forte, *et al.* 1987).

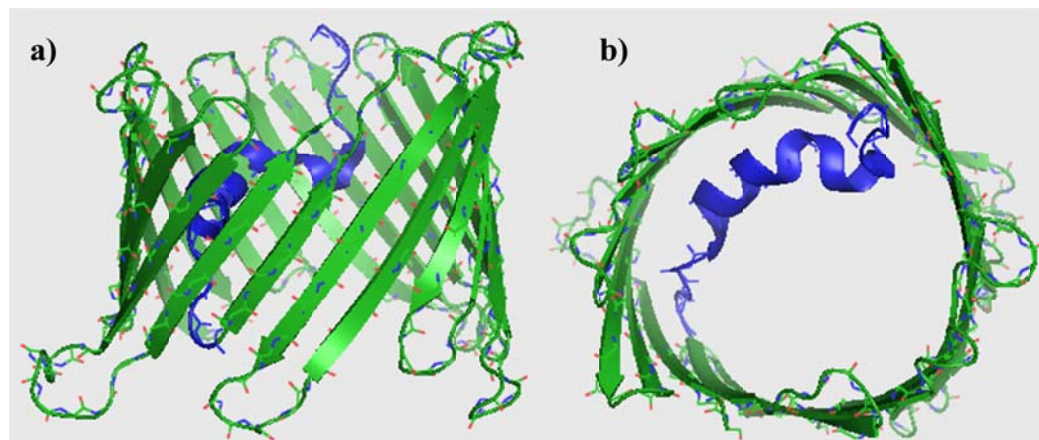


Fig. 1.1: Cartoon representation of three dimension structure of murine VDAC (PDB ID: 3EMN). The β -strands are represented in green and N-terminal α -helix is represented in blue colour. a) Cartoon representation of mVDAC1 viewed parallel to the plane of membrane. b) Cartoon representation of mVDAC1 viewed perpendicular to the plane of membrane.

The dimensions of the channel pore formed by the 19 strand β -barrel are 3.1 x 3.5 x 4 nm resembling a slightly elliptical cylinder. This is consistent with the dimensions obtained by the high resolution AFM investigations of yeast OMM (Goncalves, *et al.* 2007). The inner diameter of the pore was estimated to be 1.5 x 1 nm which would be convenient for the passage of the small molecules. The β -strands are arranged in anti-parallel fashion except for the first and last strands which are parallel aligned to close the β -barrel. Each β -strand on an average consists of \sim 10 amphipathic residues and all the strands are connected by flexible loops. The β -strands are slightly inclined relative to the β -barrel axis. The inclination varies between 27 to 46 $^\circ$ with an average inclination of 37 $^\circ$.

The N-terminal α -helix (1-25 amino acid residues) positioning in the barrel wall was not clearly indicated in the solution NMR studies. Ujwal *et al.*, clearly resolved the positioning of the N-terminal α -helix as attached to the channel wall and stabilized by a number of hydrogen bonds (Ujwal, *et al.* 2008). The helix is broken between Leu-10 and Gly-11 forming two segments of the helix. This was proposed to be important for the increased mobility of this region. Further, the multiple glycine

residues at the connecting point between the helix and the first strand of the β -barrel form the hinge region and is conserved among other mammals.

1.6. Voltage dependent gating of VDAC:

Two separate gating processes were proposed for the gating of VDAC at negative and positive transmembrane potentials *in vitro*. The dual gating mechanisms of VDAC get further support from the site-specific mutations or modifications which would specifically alter one of the gating processes (Blachly-Dyson, *et al.* 1990). Further, increase in the positive charge on the molecule has been shown to increase the steepness of the voltage dependence of both the gating processes and the converse decreases the voltage dependence. Mutations or chemical modifications of various residues have been shown to affect the voltage dependence of the molecule in a charge dependent manner (Blachly-Dyson, *et al.* 1990). Analysis of the primary structure suggests that most of these sites are located in the N-terminal 84 residues indicating that this domain moves in response to the transmembrane potential during gating. Mutation-induced charge modification of at least one residue (residue-46) was found to affect both the gating processes indicating an overlap in the gating domains.

In spite of two different gating processes operating at positive and negative voltages, the channel activity tends to be symmetrical at both the transmembrane potentials. The voltage dependent gating of VDAC results in a high conductance open state and multiple low conductance close states. The probability of finding VDAC in open state is very high at low voltages (10 mV), whereas the channel tends to close frequently and occupy multiple sub-states at high positive or negative potentials (>40 mV) (Gincel, *et al.* 2000, Hodge and Colombini 1997). The characterization of the voltage-dependent closed states revealed that the average single-channel conductance of the closed state is about half the conductance of the full open state and is cation-selective. Pavlov *et al.*, reported a large conductance cation-selective open state of VDAC. Further, they suggested that small scale conformational dynamics like movement of flexible domains in the pore could account for the changes in the charge selectivity (Pavlov, *et al.* 2005).

Based on the 3D structure of VDAC, different models for voltage-dependent gating of VDAC have been proposed. These models involve the slight movement of the N-terminal α -helix to the center to large conformational dynamics involving β -barrel (Bayrhuber, *et al.* 2008, Ujwal, *et al.* 2008). Ujwal *et al.*, proposed that the rotation of the whole N-terminal α -helix by 10° is sufficient to block the pore of the channel resulting in the closed state (Ujwal, *et al.* 2008). Hiller and Wagner proposed that the movement might involve only 11-20 amino acid residues of the helix (Hiller and Wagner 2009). However, the large conformational rearrangements involving the β -barrel suggested based on the electron microscopy and electrophysiological studies could not be ruled out (Peng, *et al.* 1992b). In deed experimental support for this kind of conformational instability of N-terminal four to five β -strands has come from the NMR spectroscopy (Villinger, *et al.* 2010). Finally, removal of N-terminal α -helix has been shown to induce conformational changes in the β -barrel of liposome reconstituted human VDAC1 suggesting the importance of the N-terminal α -helix (Abu-Hamad, *et al.* 2009). However, none of these models were found to explain the existing experimental data on VDAC.

There is no direct report of voltage dependent gating *in vivo* due to paucity of the information regarding the existence of the potential difference across the OMM. However, Brdiczka *et al.*, proposed through their calculations that inner mitochondrial membrane (IMM) potential might influence at the contact sites (Brdiczka 1991). Moreover, voltage gating of VDAC has been found to be very much important for the regulation of the metabolite and adenine nucleotide flow across the OMM. In high conductance state, VDAC is permeable to anionic metabolites like ATP, succinate, citrate and phosphate (Bowen, *et al.* 1985, Rostovtseva and Colombini 1997), whereas, in closed state, VDAC favours the conductance of positive ions including calcium (Ginzel, *et al.* 2001).

The voltage dependent gating of VDAC has been shown to be regulated by various agents including polyanions such as Konig's polyanion and Dextran sulfate (Colombini, *et al.* 1987); NADH (Zizi, *et al.* 1994), VDAC modulator (Holden and Colombini 1988) and osmotic pressure (Zimmerberg and Parsegian 1986). All these

modulators when added to mitochondria have been shown to inhibit ADP-stimulated mitochondrial respiration and also many mitochondrial kinases. Therefore, voltage dependent gating of VDAC might be playing a critical role in regulation of OMM permeability and thus mitochondrial functioning.

1.7. Extra-mitochondrial localization of VDAC:

The localization of VDAC in various sub-cellular compartments other than mitochondria is reported by many groups (Bathori, *et al.* 2000, De Pinto, *et al.* 2010b). Thinnes and co-workers for the first time identified the occurrence of VDAC in the plasma membrane which was accidentally co-purified along with human transplantation antigens (Kayser, *et al.* 1989). This was subsequently confirmed by a number of studies demonstrating the occurrence of extra-mitochondrial VDAC in various cell lines or tissues through flow cytometry, immunogold labeling and immunofluorescence techniques (Moon, *et al.* 1999). The occurrence of extra-mitochondrial VDAC has been accepted with immense criticism because the presence of a non-specific pore in the plasma membrane would be lethal to the cell (Yu, *et al.* 1995). Later, Bathori *et al.*, confirmed the presence of VDAC in the caveolae, a specific domain of the plasma membrane (Bathori, *et al.* 2000). They further purified the VDAC1 from the caveolae. The characterization of the purified VDAC1 revealed that the biophysical and biochemical characteristics were similar to that of the mitochondrial version of the protein.

The functional significance of the plasma membrane VDAC is being extensively studied. VDAC has been shown to be involved in various functions. Some of them include maxi-anion channel activity [reviewed in (Sabirov and Okada 2009)], NADH-oxidoreductase activity (Baker, *et al.* 2004) and has also been demonstrated to be a cell surface receptor for plasminogen kringle 5 (Gonzalez-Gronow, *et al.* 2003). Plasma membrane VDAC1 has also been implicated in apoptosis during various conditions including neurotoxicity induced by amyloid β -peptide during Alzheimer's disease (AD) (Marin, *et al.* 2007).

VDAC has also been detected in the sarcoplasmic reticulum compartment of skeletal muscle but the functional significance of the same is still unknown (Shoshan-Barmatz, *et al.* 1996).

1.8. Regulation of VDAC:

Mitochondria are involved in various cellular processes including the regulation of bioenergetics, inter-organelle communication, cell proliferation, aging and cell death. VDAC is known to play a central role in the regulation of the mitochondrial bioenergetics thus cellular metabolism and mitochondria mediated cell death [reviewed in (Kroemer, *et al.* 2007)]. These multiple functions of the VDAC could be realized by its regulation through various agents. The non-protein interacting partners of VDAC include ATP (Rostovtseva and Colombini 1997), NADH (Zizi, *et al.* 1994), Ca^{+2} (Gincel, *et al.* 2001), glutamate (Gincel and Shoshan-Barmatz 2004) and various therapeutic drugs affecting the apoptosis [reviewed in (Shoshan-Barmatz and Ben-Hail 2011)]. Along with these, osmotic pressure and pH also have been shown to modulate the activity of VDAC.

VDAC has been shown to interact with a wide range of proteins affecting the mitochondria mediated apoptosis. The main interaction partners include pro/anti-apoptotic Bcl-2 family proteins (Shimizu, *et al.* 1999, Shimizu and Tsujimoto 2000); kinases such as hexokinase (Pastorino and Hoek 2008) and creatine kinase (Schlattner, *et al.* 2001); cytoskeletal proteins such as actin, tubulin (Rostovtseva, *et al.* 2008, Xu, *et al.* 2001) and mitochondrial proteins such as 18 kDa mitochondrial translocator protein (TSPO) (Veenman, *et al.* 2008), cytochrome c (Roman, *et al.* 2006b) and adenine nucleotide translocator (ANT) of inner mitochondrial membrane. Most of these VDAC-protein interactions are important in the regulation of mitochondria mediated apoptosis and are discussed in the following section (1.9).

Apart from these direct binding interactions, VDAC is also shown to be regulated by post-translational modifications including phosphorylation and nitration. The phosphorylation of many of the serine and threonine residues by various kinases was mainly observed *in vitro*. A previous report from our lab demonstrated the

phosphorylation induced asymmetric modulation of VDAC channel activity by cAMP-dependent protein kinase A (Bera, *et al.* 1995). Differential phosphorylation of the VDAC isoforms in physiological conditions was shown through large scale proteomic studies (Distler, *et al.* 2007). However, the implications of the phosphorylation induced modulation of VDAC activity in both physiology and pathology requires further study. The tyrosine nitration of VDAC has been reported in various pathological conditions (Castro, *et al.* 2011). The evidence for its role *in vivo* is still lacking.

1.9. VDAC, mitochondria mediated apoptosis and human diseases:

Cell death occurs during many physiological conditions such as embryonic or immune system development or in response to infection or DNA damage or disease (Danial and Korsmeyer 2004, Elmore 2007). It follows a sequence of controlled steps leading to locally and temporally defined self-destruction and is termed as apoptosis (Kerr, *et al.* 1972). Apoptosis involves activation of a series of cysteine dependent proteases called caspases, capable of targeted protein degradation subsequently leading to organized cell demise. Two separate pathways, namely, extrinsic and intrinsic pathways are involved in the caspase activation during apoptosis (Green 2000). Mitochondria are involved in the intrinsic cell death pathway and the extrinsic cell death pathway is activated via the cell surface death receptors belonging to the tumor necrosis factor alpha (TNF- α) super family. Mitochondrial cell death pathway is stimulated by various intracellular stimuli including high levels of Ca²⁺, ROS and activation of pro-apoptotic Bcl-2 family proteins.

OMM permeabilization and release of apoptogenic proteins such as cytochrome c, SMAC, apoptosis inducing factor (AIF) and endonuclease G normally residing in the intermembrane space (IMS) into the cytoplasm is the key and primitive event during the mitochondria mediated apoptosis (Kroemer, *et al.* 2007). The released cytochrome c in association with Apaf-1 forms apoptosome and further activates the downstream caspase pathway. Many different models have been proposed for the cytochrome c release. Here we discuss only the models involving the VDAC.

One such mechanism involving VDAC is the osmotic swelling of mitochondrial matrix due to increased permeability of IMM to low molecular weight solutes causing mitochondrial permeability transition (MPT). Initial permeabilization of IMM exerts pressure on the outer membrane causing its rupture and efflux of the apoptogenic proteins such as cytochrome c from the IMS into cytosol. Such matrix swelling induced OMM rupture has been suggested to be caused by the closure of VDAC leading to the defective ATP/ADP exchange (Vander Heiden, *et al.* 2000). Growth factor removal is one typical example operating this kind of mechanism (Vander Heiden, *et al.* 2001).

A second model suggests that the cytochrome c release involves the formation of permeability transition pore (PTP) complex (a high conductance non-specific multi-protein complex comprising several components spanning both OMM and IMM. The major components of PTP include VDAC1, an OMM protein, ANT of IMM and cyclophilin D (CypD), a mitochondrial matrix protein. The direct involvement of VDAC1 and ANT in the formation of PTP is still controversial (Baines, *et al.* 2007). Although the mechanisms responsible for PTP opening and its function have not yet been resolved, many of the promoters or inhibitors of PTP such as, Ca^{2+} , inorganic phosphate, ROS, nitric oxide, gelsolin, glutamate, hexokinase, TSPO and pro/anti-apoptotic Bcl-2 family proteins have been shown to promote or inhibit PTP through the regulation of VDAC1 activity. Another model in this line has been proposed by Banerjee and Ghosh, through lipid bilayer studies on the interaction between VDAC, Bax and tBid (Banerjee and Ghosh 2004). According to this model, Bax and tBid interact with VDAC and increase its pore size and the increased pore size would be sufficient to allow the passage of cytochrome c. They further demonstrated that cyclic AMP dependent protein kinase-A mediated phosphorylation of VDAC could control the leakage of the cytochrome c (Banerjee and Ghosh 2006).

A third and more recent model suggests that homo-oligomerization of VDAC is sufficient for the OMM permeabilization and release of the pro-apoptotic proteins such as cytochrome c (Abu-Hamad, *et al.* 2006, Zalk, *et al.* 2005). This model is further supported by the recent evidences demonstrating the increase in the

oligomerization of VDAC during apoptosis. In addition, many of the apoptosis inducers have been shown to induce the oligomerization of VDAC (Abu-Hamad, *et al.* 2009). This model might explain the earlier findings showing the over-expression of VDAC induced cell death (Abu-Hamad, *et al.* 2006). The existence of supramolecular organization of VDAC in the natural membranes is not explained by this model.

VDAC being a central regulator of mitochondria mediated apoptosis, has been shown to be implicated in various human diseases caused due to mitochondrial disorders such as myocardial diseases, stroke, cancer, mitochondrial encephalomyopathies, muscular dystrophy and ageing as well as neurodegenerative disorders [reviewed in (Shoshan-Barmatz, *et al.* 2010a)]. Alterations in the regulation of PTP through modulation of VDAC channel activity has been shown to be involved in all the above mentioned diseases [reviewed in (Kroemer, *et al.* 2007)]. This could be achieved either by up/down regulation of VDAC isoforms (e.g. cancer, muscular dystrophy), altering the sensitivity to binding of various interacting partners (e.g. cancer) or by specific post-translational modifications (e.g. AD, amyotrophic lateral sclerosis).

1.10. Aims and Objectives:

Mitochondria are not only the major site of bioenergetics control in the mammalian cells but also the key site for the generation of ROS and RNS which in pathological conditions lead to severe oxidative modifications of the proteins causing mitochondrial dysfunction and cell death. Protein nitration is considered as the hallmark of such oxidative damage. Although tyrosine nitration of VDAC has been reported in various pathological conditions, the functional consequences of such nitration in the regulation of PTP remain unknown. Apart from the direct effects of oxidative stress mediators on PTP, ROS and RNS were shown to activate JNK pathway. The activated JNK has been shown to be translocated to mitochondrial sub-compartments and directly activate the PTP inducing the cytochrome c release. But there is no direct evidence for its interaction with VDAC, a key component of PTP.

Therefore, the possibility of regulation of VDAC by JNK is of considerable importance.

Supramolecular organization of VDAC has been known for long time. Another part of the work concerns the functional significance of such membrane organization of VDAC. Due to lack of proper experimental parameters to study the interactions between the VDAC molecules in an ensemble, a novel approach based on fluctuation analysis and multifractals has been used to study the existence of such functional interactions.

With the above perspective, the following objectives have been undertaken:

- a) To study the modulation of VDAC gating by peroxynitrite mediated nitration *in vitro*.
- b) To investigate the phosphorylation of VDAC isoforms by JNK and further understand the structure-function relations through Gaussian network modeling (GNM).
- c) To study the dynamics of VDAC ensemble by using noise analysis and multifractal-detrended fluctuation analysis.

**Role of Nitric oxide in biochemical
and biophysical modification of
VDAC: studies on single channel**

Chapter-2

2.1 Review of Literature:

Nitric oxide (NO) is a free radical involved in regulation of various physiological and pathological functions in all vertebrates. NO plays a key role in a wide array of biological processes such as neurotransmission, synaptic plasticity, memory formation, vascular homeostasis and inflammatory response [reviewed by (Pacher, *et al.* 2007) and references therein]. NO is produced in all mammalian tissues including brain. NO is generated either enzymatically by nitric oxide synthases (NOS) or non-enzymatically (Zweier, *et al.* 1995). Neuronal NOS (nNOS/NOS1), inducible NOS (iNOS/NOS2) and endothelial NOS (eNOS/NOS3) are the three isoforms of NOS involved in the enzymatic generation of NO. These enzymes upon activation oxidize the guanidine group of L-arginine forming NO and L-citrulline (Ignarro 1990). NO exhibits cytoprotective or cytotoxic effects in a concentration and cell type dependent manner. NO has been shown to interact with many mitochondrial proteins including electron transport chain complex III and cytochrome c oxidase (Brookes, *et al.* 2000, Brown 2001) NO is known to both promote and inhibit apoptosis in a context dependent manner (Pacher, *et al.* 2007). Specific molecular targets for NO induced anti-apoptotic effects include inhibition of Bcl-2 cleavage (Kim, *et al.* 1999), inhibition of permeability transition pore (PTP) opening (Balakirev, *et al.* 1997) and inactivation of caspases by S-nitrosylation (Li, *et al.* 1999). On the other hand, when produced in high concentrations, NO inhibits ATP synthesis and promotes PTP opening (Brookes, *et al.* 2000).

Several lines of evidence proposed the involvement of VDAC, a putative component of PTP in the oxidative stress induced pathology. VDAC has been proposed to regulate the release of reactive oxygen species (ROS) from mitochondria into the cytosol (Han, *et al.* 2003). This idea is supported by the findings that over-expression of hexokinase isoforms in HEK cells decreased the release of ROS into the cytosol and thus reduce the intracellular levels of ROS (Soshan-Barmatz, *et al.* 2008). Further, inhibition of superoxide radical ($O_2^{\cdot-}$) induced apoptosis by blockers of VDAC channel activity like DIDS, anti-VDAC antibodies suggest that $O_2^{\cdot-}$ is involved in VDAC mediated permeabilization of OMM and cytochrome c release (Madesh and Hajnoczky 2001). Sultana *et al.*, through redox proteomic approach reported the

nitration of VDAC1, a hallmark of oxidative stress, in Alzheimer's disease (AD) pathology (Sultana, *et al.* 2006). Also, nitration of VDAC1 has been shown in other tissues including heart, liver, lung and adipose tissues during diabetes and lipopolysaccharide treated conditions (Castro, *et al.* 2011). Moreover, VDAC has been shown to co-immunoprecipitate with eNOS indicating a direct interaction and complex formation (Sun and Liao 2002). This complex formation has been suggested to be important for the activation of eNOS and highly regulated modulation of VDAC by NO (Sun and Liao 2002). In spite of increasing number of reports on the involvement of VDAC in oxidative stress induced pathology the mechanism by which the ROS and RNS regulate VDAC is not completely understood. Therefore, the functional studies involving nitration of VDAC would provide more insight on the role of VDAC in the pathophysiology of oxidative stress induced cell death.

In the present part of the work, the biochemical and biophysical modifications induced by peroxynitrite on purified rat brain mitochondrial VDAC reconstituted in artificial bilayers were investigated *in vitro*.

2.2 Materials and Methods:

The details of the materials used in the present part of the work are given in Table-A1 (appendix-I).

2.2.1. Purification of VDAC from rat brain mitochondria:

Mitochondria were isolated from the rat brain according to the procedure described in (Stahl, *et al.* 1963) and VDAC was purified according to the method described in (De Pinto, *et al.* 1987b). All the steps of isolation and purification were performed at 4°C.

10 male Wistar rats (weighing 100-150 g) were starved for 15-20 hours before the experiment. These rats were then anesthetized according to the procedure approved by institutional animal ethics committee. Brain (~1.5 g each) from these rats was surgically removed, washed in chilled Solution-A (0.4 M Sucrose, 1.0 mM EDTA, pH adjusted to 7.4) and chopped into pieces. The tissue was homogenized in solution-A (2ml /g tissue) using Elvehjem-potter homogenizer with motorized

teflonpestle and more of solution-A was added to obtain a 10 ml/g suspension. The homogenate was then centrifuged at 2000g for 20 minutes in a centrifuge (Kubota 7700, Japan) to yield pellet (P1) and supernatant (S1). S1 was centrifuged at 12,000g for 15 minutes to yield crude mitochondrial fraction(P2) comprising of a tan lower layer and white fluffy upper layer and supernatant (S2). P2 was then homogenized in 6 ml of solution-B/g of original tissue and centrifuged at 12,000g for 15 minutes. The solution-B is nothing but solution-A supplemented with Ficoll to a final concentration of 8 per cent (w/v). The supernatant, S3 was discarded from the brown pellet, P3 containing pure mitochondria visibly free of contaminating white fluffy material.

The mitochondrial pellet (P3) was then suspended in solution-C (10 mM Tris-Cl, 1mM EDTA, pH adjusted to 7.4) and incubated on ice for 15 minutes to rupture mitochondria. The suspension was then centrifuged at 27,000g for 10 minutes to yield mitochondrial membrane fraction, P4 and supernatant, S4. P4 was then suspended in solution-D (solution-C supplemented with 3% (V/V) triton X 100) at a final concentration of 5 mg/ml and incubated in ice for 30 minutes. The suspension was centrifuged at 40,000g for 30 minutes and supernatant S5 was collected discarding the pellet P5.

6 ml of S5 was loaded on to a dry, suction packed Hydroxyapatite: celite-545 (2:1) column. Elution was performed with solution-D and first 20 ml containing VDAC was collected. The purity of the protein was checked by SDS-PAGE. Purified protein was distributed into aliquots of 500 μ l and stored at -70°C until further use.

2.2.2 Protein Estimation:

The protein quantification was carried out by following modified Lowry procedure (Markwell, *et al.* 1978). Calibration was performed using a BSA standard. The buffer compositions are given in appendix-II.

Protein concentrations of the samples containing Triton X-100, the detergent was first removed by the method of Chandarajan and Klein (Chandarajan and Klein 1975) and then estimated by modified Lowry's method.

2.2.3. SDS-Polyacrylamide Gel Electrophoresis (SDS-PAGE) of proteins:

SDS-PAGE was performed according to standard procedure (Laemmli 1970). Solubilized protein samples were loaded onto a minigel electrophoresis system (Miniprotean II, Bio-Rad).

SDS-polyacrylamide gels were composed of 2.1% (w/v) acrylamide stacking gel and 10% or 12% resolving gel. Electrophoresis was performed at room temperature and constant voltage 100 V. After completion of the run the gels were stained either by Coomassie blue or silver nitrate. The molecular mass determination of the protein bands was based on standard proteins (Pageruler, Fermentas, Canada). The buffer compositions for stacking and resolving gel preparation are given in appendix-II.

2.2.4. Bilayer Electropysiology of VDAC:

a) Bilayer Setup:

Fig. 2.1 shows a snapshot of the bilayer setup used for the electrophysiology experiments. The setup consists of a polystyrene cuvette with 150 μm aperture which snugly fits into a bilayer chamber. The cuvette divides the bilayer chamber into two aqueous compartments. The bilayer chamber along with the cuvette was placed on the vibration isolation table (Technical manufacturing corporation, USA). The aqueous compartments were connected to an integrating patch clamp amplifier (Axopatch 200B, Molecular Devices inc., USA) via a matched pair of Ag/AgCl electrodes (Harvard apparatus, USA) through a headstage (CV-203BU). One of the compartments receiving the analog signals from the amplifier is called the *cis* compartment and the other compartment held at virtual ground is called *trans* compartment. An interface, Digidata 1440A (Molecular Devices inc., USA) was used to connect the amplifier to the CPU of a computer. Channel currents were recorded and analyzed using a software package, pClamp 10 (Molecular Devices inc., USA). Microcal Origin 6.0 was also used for analyzing the data.

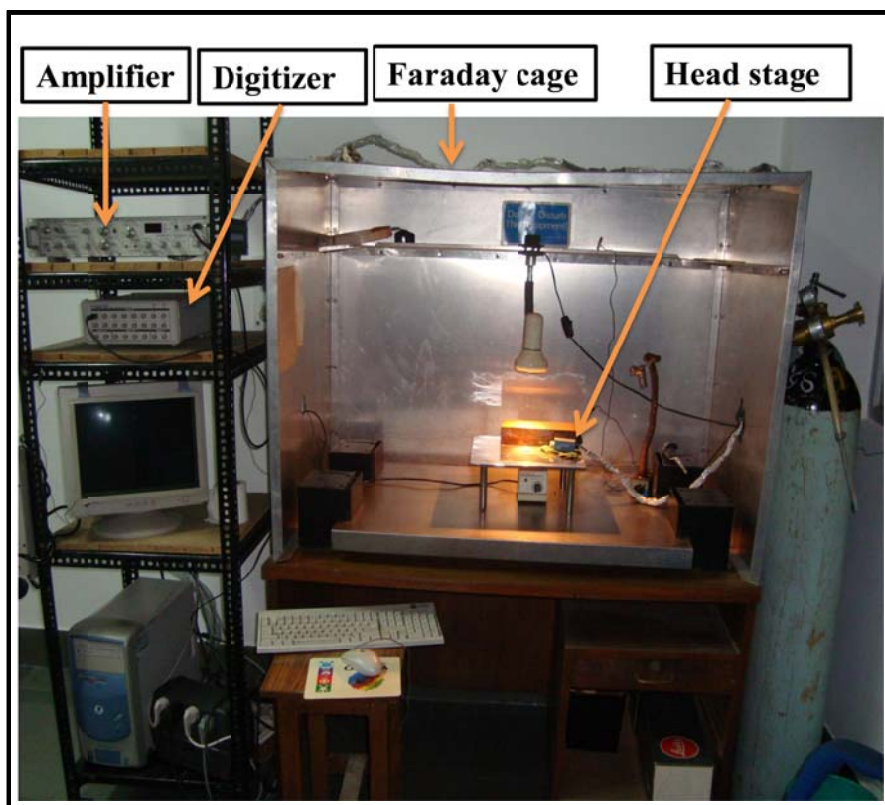


Fig. 2.1: Snapshot of the bilayer setup used for lipid bilayer studies of single and multichannel VDAC

b) Lipid Solution:

8 μl of DPhPC (25 mg/ml in chloroform) was taken in a small glass eppendorf tube. The chloroform was evaporated under slow nitrogen stream and DPhPC re-dissolved in 20 μl of n-decane. The working lipid solution was prepared afresh before each experiment.

c) Formation of Black Lipid Membrane (BLM):

Planar lipid bilayers were painted according to the procedure of Mueller *et al.*, (Mueller, *et al.* 1963). Polystyrene cuvette was washed thoroughly with DDW and then with ethanol. The cuvette was dried under nitrogen stream and DPhPC (10 mg/ml in n-decane) was painted on 150 μm aperture of the cuvette (pre-conditioning) using a fire polished glass capillary. The solvent was evaporated under slow nitrogen stream. After that, both *cis* and *trans* chambers were filled with BLM buffer (500 mM

KCl, 10 mM HEPES, 5 mM MgCl₂, pH-7.4) in such a way that both the compartments had equal levels of buffer. Ag/AgCl electrodes were dipped into the buffer of each chamber. Then DPhPC is applied onto the aperture of the cuvette using a fire polished glass capillary. This pre-conditioning was done to hasten the formation of the membrane.

d) Reconstitution of VDAC into BLM and single channel recording:

The reconstitution of purified VDAC into BLM was carried out following Benz *et al.*, (Benz 1994). After getting a leakage free membrane, purified VDAC was added to the *cis* compartment at a final concentration of 5-6 ng and was stirred continuously. Channel incorporation was indicated by a sudden jump of membrane current as observed on the computer monitor. The time for the insertion of the first channel was observed to be 20-25 minutes. For single channel recording, the *cis* chamber solution was replaced with fresh buffer devoid of VDAC immediately after the first channel insertion. The perfusion was done manually by simultaneous removal and addition of old and new buffer respectively. Once it was confirmed that membrane contained single channel, the channel currents were recorded at different clamping potentials using data acquisition software Clampex 10 (pClamp 10). The obtained data was analyzed offline using Clampfit 10 software (pClamp 10) and Microcal Origin 6.0.

e) Steady state current voltage (I-V) curve:

Steady state I-V curve was plotted from the single channel current (I) data as a function of applied voltage (V). Steady state current was measured after the exponential decay of the membrane current following the applied voltage step.

f) Determination of open probability (P_o):

The open probability (P_o) at a particular applied voltage was determined manually by calculating the fraction of total time spent by the single VDAC channel in the open state (~4 nS) at that voltage. Calculations were performed on continuous time traces of two minutes length at each applied potential. P_o calculations were performed manually.

2.2.5. Synthesis of Peroxynitrite (ONOO^-):

Peroxynitrite (ONOO^-) was synthesized by adopting the procedure described by Robinson and Beckman (Robinson and Beckman 2005) with some modifications. The synthesis was performed at room temperature. The solution required for the synthesis, acidified H_2O_2 ($0.7\text{M HCl} + 0.6\text{M H}_2\text{O}_2$), 0.6M NaNO_2 and 3M NaOH , were prepared freshly just before the start of the experiment. The setup used for the synthesis is shown in fig. 2.2.

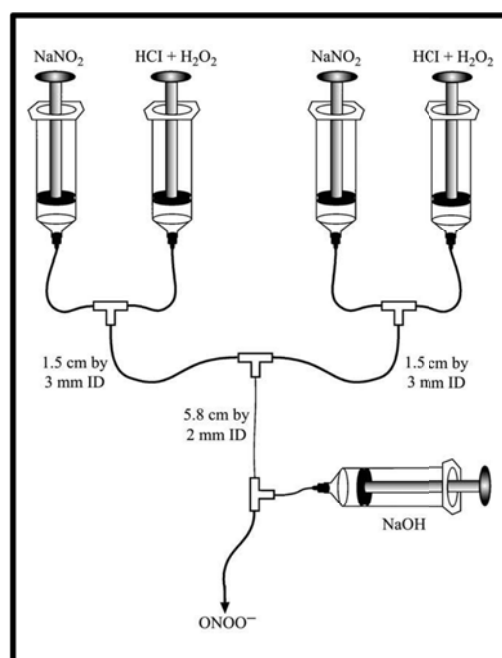


Fig. 2.2: Schematic diagram showing the setup used for synthesis of peroxynitrite (adapted from (Robinson and Beckman 2005)).

As shown in fig. 2.2, the nitrite and peroxide were allowed to react at the first set of T-junctions to form peroxynitrite and further allowed to mix at the next T-junction to ensure maximum peroxynitrite formation. Thus formed peroxynitrite has a half-life of less than 1 second in acidic conditions. Therefore the reaction is immediately quenched with an excess base (3M NaOH) at the next junction. The flow is discarded until yellow coloured solution emerges. The yellow colour is due to peroxynitrite and is collected in a separate flask buried in ice. The concentration of the peroxynitrite can be spectrally monitored at 302 nm using an extinction coefficient

of $1670 \text{ M}^{-1} \text{ cm}^{-1}$. The typical yields of peroxyxynitrite synthesized by this method are in the range of 180 – 190 mM. In our case the flow in the five syringes was manually controlled instead of using syringe pumps. This might have affected the yields. The yield in our case was ~70 mM. The peroxyxynitrite thus formed contains about 0.28 M NaCl and 0.1 M NaOH as contaminants.

The unreacted H_2O_2 was decomposed by incubating the peroxyxynitrite with MnO_2 on ice for 15 minutes. The MnO_2 was removed by filtration. MnO_2 was synthesized according to the procedure described in the Robinson and Beckman (2005). MnO_2 was prepared by treating 16% (w/v) KMnO_4 with 10 volumes of 95% ethanol and stirred overnight. The formed MnO_2 precipitate was then washed with 2-3 litres of DDW and dried at room temperature.

2.2.6. Nitration of VDAC:

Synthesized peroxyxynitrite was used to nitrate VDAC. Nitration of VDAC was achieved by addition of 1 mM ONOO^- or to aqueous solution of VDAC (for western blotting) or to the *cis* chamber of the bilayer chamber for nitration of VDAC reconstituted in artificial bilayer.

2.2.7. Western Blot analysis:

Following one dimensional SDS-PAGE, the proteins from polyacrylamide gels were transferred onto PVDF membrane (BioRad) by means of electroblotting method (Towbin, *et al.* 1979). The primary and secondary antibodies used were mouse monoclonal anti-3-Nitrotyrosine antibody (Cayman chemicals, USA) and horse radish peroxidase conjugated anti-mouse IgG respectively. Both chemiluminescence and colorimetric detection methods were used for identifying antigen-antibody interactions. The buffer compositions are given in appendix-II.

2.2.8. Lipid Bilayer experiments of Nitrated VDAC:

After getting single channel recording of VDAC, 1 mM ONOO^- was added to the *cis* chamber and stirred for 2-3 minutes. As the addition of peroxyxynitrite shifted the pH to alkaline side, the pH was adjusted to 7.4 by addition of 4 μl of 1N HCl. The

pH during the experiment was monitored by using Neutralit pH strips (Merck) and the recording was done after 5 minutes of peroxyntirite addition. All the data were analyzed by clampfit 10 (pCLAMP 10, Molecular Devices inc., USA).

2.3. Results and Discussion:

2.3.1. Purification of VDAC from rat brain mitochondria:

VDAC was purified according to the method described in the earlier section. The protein obtained was pure and devoid of any contaminant proteins as judged by single band in the silver stained polyacrylamide gel run in denaturing conditions (fig. 2.4). The molecular weight of the observed band was estimated based on molecular weight standards and was found to be ~31 KDa. The purified protein was quantified by modified Lowry method. The final concentration of purified VDAC was calculated based on BSA calibration curve (fig. 2.3) and was found to be 1 $\mu\text{g/ml}$.

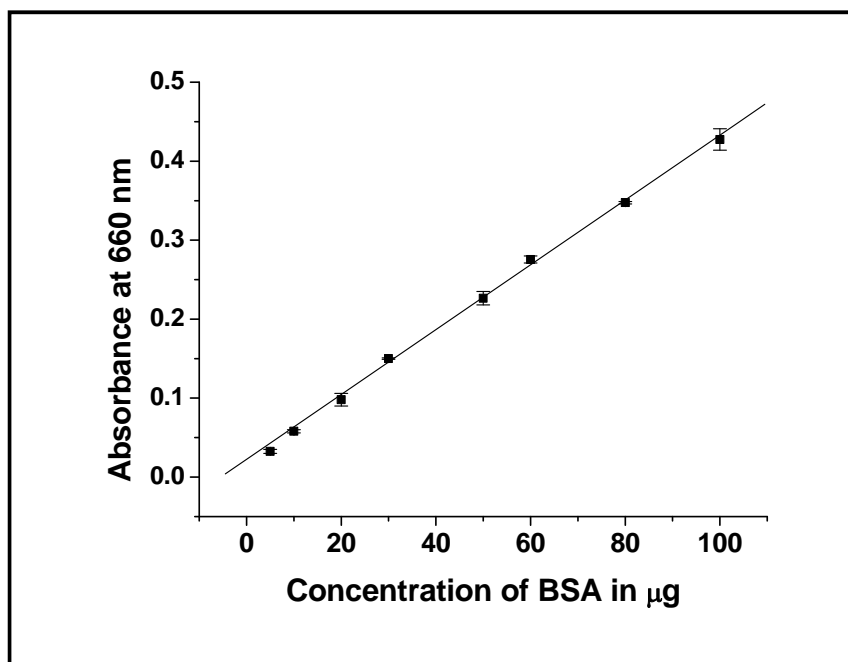


Fig. 2.3: Standard curve for protein estimation. BSA standards containing 5, 10, 20, 30, 50, 60, 80 and 100 $\mu\text{g/ml}$ were prepared in double distilled water and estimated by modified Lowry's method. Absorbance was measured at 660 nm. Values are mean \pm SE of three independent experiments.

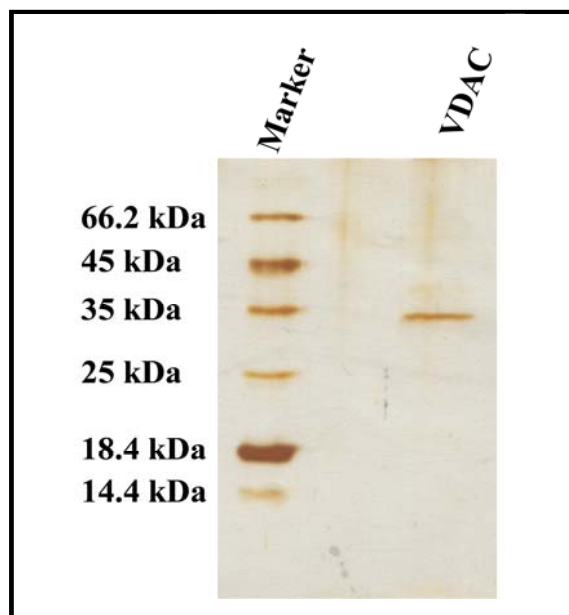


Fig. 2.4: SDS-PAGE profile of purified rat brain mitochondrial VDAC. Lane A: Molecular weight markers (molecular weights in kDa are written on the left side); Lane B: Purified Rat brain mitochondrial VDAC (~31 kDa). The polyacrylamide gel (12.5%) was stained by silver staining procedure.

2.3.2. Electrophysiological characterization of purified VDAC reconstituted in planar lipid bilayers:

The purified VDAC exhibited channel activity when reconstituted into planar lipid bilayer. The time lag between the addition of protein to the *cis* compartment of the bilayer chamber and the observation of channel activity was about 25 minutes. The channel activity was indicated by a sudden jump in the membrane current. No such increase in current was observed when only buffer was added to the bilayer chamber. Single channel reconstitution was achieved by addition of very low amounts of VDAC (~5 ng/ml to the *cis* chamber buffer). The single channel activity recorded was consistent with the earlier reports (De Pinto, *et al.* 1987a). The channel remained in full open state, (~4 nS) (fig. 2.5) for longer durations at lower applied voltages (-30 mV to +30 mV) and showed a linear current (I) – Voltage (V) relation in this region (fig. 2.6). Beyond ± 30 mV, the channel remained in sub-conductance states for longer periods. This voltage dependent gating was shown by the non-linearity in I-V curve (fig. 2.6).

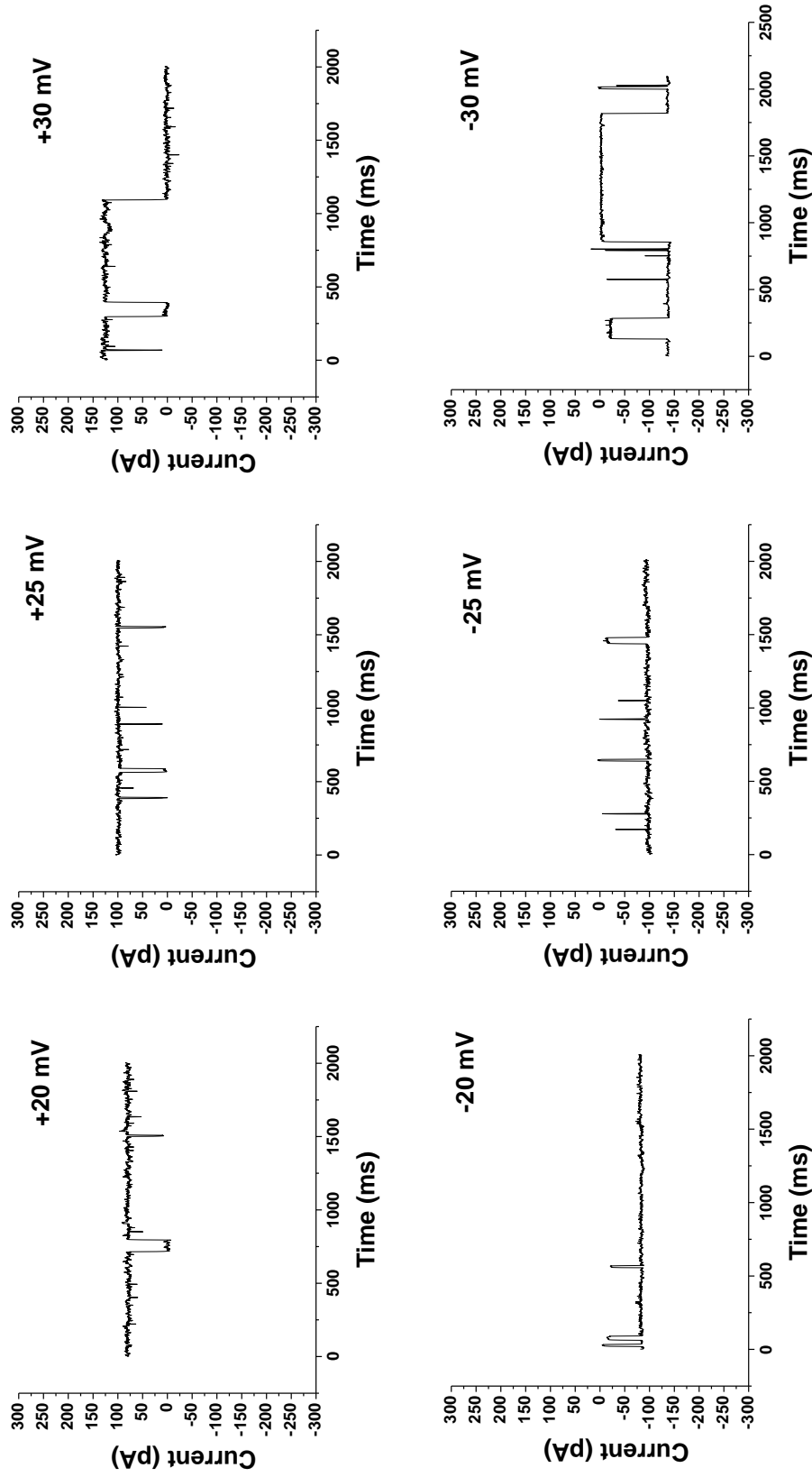


Fig. 2.5: Representative single channel current traces of purified rat brain mitochondrial VDAC reconstituted in DPhPC membranes. The recording was performed in symmetrical solution of 500 mM KCl, 10 mM HEPES, 5 mM MgCl₂, at 25 °C. Clamping potentials with respect to ground are indicated on each plot.

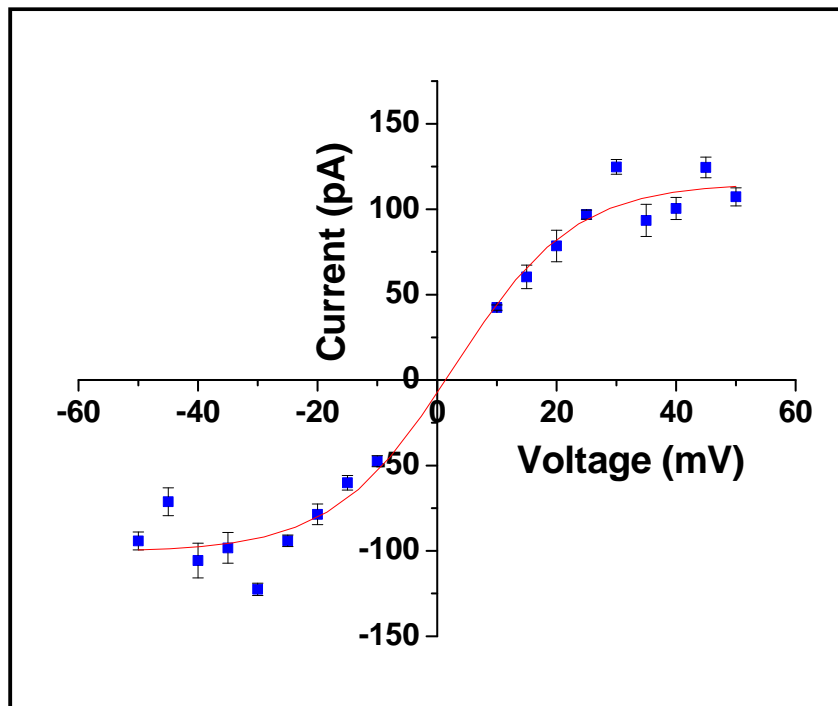


Fig. 2.6: The steady-state current-voltage relation of VDAC. Rat brain mitochondrial VDAC was incorporated in DPhPC/n-Decane bilayers with symmetrical solution of 500 mM KCl, 10 mM HEPES, 5 mM MgCl₂, at 25 °C. Data shown was recorded with Clampex (pClamp 10, Molecular Devices, USA) and analyzed using Clampfit (pClamp 10, Molecular Devices, USA). The data was fit using sigmoidal function in Origin 6.0 software.

Fig. 2.7 shows the open probability of VDAC as a function of clamping potential (V). The open probability curve was bell shaped indicating a high open probability at lower voltages, which falls down with increase in clamping potential.

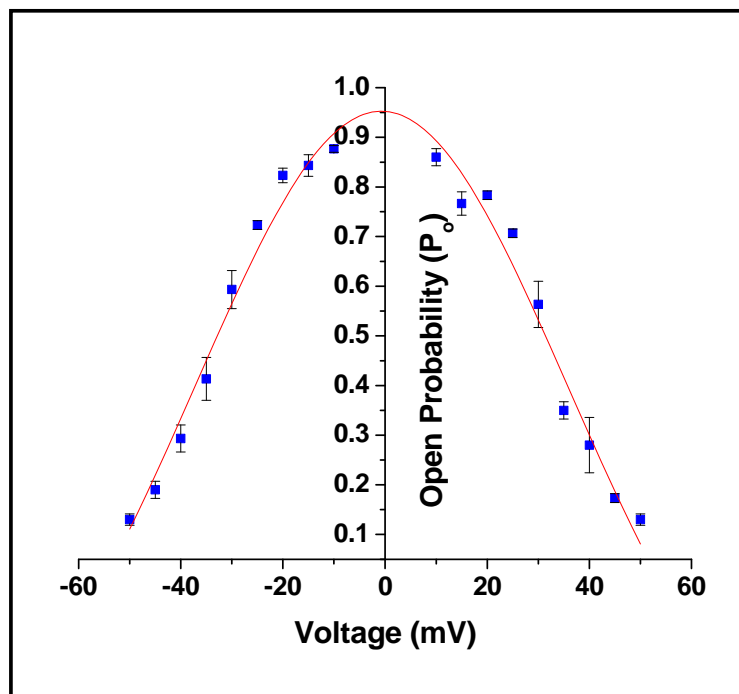


Fig. 2.7: Voltage dependence of open probability (P_o) of VDAC. P_o was calculated as a fraction of total time the channel spends in the open state. Data shown were taken from continuous current recording of two minutes for each holding potential. Values represented are mean \pm SE of three independent observations. The data was fit using Gaussian function in Origin 6.0 software.

Average single channel current (IP_o) at different applied potentials were calculated. The IP_o is defined as the product of single channel current (i) and open probability of VDAC at a given potential. The IP_o gives an idea about the ion flux across the bilayer containing VDAC. Fig. 2.8 shows that the current through VDAC single channel was maximum at 30 mV clamping potential and reduces down to a near zero value at 50 mV.

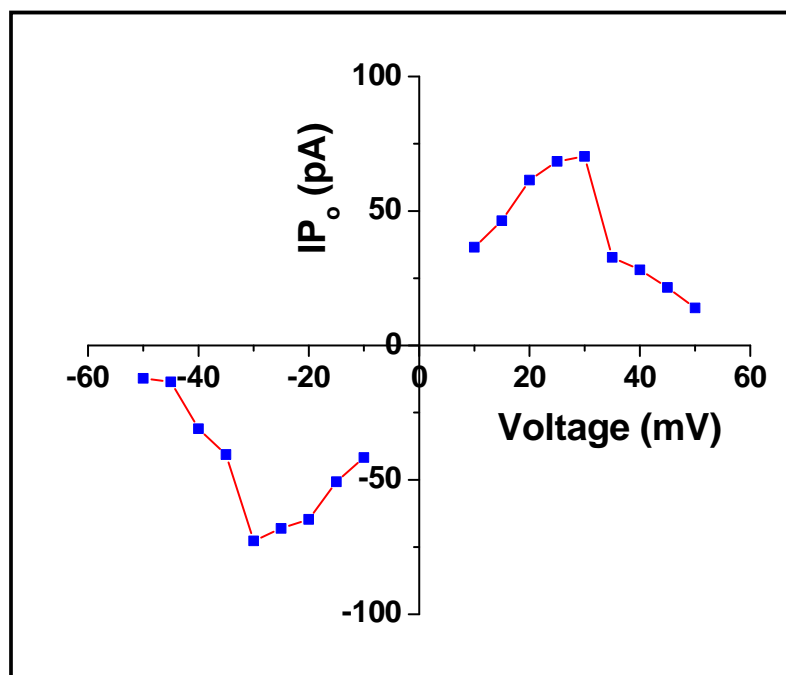


Fig. 2.8: Average single channel current (IP_o) of VDAC at various holding potentials. Average single channel current was calculated by multiplying single channel current and open probability at a given holding potential. Data was taken from fig. 2.6 and fig. 2.7.

2.3.3. Nitration of VDAC and Western blotting:

VDAC was nitrated by treating with 1mM $ONOO^-$. The nitration was further confirmed by western blotting using a monoclonal antibody for 3-Nitrotyrosine. The nitrotyrosine antibody specifically detected the $ONOO^-$ treated VDAC (fig. 2.9), but did not bind to either control VDAC or VDAC treated with peroxynitrite decomposed before adding to VDAC (negative control). This confirms the nitration of VDAC by $ONOO^-$. A faint higher molecular weight band was also visible which may correspond to the higher oligomer of nitrated VDAC.

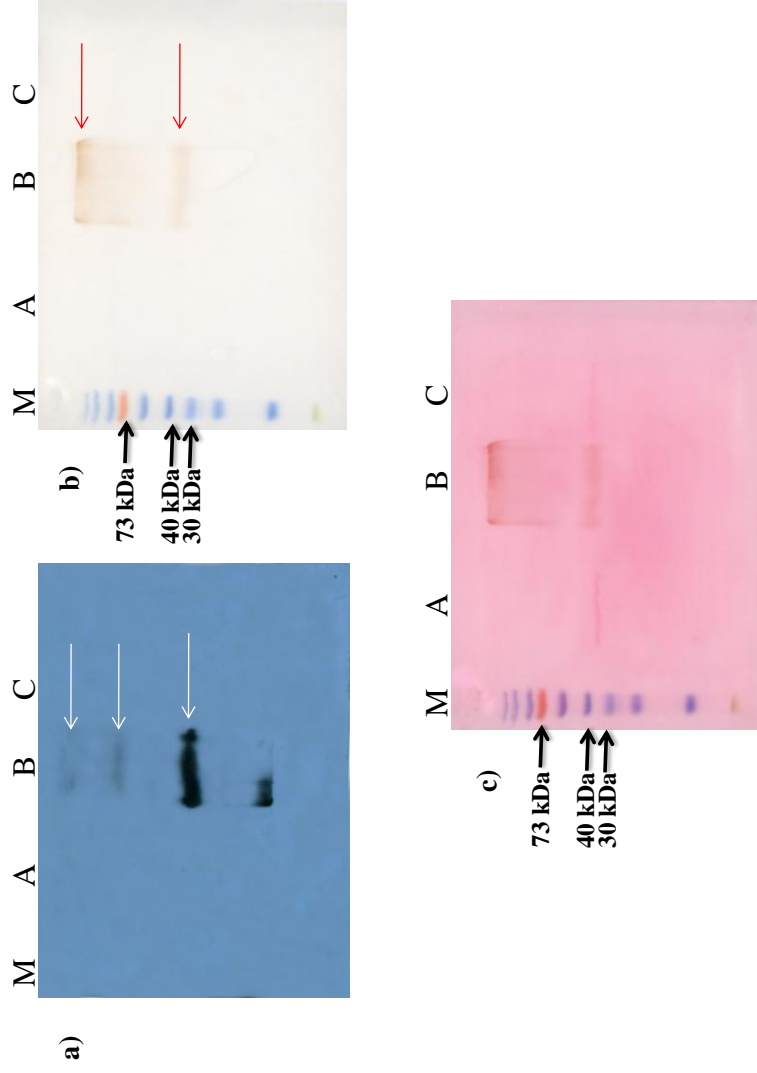
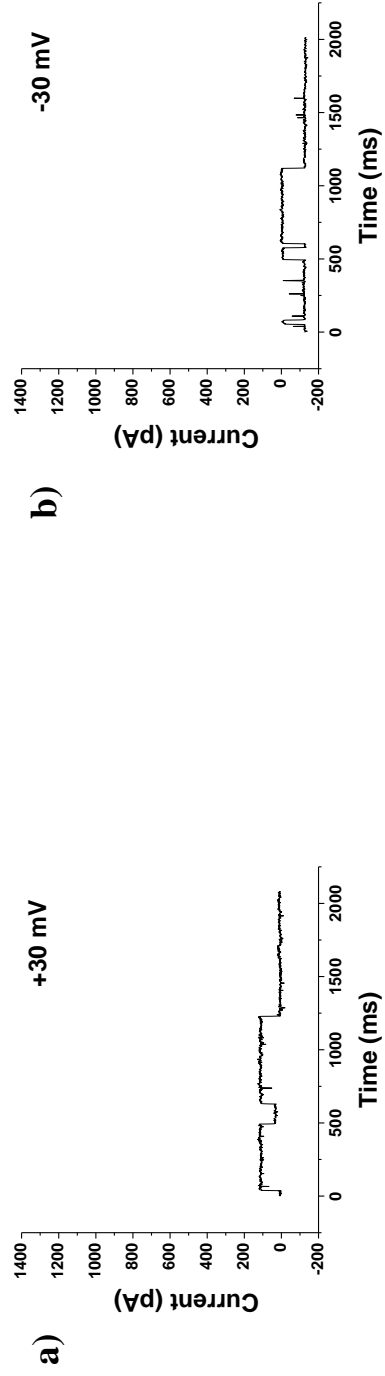


Fig. 2.9: Western Blot analysis. The nitration of VDAC treated with peroxydinitrite was visualized using a monoclonal antibody for 3-Nitrotyrosine. a) Nitrotyrosine antibody specifically detected peroxydinitrite treated VDAC in Lane B. The nitrated VDAC monomer and respective higher oligomers are indicated by white arrows. b) Colorimetric substrate also detected the nitrated VDAC in the Lane B and the bands are indicated by red arrows. Lane A contains untreated VDAC, Lane C has VDAC treated with decomposed peroxydinitrite and Lane M is pre-stained molecular weight marker (Pageruler, Fermentas, Canada) c) Ponceau stained blot showing the VDAC bands in Lane A and Lane C unreactive to the Nitrotyrosine antibody.

2.3.4. Electrophysiological characterization of Nitrated VDAC:

After successful reconstitution of single VDAC channel, the buffer in the *cis* chamber was replaced by fresh BLM buffer to avoid further reconstitution of VDAC molecules. Peroxynitrite was thawed on ice and was added to the *cis* chamber to attain a final concentration of 1 mM/ml and stirred for 5 minutes. The pH changes due to the addition of ONOO^- were neutralized by addition of 1N HCl. Significant decrease or increase in current was observed within 5 minutes after addition of ONOO^- depending on the sign of holding potential (fig. 2.10).

Native VDAC



Nitrated VDAC

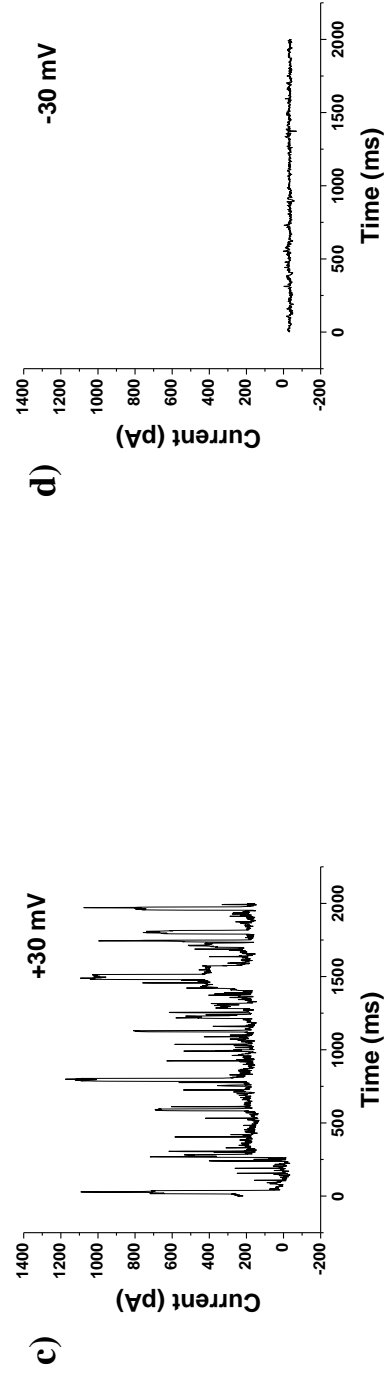


Fig. 2.10: Effect of peroxynitrite mediated nitration on VDAC gating. Continuous current traces at ± 30 mV: a) and b) Native VDAC; c) and d) Peroxynitrite treated VDAC

2.3.5. Asymmetric behaviour of nitrated VDAC:

Analysis of single channel currents of nitrated VDAC revealed that the channel after nitration behaves asymmetrically at negative and positive clamping potentials. The current amplitude of nitrated VDAC at all positive clamping potentials was found to be higher than that of the native VDAC, whereas, at negative clamping potentials, the channel remains at a closed state (fig. 2.10). Further, the average conductance of the peroxyxynitrite treated single channel VDAC was observed to be approximately ~ 5 fold higher than that of native VDAC at positive clamping potentials (fig. 2.11).

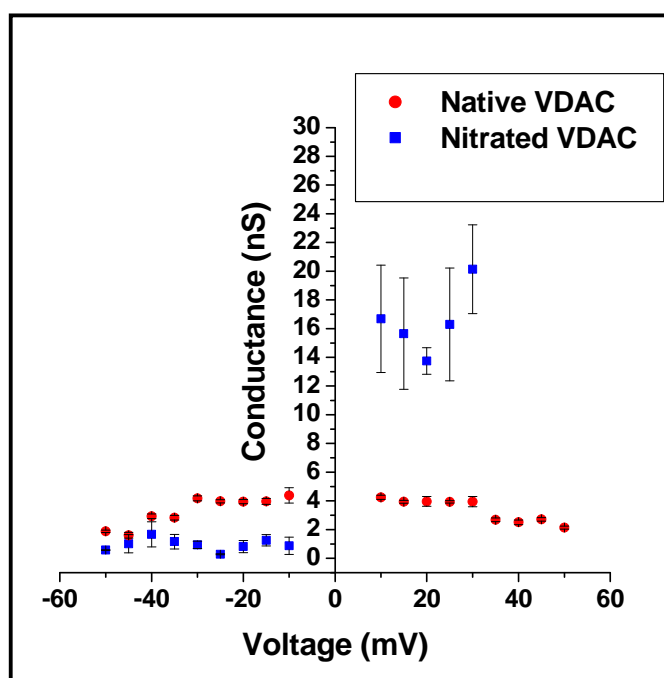


Fig. 2.11: Conductance profiles of native and nitrated VDAC. As shown, conductance profile of nitrated VDAC deviates from that of the typical double Gaussian pattern of native VDAC. In case of nitrated VDAC the conductance has very large fluctuations and for clamping voltages greater than ± 35 mV, the fluctuations in the conductance were observed to be still higher and are not presented in the plot.

Similar kind of asymmetric behaviour in case of phosphorylated VDAC has been reported (Bera and Ghosh 2001). But in their report the phosphorylation affected the gating dynamics of VDAC only at negative potentials

leaving the gating properties at positive clamping potentials unaffected. They further proposed that asymmetry in the charge distribution due to additional phosphate group is responsible for the observed asymmetry in the gating behaviour. Although, the same explanation could be extended to our case, the abnormal increase in the conductance of nitrated VDAC at positive clamping potentials remains unexplained.

There are about 11 tyrosine (tyr) residues in the primary structure of VDAC. The recently solved X-ray crystallographic structure of murine VDAC1 (Ujwal, *et al.* 2008) reveals some interesting details about the distribution of these tyr residues. Out of the 11 tyr residues, two are located on the N-terminal α -helix and the remaining nine are unevenly distributed on the 19 β -strands forming the pore. Eight of these nine tyr residues are spread on one side of the pore and the remaining one, on the other side of the barrel (fig. 2.12). Therefore, we strongly believe that the number and distribution of the tyr residues in nitrated VDAC would explain the conductance changes observed both at positive and negative clamping potentials.

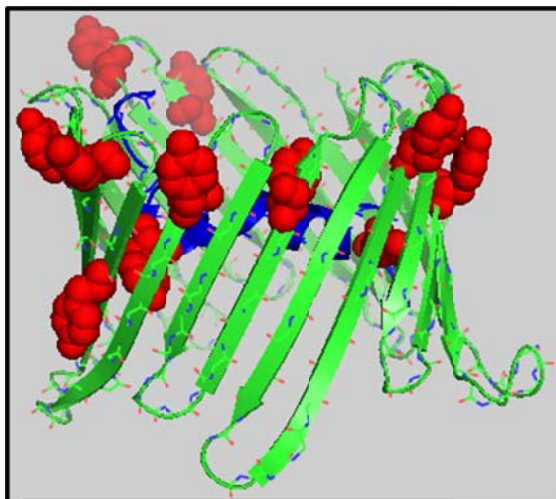


Fig. 2.12: Cartoon representation of murine VDAC1 (PDB code: 3EMN) viewed parallel to the membrane plane. The red spheres in the snapshot represent the tyr residues distributed on the mVDAC1 structure. The unequal distribution of the tyr residues is clearly visible. Pymol software was used to visualize the 3D structure.

Peroxynitrite-mediated damage of key mitochondrial proteins resulting in mitochondrial dysfunction is being recognized as the common pathway underlying the

cell death associated with various diseases such as diabetes, stroke, atherosclerosis and most of the neurodegenerative disorders (Pacher, *et al.* 2007). Peroxynitrite has been shown to induce the opening of PTP in isolated mitochondria (Borutaite, *et al.* 1999, Brookes and Darley-Usmar 2004, Brookes, *et al.* 2000, Scarlett, *et al.* 1996). Although, cysteine nitrosylation of ANT was proposed as a possible mechanism for the peroxynitrite induced PTP opening (Vieira, *et al.* 2001), this requires further confirmation. The underlying mechanisms involved in the opening of PTP in response to peroxynitrite are still not clear. VDAC, a putative component of PTP has been observed to be nitrated in a context and tissue specific manner (Castro, *et al.* 2011, Sultana, *et al.* 2006). In order to understand whether nitration of VDAC could cause the PTP opening, we studied the effect of peroxynitrite on the channel activity of VDAC *in vitro*. Our results demonstrated a ~4-5 fold increase in the conductance of VDAC at positive clamping potentials after exposure to 1 mM peroxynitrite (fig. 2.11). As a positive potential difference exist across the mitochondrial outer membrane, our results suggest that nitration of VDAC might underlie the peroxynitrite induced PTP opening. Nitric oxide has also been shown to inhibit the PTP opening in a context dependent manner (Brookes, *et al.* 2000). The channel closure observed at negative clamping potentials might be relevant in such cases.

Recently, Cheng *et al.*, demonstrated that NO affects the cardiac VDAC reconstituted in planar lipid bilayer, in a biphasic manner. They showed that physiological concentrations of NO induced closure of VDAC at both positive and negative clamping potentials whereas higher concentrations of NO failed to elicit the same response (Cheng, *et al.* 2010). These results are in striking contrast to our observations and some of the earlier observations made by different groups showing that high concentration of NO promote PTP opening (Borutaite, *et al.* 1999, Brookes, *et al.* 2000, Vieira, *et al.* 2001). The reasons for the discrepancies in the observations require further detailed investigation.

Taken together our results suggest that nitration of VDAC plays a crucial role in regulation of PTP opening in a context dependent manner. Further, we suggest that the potential difference across the outer mitochondrial membrane might be the key regulator of the context dependent responses *in vivo*.

Phosphorylation of VDAC: studies on structure-function relationship

Chapter-3

3.1. Review of Literature:

Oxidative stress induced mitochondrial-mediated cell death has been demonstrated to be the major pathway implicated in neuronal cell death associated with various neurodegenerative disorders, aging, cerebral ischemia and traumatic brain injury (Kroemer, *et al.* 2007, Pacher, *et al.* 2007). Several lines of evidence presented the direct effects of ROS and RNS in mitochondrial dysfunction and induction of mitochondrial membrane permeabilization causing neurodegeneration (Condo, *et al.* 2006, Gakh, *et al.* 2006, Kruman, *et al.* 1997, Vieira, *et al.* 2001). Apart from these direct effects, ROS and RNS have been shown to induce c-Jun N-terminal kinase (JNK, also known as stress activated protein kinase (SAPK)), a member of mitogen-activated protein kinase (MAPK) subfamily (Shen and Liu 2006).

JNK is considered as a central mediator underlying the neuronal cell death in mammalian brain, but also involved in regulation of neuronal plasticity and regeneration (Coffey, *et al.* 2000, Tararuk, *et al.* 2006). A total of 10 splice variants of three major isoforms JNK1, JNK2 and JNK3 generated from three different genes *jnk1*, *jnk2* and *jnk3* comprise the JNK family in mammals (Gupta, *et al.* 1996). While, JNK1 and JNK2 isoforms are expressed in all tissues, JNK3 expression is limited to brain, heart and testes (Gupta, *et al.* 1996, Mohit, *et al.* 1995). Phosphorylated JNK has been shown to modulate the activity of a number of nuclear and non-nuclear substrates in a context dependent manner (Bogoyevitch and Kobe 2006). The existence of mitochondrial pools of JNK has been demonstrated in neuronal and non-neuronal cells (Putchu, *et al.* 2002, Putchu, *et al.* 2003, Schroeter, *et al.* 2003, Zhou, *et al.* 2008, Zhou, *et al.* 2009). Especially the mitochondrial presence of JNK is of great interest due to its role in the activation of pro-apoptotic Bcl-2/BH3 only proteins and the release of cytochrome c during stress induced mitochondria-mediated apoptosis.

The differential distribution of JNK1 and JNK2 isoforms has been demonstrated in PC12 cell mitochondria in normal conditions and following oxidative stress (Eminel, *et al.* 2005). Another report from the same group recently demonstrated the alterations of the activated JNK isoforms following cerebral ischemia (Zhao and Herdegen 2009). They have shown that following transient

ischemia, the phosphorylated JNK3 dominates the mitochondrial JNK pool and was responsible for the induction of the mitochondrial permeability transition pore (MPTP) and cytochrome c release. However, the mechanism by which the JNK3 induces the formation of MPTP is still unclear. At this juncture, we would like to hypothesize that modulation of either components of the MPTP complex or the regulators of MPTP through site specific Phosphorylation might underlie the pro-apoptotic activities of JNK.

VDAC is one such putative MPTP component of the OMM which has been shown to be implicated in the cytochrome c release. VDAC has also been shown to be phosphorylated by various mitochondrial and cytosolic kinases (Baines, *et al.* 2003, Bera, *et al.* 1995, Liberatori, *et al.* 2004). Recently, Distler *et al.*, (Distler, *et al.* 2007) identified the phosphorylation sites of VDAC by MALDI-TOF showing that the three isoforms VDAC1, VDAC2 and VDAC3 from rat liver are phosphorylated at different sites. The effects of phosphorylation on VDAC were mostly studied *in vitro*. Bera and Ghosh (Bera and Ghosh 2001) showed that PKA-mediated phosphorylation of reconstituted single channel VDAC resulted in reduced single channel current at negative clamped potentials. c-Raf kinase has been shown to interact with VDAC and prevented its reconstitution into lipid bilayers, yet phosphorylation of VDAC by c-Raf was not detected (Le Mellay, *et al.* 2002). In addition, studies on VDAC1 mutants for potential phosphorylation sites i.e. Ser-12 and Ser-103 to Alanine could attenuate the endostatin induced upregulation of VDAC1 expression and thus abolished the endostatin induced PTP opening in endothelial cells (Yuan, *et al.* 2008).

Keeping in view the above facts, as described in this part of the work we made an attempt to examine the phosphorylation of VDAC1 and VDAC2 isoforms by recombinant active JNK3 *in vitro*.

3.2. Materials and Methods:

The details of the materials used are given in Table-A1 (appendix-I)

3.2.1. Purification of VDAC: VDAC was purified according to the procedure described in section 2.2.2.

3.2.2. *In vitro* kinase reaction: *In vitro* kinase assay was performed as follows:

4 µg of purified rat brain mitochondrial VDAC was precipitated with chilled acetone and was resuspended in 12 µl of kinase buffer (20 mM MOPS-EDTA, pH-7.2). 0.1 µg (1µl) of recombinant active JNK3 and 10 µl of [γ - 32 P] ATP mix (containing 6 µCi and 56 µM of unlabelled ATP in 10 mM Tris-Cl, pH-7.4) were added to it. The total volume of reaction mixture was adjusted to 30 µl by adding 7µl of kinase buffer and incubated at 30 °C for 30 minutes. After completion of the incubation period the reaction was terminated by adding 10 µl of SDS-PAGE sample buffer (4X). The incorporation of 32 P radioisotope was analyzed by electrophoresis on 12.5 % SDS-PAGE and autoradiography. A control for the kinase reaction was maintained without addition of JNK3 to the reaction mixture. For samples to be processed further for mass spectrometry, only unlabeled ATP was used for phosphorylation.

3.2.3. Recombinant expression of rVDAC1 and rVDAC2 isoforms in *E. coli*:

a) *E. coli* strain:

BL21 CodonPlus strain was used for cloning and expression of rVDAC1 and rVDAC2 isoforms. The cultures were grown in Luria-Bertani (LB) broth (DIFCO) containing 1% tryptone, 0.5% yeast extract and 0.5% sodium chloride. Chloramphenicol at a final concentration of 25 µg/ml was used as a selection marker for BL21 CodonPlus cultures. In case of bacteria harboring pASK plasmid, a double selection was made using antibiotics, chloramphenicol and ampicillin at final concentrations of 25 µg/ml and 100 µg/ml respectively. The cultures were grown at 37 °C.

b) Transformation of *E. coli*:

BL21 CodonPlus competent cells were prepared using CaCl₂ method. Briefly, a single colony was inoculated into 10 ml of LB broth and grown for 12-16 hours. 5 ml of the culture was then inoculated into 500 ml LB and the culture was incubated at 37°C till it attained an OD (A_{600}) of 0.5. The cells were then harvested at 4°C and resuspended in ice cold TfbI buffer (30 mM potassium acetate, 50 mM MnCl₂, 100

mM KCl, 10 mM CaCl₂, 15% glycerol; final pH was adjusted to 5.8 using acetic acid). The suspension was incubated on ice for 30 minutes and the cells were harvested again. The cell pellet was resuspended again in 20 ml TfbII buffer (10 mM Na-MOPS (pH-7), 75 mM CaCl₂, 10 mM KCl, 15% glycerol) and distributed into aliquots of 100 µl and frozen at -80 °C until use.

For transformations, 100 µl aliquots of cells were thawed on ice and 50 ng of DNA was added to the cells and kept on ice for 20-30 minutes and then heat shock was given by incubating the cells at 42 °C for 1 minute. The cells were immediately transferred to ice and incubated in ice for 5 minutes for recovery. Then 900 µl of LB was added and incubated for 1 hour at 37 °C with mild shaking. Cells were then plated on LB agar with ampicillin (100 µg/ml) and chloramphenicol (25 µg/ml) as selection markers and incubated at 37 °C overnight.

c) Plasmid isolation and Restriction digestion:

Plasmid DNA was isolated from minicultures (3-4 ml) by alkaline lysis method as described by Sambrook *et al.*, (2000). Plasmid DNA used for sequencing was isolated from minicultures using spin column purification as per manufacturer's instructions (Qiagen mini-prep kit). Restriction digestions were also performed as described in (Sambrook and Rusel 2000). The restriction enzymes were purchased from Fermentas (Canada).

d) RNA isolation and RT-PCR:

Total RNA was isolated from 100 mg of frozen rat brain tissue by using TRIzol reagent (Invitrogen, USA) according to the manufacturer's instructions. About 3 µg of RNA was treated with 25 U of DNase I (Fermentas, Canada) in a 20 µl reaction containing 10 mM Tris-Cl (pH-7.5), 2.5 mM MgCl₂, and 100 µM CaCl₂, at 37 °C for 30 minutes. The reaction was stopped by the addition of 2.5 mM EDTA and incubating the reaction at 65 °C for 10 minutes.

About 1µg of Dnase I treated RNA was used for cDNA synthesis. The total volume of the reaction mixture was 50 µl containing 50 mM Tris-Cl (pH-8.3), 50 mM

KCl, 5 mM MgCl₂, 10 mM DTT, 1 mM dNTP mix (Cinnagen, Iran), 4 U RNase inhibitor (Ribolock RNase inhibitor, Fermentas, Canada), 40 U MuLV reverse transcriptase (Applied Biosystems, USA). The cDNA synthesis was primed by using 2 pmoles of oligo dT (Sigma-Aldrich). The reaction mixture was incubated at 48 °C for 45 minutes, followed by heat inactivation of the enzyme at 94 °C for 5 minutes. The cDNA was aliquoted and stored at -20 °C until use.

e) Primer Design:

The primers were designed to specifically recognize *VDAC1* and *VDAC2* genes using available on-line computer software (<http://frodo.wi.mit.edu/~primer3/>) and published sequences in NCBI GenBank database. The sequences of primers used in the present work are given in the Table 2.1. The 5' end of the forward and reverse primers was added with restriction sites for *Bam*HI and *Xho*I restriction enzymes respectively. Further, the forward primer has Factor XA protease cleavage site for removing His-tag from the protein.

Table-2.1: Primer sequences

| Protein | Primers |
|---------|--|
| rVDAC1 | F:5'-ACATGGGATCCATCGAAGGGCGCATGGCTGTGCCTCCCACATATGCTG-3' R: 5'- GTCGACCTCGAGTTATGCTTGAAATTCAG-3' |
| rVDAC2 | F:5'-ACATGGGATCCATCGAAGGGCGCATGGCTGAATGTTGTGTACCGGTAT-3' R: 5'- GTCGACCTCGAGTTAAGCCTCCAATCCAA -3' |

f) Polymerase chain reaction:

The subsequent amplification of second strand of rVDAC1 and rVDAC2 cDNA was performed by PCR, using Phusion HF DNA Polymerase (Finnzymes, Finland). The PCR was performed in a 50 µl reaction for each of the two isoforms separately. The reaction mixture contained 1X Phusion HF buffer (containing 1.5 mM MgCl₂; other components unknown), 200 µM dNTP mix, 2 pmoles each of the forward and reverse primers (Eurofins genomics, India), 0.5U Phusion High Fidelity

DNA polymerase (Finnzymes, Finland) and milliQ water was finally added to adjust the final reaction volume to 50 μ l.

The PCR conditions were set as 30 cycles of cDNA denaturation at 98°C for 10 sec (after initial denaturation of 98°C for 3 min), 59°C (AT) for 30 sec and primer extension at 68°C for 45 sec with a final extension step of 68°C for 9 minutes. The AT for the primers specific to both *VDAC1* and *VDAC2* was maintained same. The PCR products were checked on 1% agarose gel and the molecular size of the amplified products was estimated using a 1 KB DNA ladder (Fermentas, Canada) run along with the PCR products. The amplicons corresponding to molecular size of *VDAC1* and *VDAC2* were sliced and then eluted from the gel using QIAquick PCR purification kit (Qiagen) following the manufacturer's instructions.

g) Cloning of *rVDAC1* and *rVDAC2*:

The gel eluted products were then cloned into the *Bam*HI and *Xho*I sites of pASK-IBA43plus (IBA BioTAGnologies, Germany) to create the plasmid pASK-V1 and pASK-V2. The pASK-V1 and pASK-V2 were then transformed into BL21 CodonPlus cells as described above. The specificity of the cloned products was further confirmed by DNA sequencing using rVDAC specific primers.

h) Overexpression of *rVDAC1* and *rVDAC2* in *E. coli*:

The BL21 CodonPlus cells harboring pASK-V1 and pASK-V2 were grown at 37°C till an OD₆₀₀ of 0.5 and then protein expression was induced by treating the cultures with 200 ng/ml of anhydrotetracycline (IBA BioTAGnologies, Germany). The cultures were incubated for another 3 hours. After the incubation, cells were harvested by centrifugation and analyzed for protein overexpression.

i) Purification and refolding of His- *rVDAC1* and His-*rVDAC2* isoforms:

The purification and refolding of his tagged rVDAC1 and rVDAC2 isoforms was carried out following the one step on-column affinity refolding purification procedure described by Shi *et al.*, (Shi, *et al.* 2003). Briefly, harvested cells were resuspended in 1:50 (v/v) of buffer A (20 mM Tris-Cl (pH-7.9), 200 mM NaCl), lysed

on ice by sonication, and the lysate clarified by centrifugation at 10,000g. The inclusion bodies in the pellet were solubilized in buffer B (1:20 v/v 20 mM Tris-Cl, pH-7.9, 500 mM NaCl, 4M Guanidium-HCl and 10% glycerol) for 30 minutes with gentle stirring. The supernatant was collected after centrifugation at 18,000g for 20 minutes.

The supernatant containing 1 mg of total solubilized protein was loaded on to the 0.5 ml of Ni-NTA superflow beads (Qiagen, Germany) pre-equilibrated with buffer B. The column was extensively washed with 5 column volumes of buffer B and then a 3-step wash was performed with 3 volumes buffer B mixed with buffer C (2% LDAO, 20 mM Tris-Cl, pH-7.9, 500 mM NaCl and 10% glycerol) and 10 mM imidazole (B:C=1:3, 1:7 and 1:15 respectively). To ensure complete refolding of the protein, the column was further washed with additional 10 volumes of buffer C with 10 mM imidazole. Finally, the His-tagged rVDAC1 and rVDAC2 proteins were eluted with 4 bed volumes of buffer c supplemented with 100 mM imidazole. All the above steps were performed at 4 °C.

Further, the obtained refolded protein was applied to Sephadex G-15 column and eluted either with buffer containing 10 mM Tris-Cl (pH 7.4), 0.1% LDAO or 20 mM MOPS-EDTA (pH-7.4), 0.1% triton X 100 to obtain homogeneous population of protein.

3.2.4. Trypsin digestion:

Coomassie Blue-stained protein bands were excised from the corresponding SDS-polyacrylamide gels and destained with 50% acetonitrile in 50 mM ammonium bicarbonate for 1 hour with three intermittent changes of the solution. The supernatants were replaced with 10mM DTT (Sigma) in 50 mM ammonium bicarbonate solution to reduce the proteins for 15 min at 56 °C. The supernatant was discarded and 20 mM Iodoacetamide (Sigma) in 50 mM ammonium bicarbonate was added and incubated in dark for 15 min at RT to alkylate the proteins. The gel pieces were collected, washed three times with 200 µl of 50 mM ammonium bicarbonate for 15 min at RT and then dried *in vacuo*. The gel pieces were rehydrated with 3.0 µl of

12.5 ng/ μ l of sequencing grade modified trypsin gold (Promega) in 50 mM ammonium bicarbonate, 10% acetonitrile and incubated for 60 min at RT. Further, 50 μ l of 10% acetonitrile in 50 mM ammonium bicarbonate was added and the digestion of proteins was continued for 18 h at 37 $^{\circ}$ C with agitation. The supernatant was collected and the gel pieces were extracted for 40 min at 37 $^{\circ}$ C with successive 50 μ l aliquots of 0.1% trifluoroacetic acid and 50% acetonitrile. The combined extracts were concentrated using Speed Vac.

3.2.5. LC MALDI separation of peptides:

This was performed in the Central Instrumentation Facility in the University of Delhi South Campus. Briefly, the peptide extract was reconstituted in the 40 μ l of 98% Water, 2% Acetonitrile and 0.1% TFA. The aliquot of 12 μ l of digested peptide was separated on Chromolith CapRod Monolithic capillary column (150 mm \times 0.1 mm RP-18 endcapped). Simultaneously, the eluted peptides were spotted on the LC MALDI plate at intervals of 7 sec after mixing of α -cyano-4-hydroxycinnamic acid matrix in ratio of 1:1. The LC MALDI plate was analyzed on AB Sciex 4800 Plus TOF/TOF analyzer in reflector ion mode. To identify the peptide and its phosphorylation, peptide masses obtained from the mass spectrometric analysis were searched using the Protein Pilot 2.0 software in the MSDB database. In the Protein Pilot search, phosphorylation emphasis was incorporated as special search factor along with the gel based ID. Detected protein threshold was fixed at a confidence score of 99.9%. For the identification of phosphorylation of peptides in rVDAC2, ABI Q-TRAP MS/MS analyzer in neutral loss scanning mode was used. The obtained peptide masses were searched using Mascot search engine.

The LC gradient for the separation of the peptide was made from two solvent system solvent A (98% Water, 2% Acetonitrile and 0.1% Trifluoroacetic acid) and Solvent B (98% Acetonitrile, 2% Water and 0.1% Trifluoroacetic acid). Trypsin digested peptides were desalted with solvent A for 30 min on Cap-trap C18 column with the flow rate of 20 μ l in the reverse direction. After desalting, the peptides were eluted from the column with 60min gradient of solvent A and B in the following steps: 5-10% B in 7 min, 10-35% B in 18min, 35-50% B in 10 min, 50-90% B in 2

min and then the column was washed for 5 min at the same gradient. Finally, the column was equilibrated with the solvent A for 15 min. Most of the peptides were extracted between the 10 min to 30 min. All the peptides were spotted after every 7 sec on LC MALDI plate with CHCA. The flow rate of the solvent was 2.2 $\mu\text{l}/\text{min}$.

3.2.6. Gaussian Network Modeling (GNM):

The motions of the proteins in solution are seemingly quite complex and involve transition among a continuum of infinite number of conformational sub-states (e.g. conformational transitions between open and closed states). But the proteins in their native condition (either open or closed state in case of ion channels) are much simpler, as they are limited to a subset of conformations. These fluctuations can be studied to understand the molecular mechanisms of their functions. Another interesting feature of protein dynamics is that these fluctuations involve correlated motions of large number of atoms, residues or even entire domains which underlie the biological function. GNM was proposed by Bahar *et al.*, (1997) to explore the collective dynamics of the proteins based on the topological constraints in the 3D structure of the protein. GNM describes the 3D structure of the protein as an elastic network of contacts between all α -carbons (both bonded and non-bonded) connected by harmonic springs within a cut-off distance r (Bahar, *et al.* 1997). Then, the internal Hamiltonian of the network can be written as:

$$V = \frac{1}{2} \gamma [\Delta R^T (\Gamma \otimes E) \Delta R], \quad 3.1$$

where, γ is the force constant, E is the third order identity matrix; ΔR represents X, Y and Z components of the fluctuation vectors considered for all $\Delta R_1, \Delta R_2, \dots, \Delta R_N$, where N is the number of residues; Superscript T represent transposition and \otimes is the direct product.

Γ is Kirchhoff matrix, an N X N symmetric matrix encoded with information about contact topology. The ij^{th} off-diagonal element of the Kirchhoff matrix is assigned with a value of -1 or 0 based on presence or absence of contacts between the i and j α -carbons respectively. The value of the i^{th} diagonal element is evaluated as the

negative sum of all the elements of the i^{th} row (or column). This value gives the coordination number of specific site i .

Modal decomposition of Γ by eigenvalue transformation yields in a total of $n-1$ modes of motion. The eigenvalues (λ_i) represent the frequencies of the modes and the eigenvectors (u_i) define the shapes of the modes.

The correlation $[\Delta R_i \cdot \Delta R_j]_k$ contributed by the k^{th} mode was found from the equation

$$[\Delta R_i \cdot \Delta R_j]_k = \left(3kT/\gamma\right)[\lambda_k^{-1} \mathbf{u}_k \mathbf{u}_k^T]_{ij} \quad 3.2$$

where, u_k is the k^{th} eigenvector of Γ , λ_k is the k^{th} eigenvalue and T is the absolute temperature. The low frequency modes called the slow modes, are important for the biological functions of the molecule and the fast modes are high frequency modes involved in structural stability of the protein. The first twenty slowest modes and twenty fastest modes were further considered for further analysis. oGNM server (http://ignm.cccb.pitt.edu/GNM_Online_Calculation.htm) was used for the computation of the collective modes of motion of the amino acid residues in the three dimensional structure of VDAC1 (PDB ID. 3EMN). A cut-off of 8 Å was used for the computation of Kirchhoff's matrix.

3.3. Results and Discussion:

3.3.1. Purification of rat brain mitochondrial VDAC:

VDAC was purified from rat brain mitochondria as described in section 2.2.1.

3.3.2. In vitro kinase assay:

When purified rat brain mitochondrial VDAC was incubated with recombinant active JNK3 and γ - ^{32}P - labeled ATP, it showed the incorporation of labeled phosphate indicating the phosphorylation of the VDAC (fig. 3.1, Lane A). The negative control without JNK3 did not show any incorporation of γ - ^{32}P - labeled ATP (Fig. 3.1, Lane B). Two major higher molecular weight bands are visible in the autoradiogram (Fig. 3.1, Lane A) based on their molecular weight were thought to be the higher oligomers of the monomeric VDAC. The observation of phosphorylation of VDAC raised some

important questions whether all the three isoforms are phosphorylated by JNK or not? Assuming that all the VDAC isoforms are phosphorylated by JNK, the next important question asked was whether all the three isoforms are phosphorylated at the same positions or not? In order to address these concerns, VDAC isoforms were overexpressed in *E. coli* and the refolded *in vitro*, purified rVDAC1 and rVDAC2 isoforms were used for further studies. As there were no reports available demonstrating the association of VDAC3 with apoptosis, the rest of the work was focused only on VDAC1 and VDAC2 isoforms.

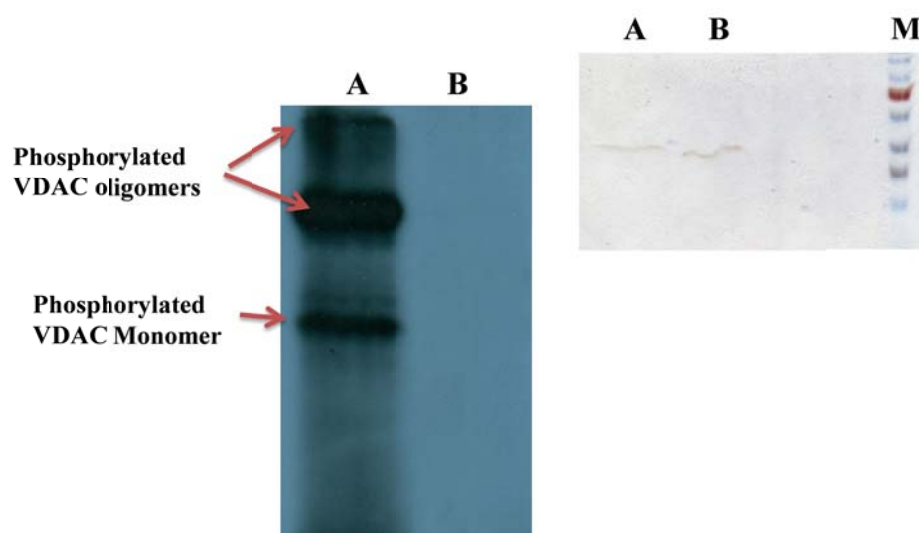


Fig. 3.1: Autoradiogram showing phosphorylated VDAC. Lane A: Purified VDAC+ Recombinant active JNK3 + [γ - 32 P] ATP mix and Lane B: Purified VDAC+ [γ - 32 P] ATP mix. The inset shows the silver stained gel exposed to the X-ray film.

3.3.3. Cloning of rat brain VDAC1 and VDAC2 into pASK for overexpression in E.coli:

The cDNA of rat brain mitochondrial genes was prepared by RT-PCR using oligo-dT primers from the total rat brain mRNA. The amplification of *VDAC1* and *VDAC2* cDNA was achieved by PCR reaction of total cDNA using specific primers (Table-3.1). Fig. 3.2 shows the specific amplification of *VDAC1* and *VDAC2*. The molecular sizes of *VDAC1* and *VDAC2* are 885 bp and 920 bp, respectively. The *VDAC1* and *VDAC2* bands were cut and eluted from the agarose gels and cloned into

*Bam*HI - *Xho*I sites of pASK-IBA43 expression vector (as described in section 3.2.3.). The pASK-V1 and pASK-V2 cloned plasmids were transformed into BL21 CodonPlus and screening for clones was done by isolation of the plasmid DNA from minicultures, followed by restriction digestion analysis. Digestion of plasmid DNA with *Bam*HI and *Xho*I released the expected 885 and 920 bp bands (Fig. 3.3). The sequences were further confirmed by DNA sequencing.

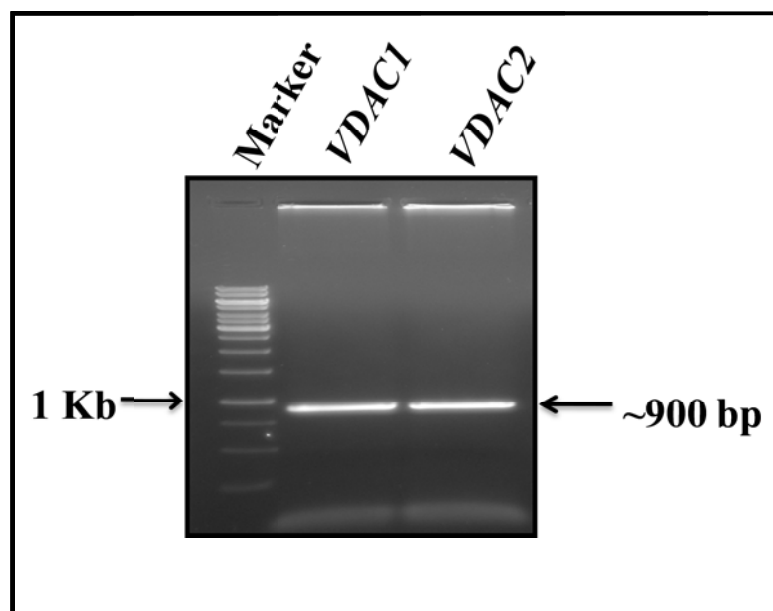


Fig. 3.2: Amplification of *VDAC1* and *VDAC2* cDNA

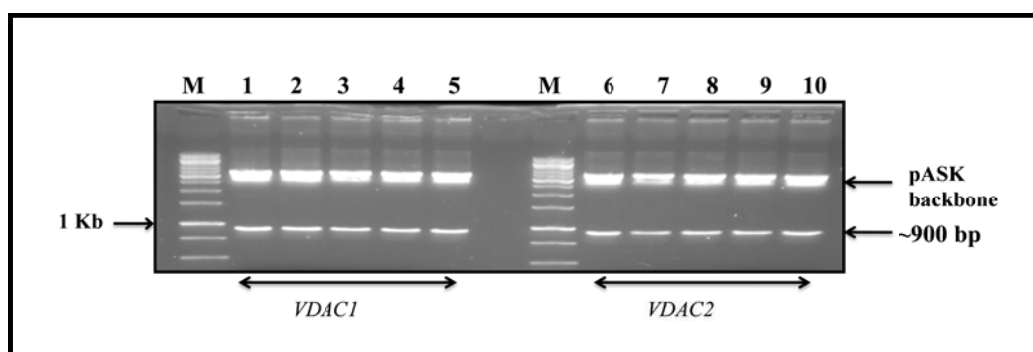


Fig. 3.3: Clone confirmation of *VDAC1* and *VDAC2* by double digestion using *Bam*HI and *Xho*I restriction enzymes. Lanes 1-5 correspond to *VDAC1* and lanes 6-10 correspond to *VDAC2*.

3.3.4. Overexpression, refolding and purification of rVDAC1 and rVDAC2 isoforms:

The rVDAC1 and rVDAC2 isoforms were over expressed in BL21 CodonPlus cells (as described in section 3.2.3). The cells were harvested and assessed for overexpression of rVDAC1 and rVDAC2 isoforms. The SDS-PAGE showed that both the isoforms were expressed in the pellet forming inclusion bodies (Fig. 3.4).

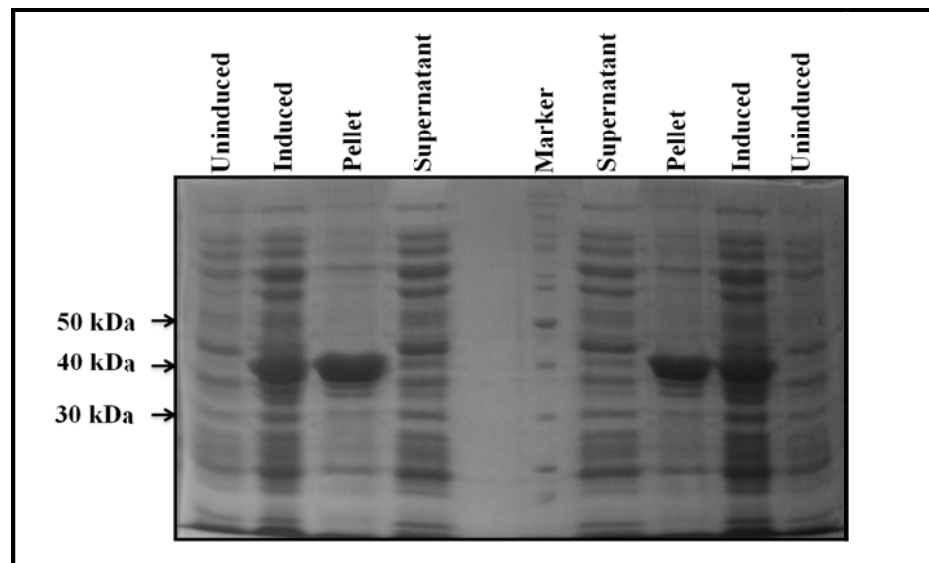


Fig. 3.4: Coomassie stained SDS-PAGE (10%) showing the over-expression of rVDAC1 (left half) and rVDAC2 (right half).

The rVDAC1 and rVDAC2 were refolded and purified from the inclusion bodies according to the method of Shi *et al.*, (2003) as described in section 3.2.3. The eluted fractions were analyzed by SDS-PAGE and the bands were visualized by coomassie staining. A single band was observed in 2nd, 3rd and 4th eluted fractions in case of both rVDAC1 and rVDAC2 isoforms (Fig. 3.5a & b). The molecular weight of the recombinant proteins was observed to be ~40 KDa. Similar observation was reported in case of overexpression of *Paralichthys olivaceus* VDAC (Lu, *et al.* 2007). The identity of the expressed protein was further confirmed by mass spectrometry.

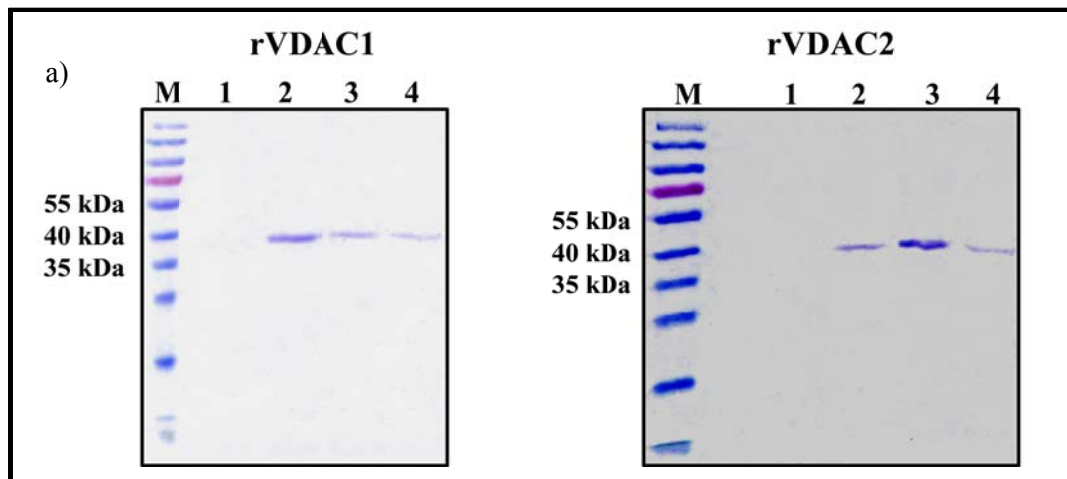


Fig. 3.5: Affinity purification of recombinant VDAC isoforms. rVDAC isoforms were eluted in 2nd, 3rd and 4th fractions. a) rVDAC1 and b) rVDAC2.

3.3.5. Differential Phosphorylation of VDAC isoforms:

The rVDAC1 and rVDAC2 isoforms were incubated with recombinant active JNK3 and unlabeled ATP in separate reactions *in vitro* (as described in section 3.2.2). The reaction mixture was run on SDS-PAGE and the bands were visualized by coomassie staining protocol. The rVDAC1 and rVDAC2 bands were processed for trypsin digestion and LC-MALDI (as described in section 3.2.4 and section 3.2.5).

Both VDAC1 and VDAC2 isoforms were found to be differentially phosphorylated by JNK3. VDAC1 was found to be phosphorylated at three different sites Thr-19, Thr-116 and Ser-260 whereas, VDAC2 was found to be phosphorylated at a single site Ser-179. Fig. 3.6 and Fig. 3.7 show the MS/MS spectra showing y/b-ion series of the peptides carrying phosphorylation at the above-mentioned residues respectively. While the peptides from native rVDAC1 and rVDAC2 were found to be negative to neutral loss scanning.

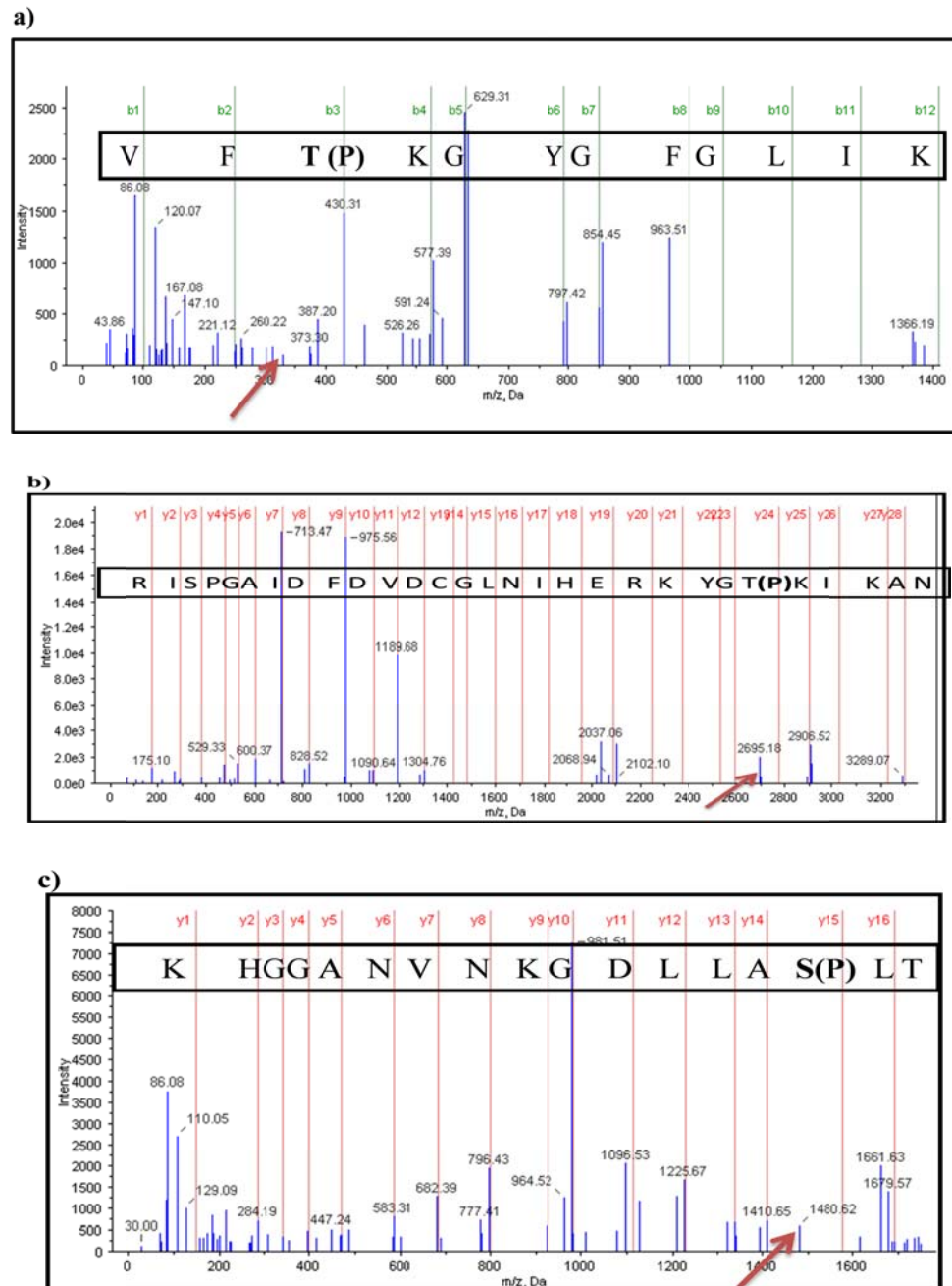


Fig. 3.6: y/b-ion series of phosphopeptides of rVDAC1 and the positions are marked by an arrow. a) Thr-19, b) Thr-116 and c) Ser-260 residues.

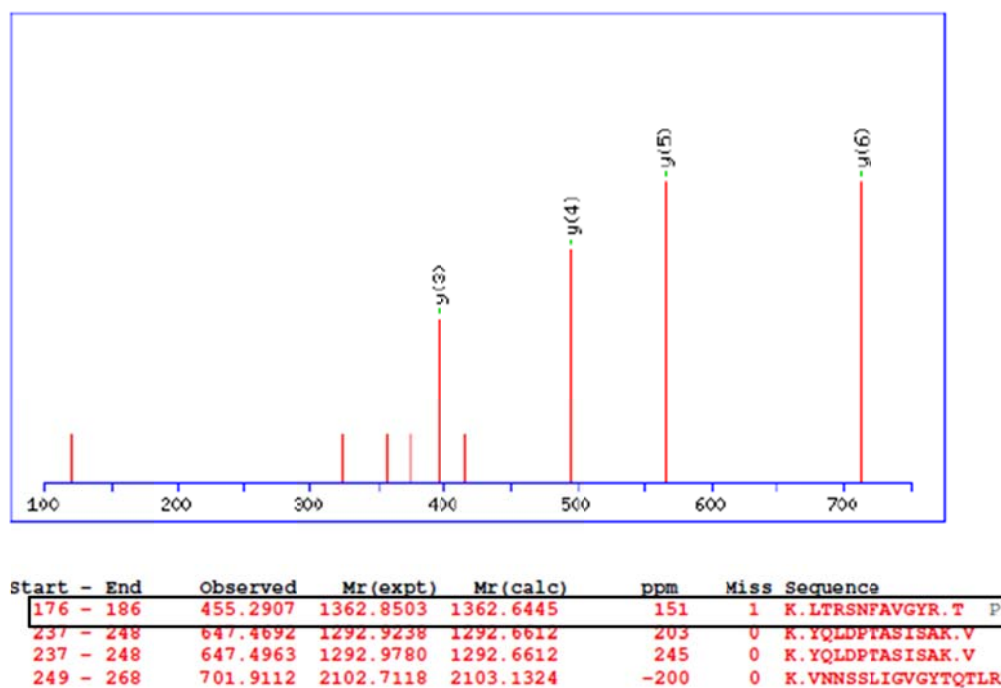


Fig. 3.7: y-ion series of phosphorylated peptide of rVDAC2 obtained by neutral loss scanning in ABI Q-TRAP MS/MS instrument. The sequence of the peptide shows Ser-179 phosphorylation is highlighted in the list.

3.3.6. Sequence analysis of VDAC1 and VDAC2:

The protein sequences of *Rattus norvegicus* VDAC1 (NCBI Accession No. NP_112643) and VDAC2 (NCBI Accession No. NP_112644) were aligned with the respective sequences from other chordates available in the NCBI database. The aligned sequences have >97% sequence homology in case of both VDAC1 and VDAC2. The identified phosphorylation sites of VDAC1 were found to be present in almost all the aligned chordate VDAC sequences. But in case of VDAC2, the identified phosphorylation site Ser-179 was found to be highly variable. Fig. 3.8 shows the identical and similar portions of the aligned sequences of VDAC1 (Fig. 3.8a) and VDAC2 (Fig. 3.8b). Further, the evolutionary conservation scores of the individual amino acid residues in VDAC1 and VDAC2 were calculated by using Conseq server (http://conseq.tau.ac.il/index_old_ver.html). The colour-coded conservation scores of VDAC1 and VDAC2 amino acid residues were given in Fig. 3.9. The evolutionary conservation scores suggest that both Thr-19 and Thr-116

b)

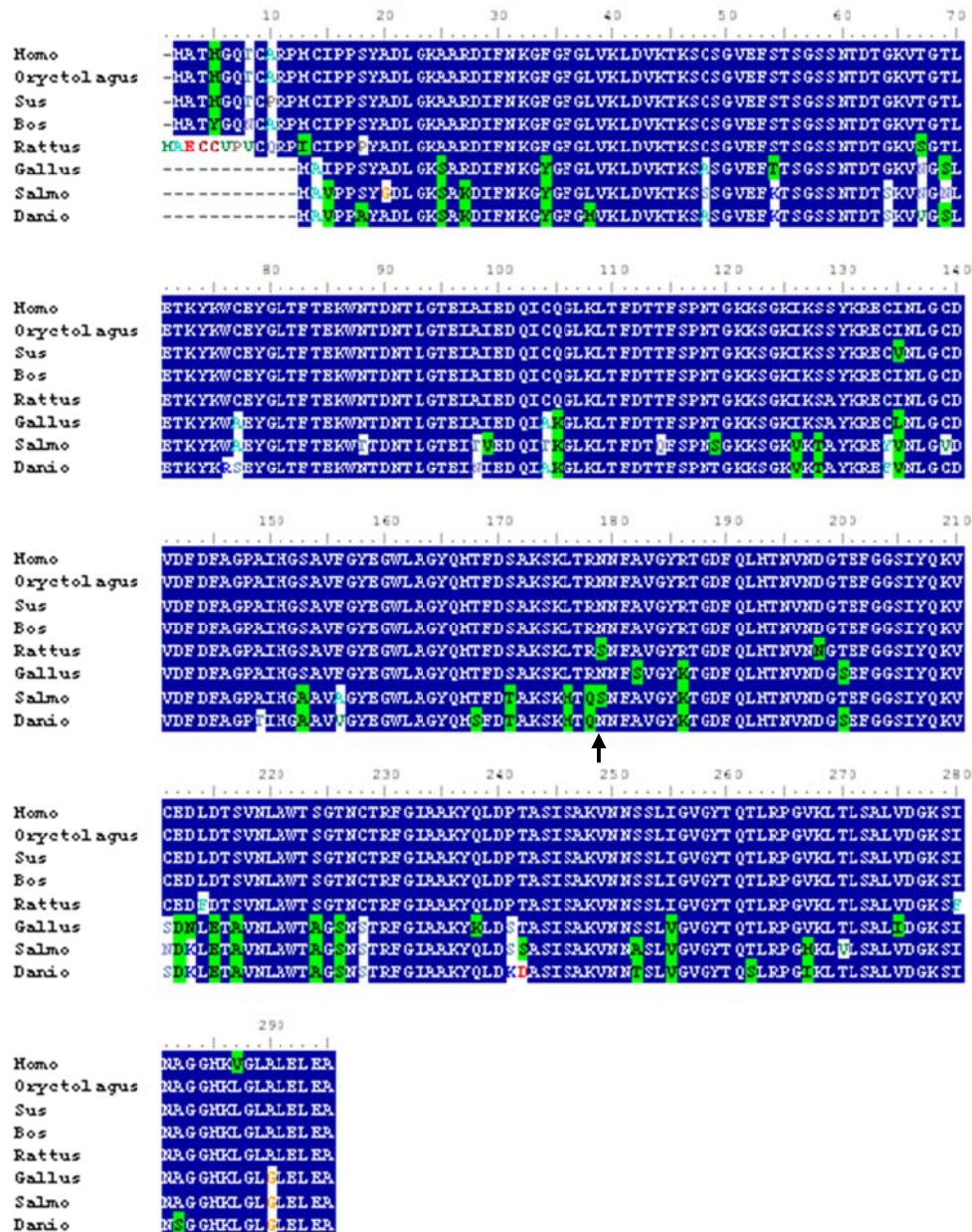


Fig. 3.8: Multiple sequence alignment of a) VDAC1 and b) VDAC2 sequences of selected chordates (NCBI database) using ClustalW. The blue background colour indicates identity of the amino acid residues; green background colour indicates similarity and the white background colour indicate dissimilarity. The identified phosphorylated residues are indicated by arrow head.

a)



b)

**Legend:**

The conservation scale:



- Insufficient data - the calculation for this site was performed on less than 10% of the sequences.

Fig. 3.9: Colour coded evolutionary conservation scores of (a) VDAC1 and (b) VDAC2 amino acid residues. The identified phosphorylated residues are marked by an arrow head.

3.3.7. Gaussian Network Modeling (GNM) of VDAC1:

The three dimensional structure of the protein provides the topological arrangement of the amino acid residues in the native folded conditions. The stability of the native structure is ensured by a network of hydrogen bonds and inter-residue attractive forces. These effects increase the packing density and lead to the fluctuations of the residues in the folded state. GNM has been successfully employed to identify the key residues important for the structural stability and various biological functions, by modal decomposition of the residue fluctuations in a three dimensional structure of the protein (Rader, *et al.* 2006).

The crystal structure of mouse VDAC1 has been resolved by Ujwal *et al.*, (2008). As the mouse and rat VDAC1 protein sequences are identical, the coordinates of the murine VDAC1 (PDB ID: 3EMN) were used for GNM. In order to envisage the importance of the Thr-19, Thr-116 and Ser-260 amino acid residues in the native VDAC1, fast and slow collective modes were computed (as described in section 3.2.6).

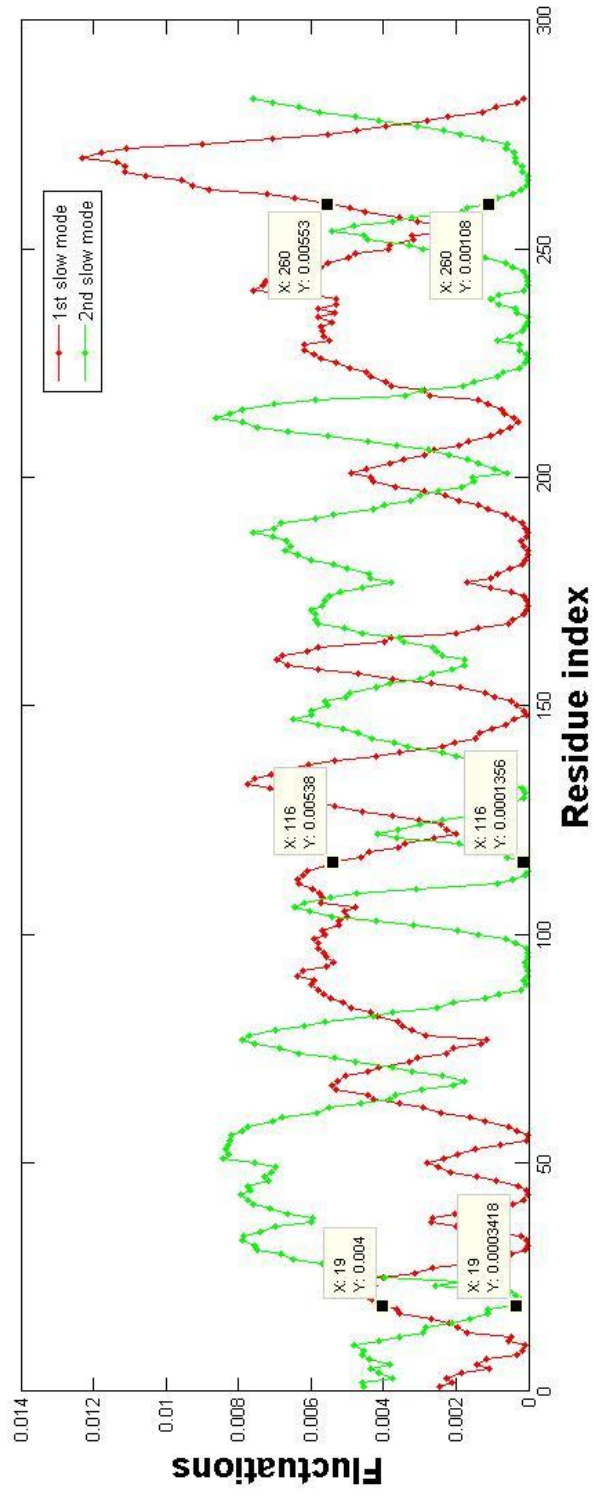


Fig. 3.10: First and second principal slow modes calculated for three dimensional structure of murine VDAC1. The data tips show the intensity of the fluctuations of Thr-19, Thr-116 and Ser-260 residues in the first and second principal slow modes.

Fig. 3.10 shows the first and second slowest modes of motion. These slow modes involve motion of the entire molecule as indicated by broad and delocalized peaks in the plot (Fig. 3.10). The immobilized residues (residues at the minima) in the slowest mode correspond to the amino acid residues forming the hinge bending regions. The amino acid residues occupying the minima positions in the two modes are exactly opposed. This is caused due to symmetric nature of the molecule. The eigen value of the first two modes are very close to each other further supporting the symmetric nature. Therefore, the average of the first two modes was considered. Fig. 3.11 shows the mean fluctuations of the first two slowest modes. Although the three amino acid residues, Thr-19, Thr-116 and Ser-260 have minimum fluctuations, they could not be considered as the hinge regions as their motion is not completely constrained. Based on the above results, the role of the above-mentioned residues in biological functions could not be predicted based on the slow mode fluctuations.

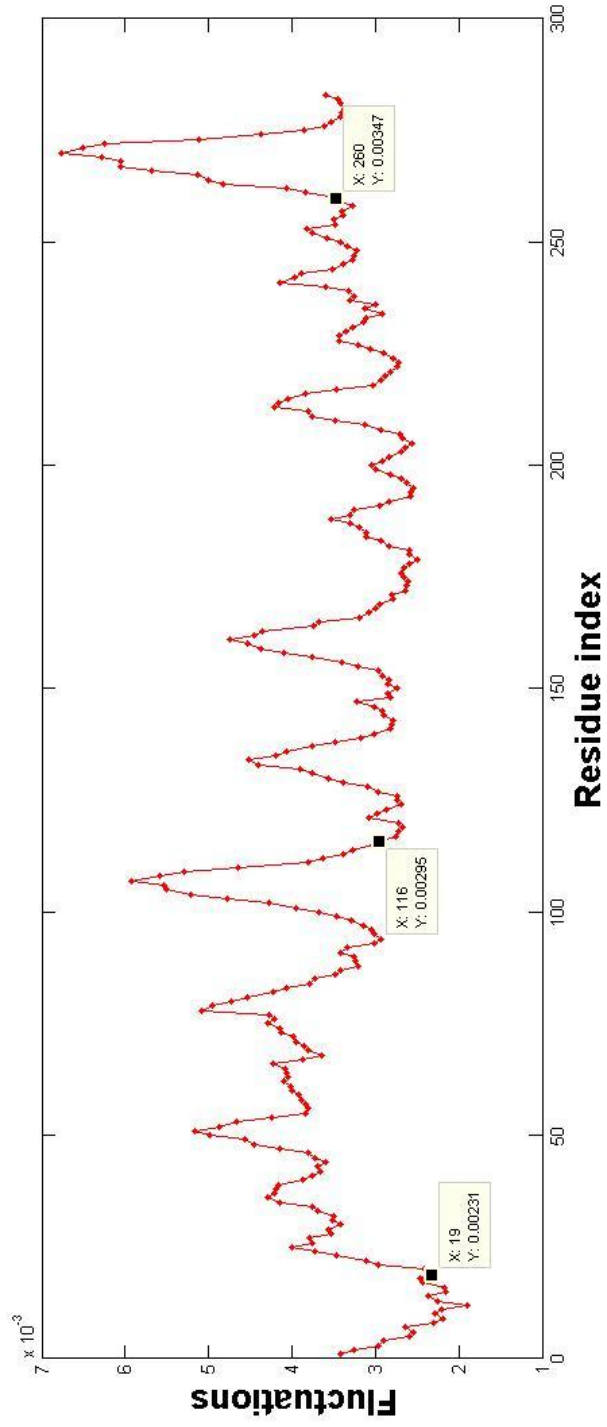


Fig. 3.11: Plot showing the average of first two slowest modes. The data tips show the intensity of the fluctuations of Thr-19, Thr-116 and Ser-260 residues.

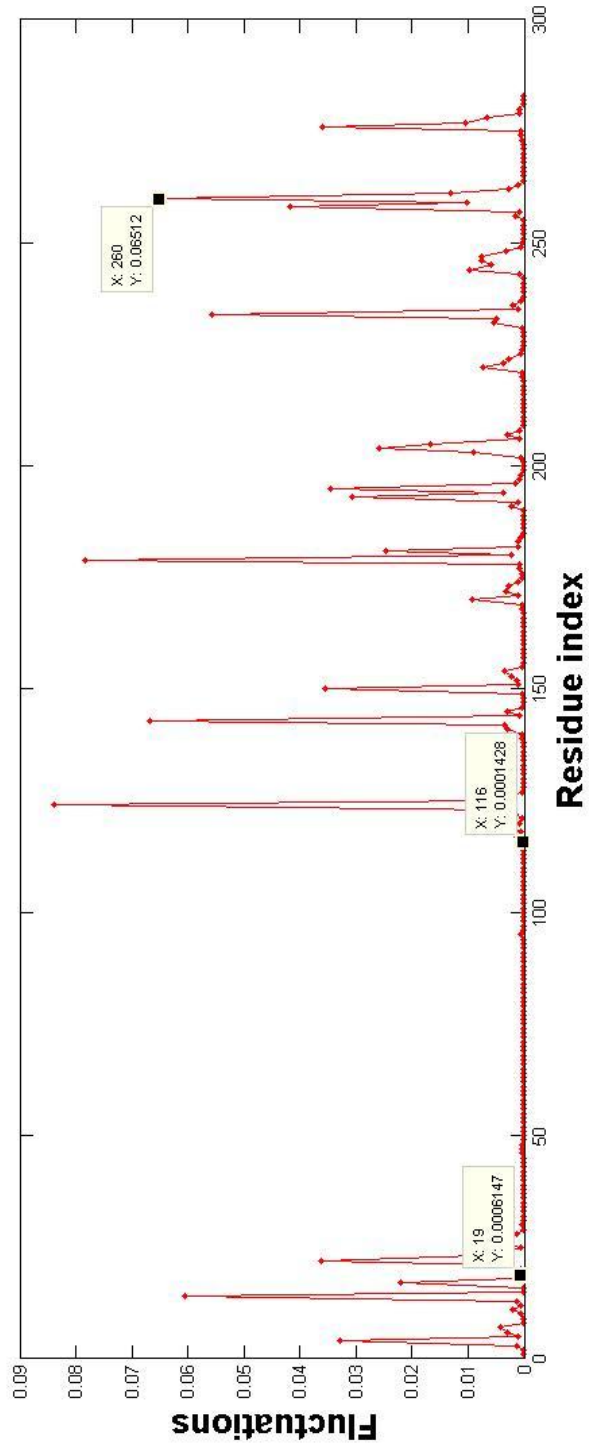


Fig. 3.12: Plot showing average of the first ten fastest modes. The data tips show the intensity of the fluctuations of Thr-19, Thr-116 and Ser-260 residues.

Fig. 3.12 shows the mean fluctuations of the fastest ten modes. Unlike the slow mode fluctuations, the fast modes are highly localized and involve only a few peaks, as in Fig. 3.12. The peaks here refer to the amino acid residues that have a high concentration of local energy and highly constrained in motion. Ser-260 residue, but not the other two residues, forms such a peak. This indicates that the Ser-260 residue is very much important for the folding and structural stability of the VDAC1. Any modification at this site, phosphorylation in our case, may result in structural abnormalities of VDAC1. In specific, phosphorylation induced modulation of expression levels of VDAC1 has been demonstrated to be associated with endostatin-mediated apoptosis (Yuan *et al.*, 2008). Therefore, we anticipate that phosphorylation of Ser-260 residue before the incorporation of VDAC1 into the mitochondrial membrane, might affect its insertion. Due to lack of structural data for VDAC2 isoform, the role of Ser-179 position in VDAC2 could not be predicted. However, the results presented here require further study.

Dynamics of VDAC multichannels: computational analyses

4.1. Review of Literature:

While it is established that the functional unit of VDAC is a monomer, a substantial body of evidence supports its tendency to form oligomers both *in vivo* and *in vitro*. Spatial organization of VDAC was initially observed even before its functional characterization. Arrays of stain filled pores were detected in the electron micrographs of negatively stained plant outer mitochondrial membranes and were later identified as VDAC (Parsons 1965). Similar kind of oligomeric pattern was observed by electron microscopy of two dimensional VDAC crystals either spontaneously formed in the OMM (Mannella 1982) or formed by lipid withdrawal from OMM (Mannella 1998). Self-association of VDAC is not limited to native membranes and it was also observed in the crystals of human VDAC reconstituted in artificial bilayers (Dolder, *et al.* 1999).

Recent high resolution atomic force microscopic imaging of native OMM unveiled non homogeneous distributions of VDAC with hexagonally packed high density regions and low density regions with self-assemblies having one to twenty molecules of VDAC. These results were first observed in yeast mitochondria (Goncalves, *et al.* 2007) and later confirmed in potato tuber mitochondria (Hoogenboom, *et al.* 2007). The low density regions displayed association and dissociation of VDAC molecules and were found to be in dynamic equilibrium (Goncalves, *et al.* 2007). This association-dissociation equilibrium resulting in variations in surface density of VDAC molecules has been suggested to be important for the modulation of channel function (Hoogenboom, *et al.* 2007). Although, the above evidences suggest the ability of VDAC to spontaneously self-organize into oligomers, the functional significance of such spatial organization remains unclear.

Organized VDAC clusters have been proposed to act as anchor points for the interaction of various cytosolic and mitochondrial proteins including kinases, cytochrome c, motor proteins and various pro/anti apoptotic proteins (Adams, *et al.* 1991, Banerjee and Ghosh 2004, Brdiczka 1990, Brdiczka, *et al.* 1994, Cheng, *et al.* 2003, Roman, *et al.* 2006a, Schlattner, *et al.* 2001, Shimizu, *et al.* 1999). In fact, it has been reported that the relative levels of VDAC isoforms in the arrays are responsible

for the tissue specific regulation of hexokinase binding to OMM (Blachly-Dyson, *et al.* 1993, Poleti, *et al.*), which has been shown to play a key role in regulating the apoptosis in cancer cells (Mathupala, *et al.* 2006) and also more than 50 putative interacting partners of VDAC have been identified (Roman, *et al.* 2006b) suggesting a more complex regulation of VDAC.

Recent evidences suggest that oligomerization of VDAC is associated with the release of cytochrome c into the cytosol during mitochondria-mediated apoptosis (Abu-Hamad, *et al.* 2009, Keinan, *et al.* 2010, Shoshan-Barmatz, *et al.* 2010b) These reports support an earlier model that proposed the formation of central mega channel delimited by tetrameric VDAC as responsible for the regulation of release of apoptogenic molecules from mitochondrial IMS to cytosol (Zalk, *et al.* 2005). It has to be noted here that the results of Zalk *et al.*, 2005, Abu-Hamad *et al.*, 2009 and Kienan *et al.*, 2010 demonstrated association of apoptosis induction with oligomerization of VDAC alone but not the formation of central megachannel. Moreover, none of these reports could explain the spatial organization of VDAC observed in the native OMMs.

The gating kinetics of VDAC either recorded from reconstituted channel ensembles or from membrane patches were found to be different from that of reincorporated single channel kinetics (Moran, *et al.* 1992, Tedeschi, *et al.* 1987). This difference in behaviour was proposed to be due to protein-protein interactions either between the closely apposed VDAC molecules or between VDAC and other membrane bound enzymes like creatine kinase (Saks, *et al.* 1993). Also, two kinds of channel activity have been reported for the VDAC2 isoform expressed in yeast (Xu, *et al.* 1999). These reports suggest that modulation of channel activity could be a likely explanation for the observed supramolecular complexes of VDAC. In fact, this kind of clustering mediated tuning of the channel activity has been demonstrated for different ion channels from various sources (Baddeley, *et al.* 2009, Grage, *et al.*, Marx, *et al.* 1998, Molina, *et al.* 2006) and is observed to confer enhanced signaling capabilities to the clusters. Therefore, it is important to understand the nature of interactions among the channel molecules in the clusters.

There are many models and methods proposed for investigating the collective behaviour of channels (Keleshian, *et al.* 2000, Kenyon and Bauer 2000, Yeramian, *et al.* 1986). Most of these methods are based on estimations of steady-state distribution of mean channel life time (dwell time distribution) and conductance of the channels in comparison with that of behaviour of single reincorporated channel *in vitro*. But neither of the parameters gives a clear idea about the nature of interactions between the channels in an ensemble (Kenyon and Bauer 2000, Yeramian, *et al.* 1986). Further, existence of multiple subconductance states adds another layer of complexity to these kinds of analysis. Complexities in multichannels have been discussed earlier by different groups invoking fractals (Astashev, *et al.* 2007, Lowen, *et al.* 1999). The complex nature of channel-channel interactions may thus be studied using fractals as it provides a promising tool to investigate self-similar structures as observed in complex systems.

The notion of 'Fractals' was introduced by Mandelbrot (Mandelbrot 1977, Mandelbrot 1982) which enables quantification of self-similar structures in a complex system from observed statistical scaling at various spatial/temporal scales (Bassingthwaighte 1994, Lopes and Betrouni 2009). The fractal behaviour is mainly characterized by the power laws e.g., $N=S^D$, where N is the number of small pieces that go into the larger one and S is the scale to which the small pieces compare to the larger one and D is the dimension. Various physiological processes including heart beat (Ivanov, *et al.* 2001), human gait (Hausdorff, *et al.* 1996), brain dynamics (Wink, *et al.* 2008) have been shown to follow fractal dynamics in healthy conditions and deviations from this fractal behaviour have been reported in case of heart failure, Parkinson's and other neurodegenerative disorders (Goldberger, *et al.* 2002).

Liebovitch *et al.*, proposed 'Fractal model' to explain the physical basis of the observed kinetics in single ion channel (Liebovitch, *et al.* 1987). According to this model, during the transition between the distinct conformational states (open and closed), the ion channel is expected to pass through a number of conformational sub-states leading to fluctuations, possibly correlated. Therefore, fractal analysis of ion channel current fluctuations directly reflects the coordination between the conformational dynamics of the ion channel. Single channel kinetics of various ion

channels have been demonstrated to exhibit temporal fractal patterns with varying degrees of correlations between the transitions (Astashev, *et al.* 2007, Kazachenko 2007, Liebovitch, *et al.* 1987, Manna, *et al.* 2007). Recently, multifractal model has been proposed to explain the single channel kinetics of ion channels (Grinevich 2007). Multifractals are more complex than monofractals and contain interwoven fractal subsets with different fractal dimensions which are characterized by local Hurst exponents at different scales when compared to a single constant Hurst exponent in case of a monofractal (Kantelhardt, *et al.* 2002).

In the present part of the work, we applied non-linear time series analysis techniques to study the collective behaviour of VDAC ensemble. This part of the work involves analysis of macroscopic current steps recorded from the PLB reconstituted VDAC multichannels adapting the multifractal-detrended fluctuation analysis (MF-DFA) [cf. (Kantelhardt, *et al.* 2002)].

4.2. Materials and Methods:

The details of the materials used in the present part of the work are given in Table-A1 (appendix-I).

4.2.1. Purification of VDAC: VDAC was purified from rat brain mitochondria according to the procedure described in section 2.2.2 of chapter-2.

4.2.2. Reconstitution of VDAC into Planar lipid bilayers and multichannel recording: The formation of planar lipid bilayers and reconstitution of VDAC was similar to that of the procedure described in the section 2.2.3 of chapter-2 except for the addition of protein. Here ~20ng of purified VDAC was added to the *trans* chamber in order to allow multichannel reconstitution.

4.2.3. Analysis of Macroscopic current records:

a) Cumulative open states of ion channel ensemble: The ionic current records of VDAC multichannels reconstituted in artificial bilayers show discrete current steps. As discussed earlier, the channel activity in a channel ensemble deviates from the single channel activity. Further, the extent of such deviation is not established for

VDAC. Therefore, it is not possible to accurately calculate the number of channels underlying each observed current step. In the present part of the work, each current step is denoted by a discrete current step factor (γ) which represents the current fold increase in comparison to single channel current. The γ value for each current step analyzed is defined as follows:

$$\gamma = \frac{I_m}{I_s} \quad 4.1$$

Where, I_m is the average membrane current of each discrete current step recorded at an applied potential V and I_s is the average single open channel current of VDAC at the same applied potential V . The discrete current steps with the value of γ greater than one were considered for analysis. The analyzed current traces were of length 1024 data points (sampled at 1 kHz).

b) Power Spectra: The fluctuations (noise) associated with any dynamical process carry important information regarding the dynamics of the system. The power spectrum is the most common way to characterize the noise based on the distribution of the spectral densities among the various frequencies present in the signal. A power spectrum expresses the relation between the time domain and frequency domain descriptions of any physical process and is obtained by converting the time scale to frequency scale through fourier transform (FT). The FT can be written as follows

$$S(f) = \int_{-\infty}^{+\infty} s(t).e^{-2\pi ift} dt \quad 4.2$$

Power spectra of the current steps with different γ values recorded at various applied potentials were estimated by the method of fast fourier transform (FFT). The FFT routine in microcal origin 6.0 was used for this purpose. The noise structure was found from the value of slope of the double logarithmic plot of the Power spectral density, $S(f)$ and frequency (f).

c) Multifractal-Detrended Fluctuation Analysis: Following Kantelhardt *et al.*, 2002, the generalized multifractal DFA (MF-DFA) procedure is used to determine the parameters characterizing the multifractal behaviour of the macroscopic ionic current time series, x_k . In doing so, we define the profile as

$$Y(i) \equiv \sum_{k=1}^i [x_k - \langle x \rangle], \quad i = 1, \dots, N. \quad 4.3$$

Dividing $Y(i)$ into $N_s \equiv \text{int}(N/s)$ non-overlapping segments of equal length s , the local variance is determined as:

$$F^2(v, s) \equiv \frac{1}{s} \sum_{i=1}^s \{Y[(v-1)s + i] - Y_v(i)\}^2, \quad 4.4$$

for each segment $v, v = 1, \dots, N_s$.

Here the trend, $Y_v(i)$, taken as a quadratic fit, has been used to detrend the profile in each segment. The generalized fluctuation function, $F_q(s)$, $q \neq 0$, is obtained by averaging over all the segments as follows

$$F_q(s) \equiv \left\{ \frac{1}{2N_s} \sum_{v=1}^{2N_s} [F^2(v, s)]^{q/2} \right\}^{1/q}. \quad 4.5$$

For $q = 0$, a logarithmic averaging procedure is employed to find the fluctuation function $F_0(s)$ as:

$$F_0(s) \equiv \exp \left\{ \frac{1}{4N_s} \sum_{v=1}^{2N_s} \ln[F^2(v, s)] \right\}. \quad 4.6$$

For long-range correlations existing in the series, $F_q(s)$ scales with s , as a power law,

$$F_q(s) \sim s^{h(q)}, \quad 4.7$$

where $h(q)$ defines the generalized Hurst exponent. For monofractal case, $h(q)$ is a constant, while for multifractal behaviour of the system it varies with q . Further, multifractals are also characterized by the scaling index $\tau(q)$ and singularity spectrum $f(\alpha)$ defined as:

$$\tau(q) = qh(q) - 1; \alpha = \tau'(q) \text{ and } f(\alpha) = q\alpha - \tau(q). \quad 4.8$$

Here, α is the singularity strength or Hölder exponent, while $f(\alpha)$ encodes all the global scaling information (Glazier and Libchaber 1988).

A custom written MATLAB code based on the above algorithm was used to reveal the multifractal properties of the experimental time series. The performance of the MATLAB code was tested on the following synthetic time series-

a) **Binomial fractal time series (BFT)**: We may express the BFT as:

$$x_i = \alpha^{n_{max}-n(i-1)} b^{n(i-1)} \quad 4.9$$

where $0.5 < a < 1$ and $n(i)$ is the number of digits equals to 1 in the binary representation of the index i . The simulated time series is shown in the fig. 4.1.

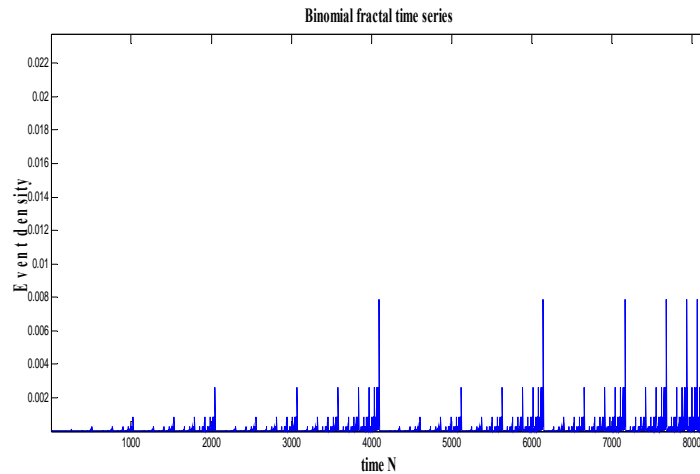


Fig. 4.1: Simulated time series of binomial fractal model.

b) **Elementary cellular automata (ECA)**: We may express ECA as:

$$x_n^{t+1} = [x_{n-1}^t + r x_n^t + x_{n+1}^t] \text{mod } 2 \quad 4.10$$

where $r=0$ and the first row pulse is indicated by "...010...". The simulated ECA series is shown in the fig. 4.2.

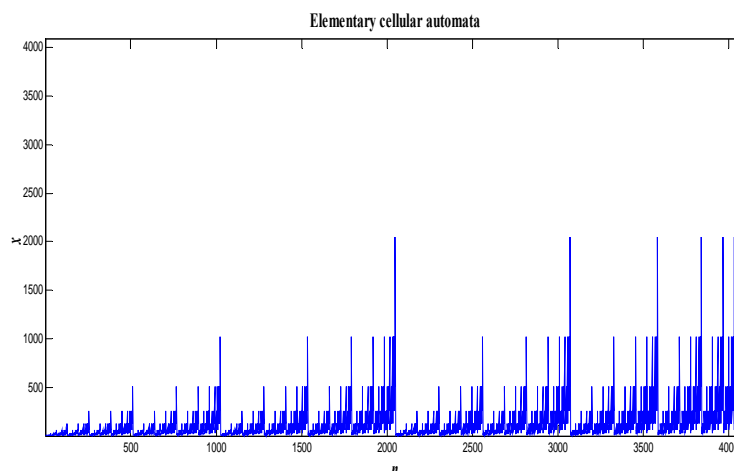


Fig. 4.2: Simulated time series of Elementary cellular automata

d) Surrogate time series: There are many need based algorithms to generate surrogate time series from simple random shuffling of the time series to digitally filtered shuffled surrogate algorithm (Dolan and Spano 2001). In our analysis, we used simple random shuffling algorithm. This algorithm involves random permutation of the original data and the resultant surrogate includes the data in a complete random order.

4.3. Results and Discussion:

The macroscopic ionic currents at various holding potentials were recorded after reconstitution of VDAC ensemble into bilayer lipid membranes. Fig. 4.3 show a representative current time series recorded at an applied potential of +30 mV. Each discrete step in the fig. 4.3 was due to the cumulative activity of varying number of channels and is indicated here after by γ factor calculated for each step according to the eq. 4.1. A single discrete current step was shown in the inset of the fig. 4.3 (pl. see figure legend for details). The fluctuations in the current step represent the conformational dynamics of ion channels in the membrane.

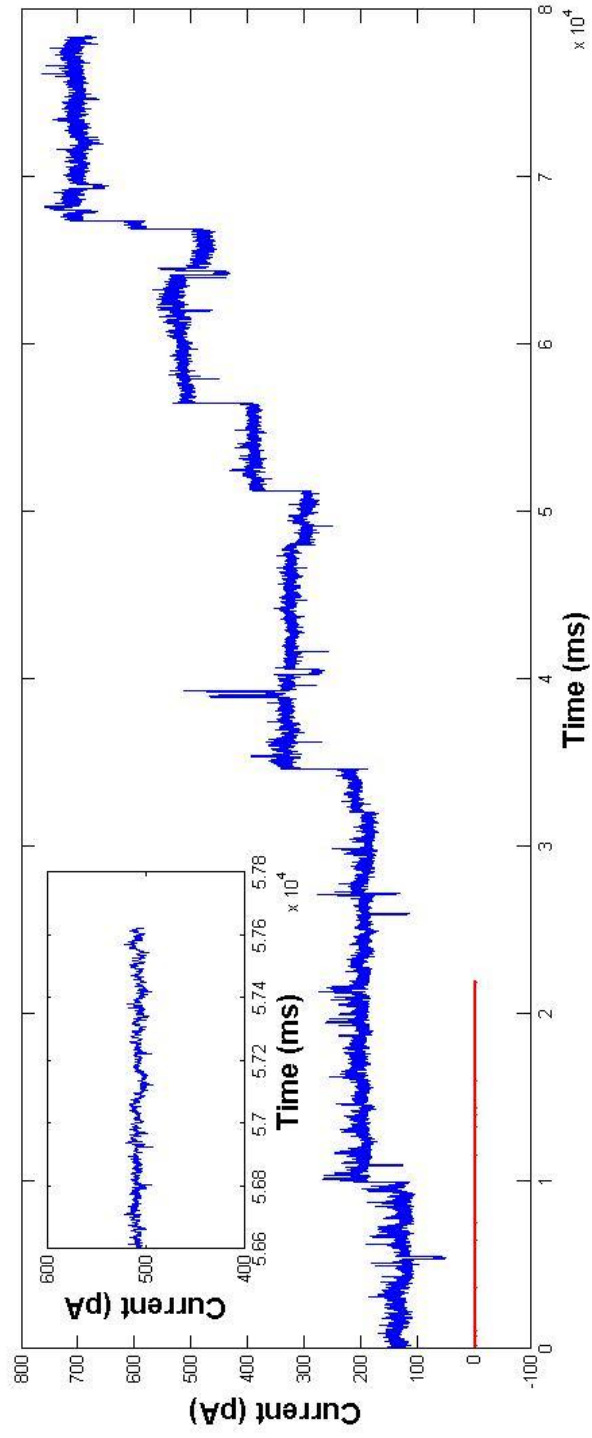


Fig. 4.3: Representative VDAC multichannel current recording at $V = +30$ mV. The inset shows a representative current step with $\gamma = 4$, $V = +30$ mV. The baseline is represented in red colour.

In order to probe the collective behaviour of VDAC ensemble and to identify the nature of interactions underlying the collective behaviour, the fluctuations associated with discrete current steps in the macroscopic ionic current recording of VDAC multichannels were analyzed using various non-linear dynamics tools which include FFT and MF-DFA.

4.3.1. Power Spectrum: The fast fourier transform of the discrete current steps with varying γ and V revealed a power law noise or usually called as $1/f$ noise associated with the fluctuations in the current steps. Fig. 4.4 shows the power spectrum for the current step displayed in the inset of fig. 4.3. The slope values of the power spectra along with their regression error are given in the table 4.1. The slopes range from 0.74 - 1.23. The $1/f$ power law noise in the macroscopic current fluctuations clearly indicates the presence of long-range correlations in the time series.

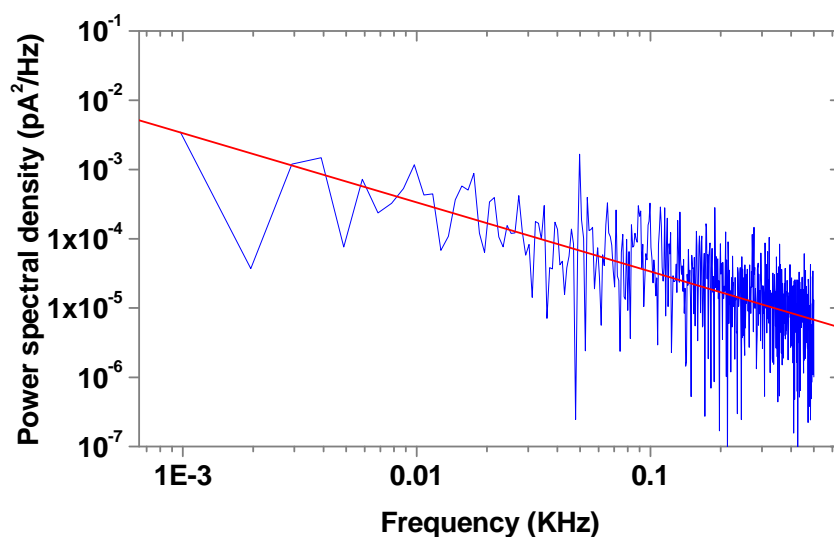


Fig. 4.4: Power spectrum of the representative current trace shown in the inset of fig. 4.3. The slope of the power spectrum is equal to -0.9977 ± 0.0607 .

Two major theories have been put forth to explain the origin of power law noise in both simple and complex systems: Interaction-dominance and component dominance [reviewed in (Diniz, *et al.* 2010)]. In the first case, the $1/f$ noise in the

complex system arises due to the dynamic non-linear interactions between the individual constituents of the system. On the other hand, the latter approach suggests that the intrinsic activities of the system constituents are more dominant in determining the observed performance than that of the interactions among the constituents.

Table-4.1: Power law exponent values of $S(f)$ vs f plots for all the current steps analyzed

| γ | Slope of the Power Spectral Density (α) |
|------------------------------------|--|
| Applied Potential (V) = +20 mV | |
| 3 | -1.04998 ± 0.05664 |
| 4 | -1.16111 ± 0.0597 |
| 11 | -1.23611 ± 0.08985 |
| $V = +25$ mV | |
| 7 | -0.82474 ± 0.05862 |
| 8 | -1.00761 ± 0.09445 |
| 9 | -0.88604 ± 0.05603 |
| $V = +30$ mV | |
| 3 | -0.74079 ± 0.03901 |
| 4 | -1.11278 ± 0.06025 |
| 7 | -1.12478 ± 0.05757 |
| $V = -20$ mV | |
| 2 | -0.78017 ± 0.03965 |
| 4 | -0.98847 ± 0.05563 |
| 6 | -1.1601 ± 0.0559 |
| 19 | -0.98874 ± 0.05959 |
| $V = -25$ mV | |
| 2 | -1.25778 ± 0.09742 |
| 3 | -0.95531 ± 0.05875 |
| 5 | -1.17733 ± 0.05823 |
| 17 | -1.205 ± 0.05512 |
| 19 | -1.19009 ± 0.05682 |
| $V = -30$ mV | |
| 5 | -0.75781 ± 0.0577 |
| 9 | -1.27828 ± 0.05672 |
| 13 | -0.8591 ± 0.05274 |
| 14 | -1.11571 ± 0.05472 |

Various reports in the past have demonstrated modulation of VDAC activity in an ensemble (Bathori, *et al.* 1998, Moran, *et al.* 1992, Tedeschi, *et al.* 1987). The likely reason for the observed channel activity modulation could be the interactions between the single channels of VDAC in homooligomers (Bathori, *et al.* 1998). Many other evidences revealed the inherent tendency of VDAC to form oligomers in both *in vivo* and *in vitro* conditions (Goncalves, *et al.* 2008, Raschle, *et al.* 2009). Therefore, in our case, we speculate that the long-range dependence in the macroscopic current records could be a result of dynamical nonlinear interactions between the single VDAC channels (interaction-dominance). However, the $1/f$ nature of power spectra does not provide any evidence for such interactions underlying the long-range correlations. So as to understand the nature and origin of possible interactions in our case, we further analyzed the time series in the frame work of MF-DFA.

4.3.2. Multifractal-detrended fluctuation analysis: The selected current traces with varying γ at applied potentials -30 mV, -25 mV, -20 mV, +20 mV, +25 mV and +30 mV extracted from the macroscopic ionic current time series were analysed using the MF-DFA procedure as described above. It may be noted that in the MF-DFA procedure, the detrending method used is likely to remove the small baseline drift, if any, in the time series. The parameters considered for describing its fractal properties are (1) Generalized fluctuation function, $F_q(s)$, (2) Generalized Hurst exponent, $h(q)$, (3) Multifractal scaling exponent, $\tau(q)$ and (4) Singularity spectrum, $f(\alpha)$.

a) Generalized Fluctuation function ($F_q(s)$) and Generalized Hurst Exponent ($h(q)$): $F_q(s)$ is estimated from the time series profile according to the eq. 4.5 (for $q \neq 0$) and 4.6 (for $q = 0$). Fig. 4.5 shows the scaling of the generalized fluctuation function, $F_q(s)$, with $s = 2^{(L-1)}$, ($L = 3, 4, \dots, 8$) for different q values. This follows a power law defined in the eq. 4.7. The slope values of the double logarithmic plots of $F_q(s)$ vs s , give the average values of generalized hurst exponent ($h(q)$). The q -dependence of thus obtained generalized Hurst exponent, $h(q)$ is shown in fig. 4.6. The observed variation of $h(q)$ with the order q clearly suggest the multifractal nature of the various time series considered. In case of monofractal behaviour, $h(q)$ will be independent of the order q .

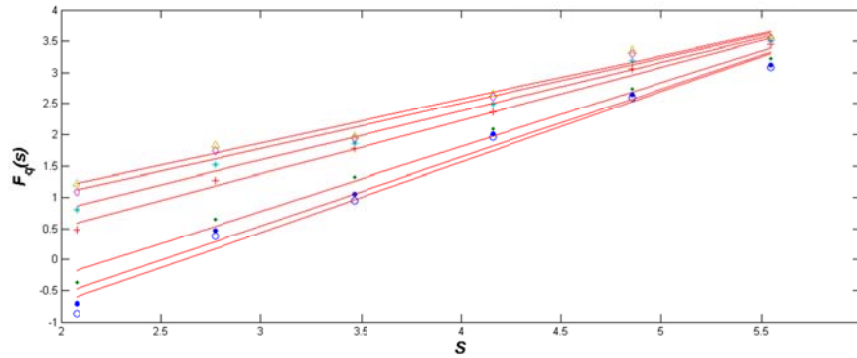


Fig. 4.5: The logarithmic plots of $F_q(s)$ vs s at $q = -15$ (o), $q = -5$ (•), $q = 2$ (+), $q = 5$ (*), $q = 10$ (◊) and $q = 15$ (▲) for the representative trace mentioned in the inset of Fig. 4.3 with $\gamma = 4$, $V = +30$ mV.

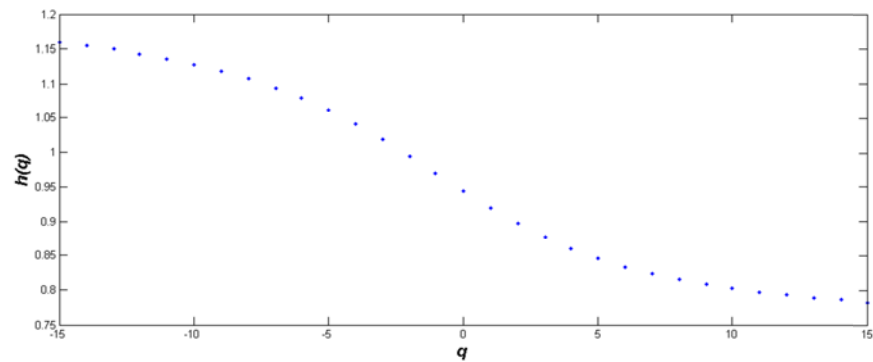


Fig. 4.6: The plot showing the q dependence of generalized Hurst exponent, $h(q)$, for the representative trace mentioned in the inset of Fig. 4.3.

In Table-4.2, we list the values of the global Hurst exponent, $h(2)$ (also known as correlation dimension) for different cases. The nature of the time series will be treated as long-term correlated/persistent, uncorrelated/purely random or negatively correlated/anti-persistent depending on whether $h(2) > 0.5$, $= 0.5$ or < 0.5 respectively. Since $h(2)$ values are greater than 0.7, we find the evidence of the existence of the long range correlations in the system.

Table-4.2: Correlation dimension values of all the current steps analyzed and their randomized surrogates

| γ | Correlation dimension [$h(2)$] | Correlation dimension of Surrogate time series [$h^{su}(2)$] |
|------------------------------------|----------------------------------|--|
| Applied Potential (V) = +20 mV | | |
| 3 | 0.9504 | 0.5552 |
| 4 | 0.9365 | 0.4716 |
| 11 | 1.05914 | 0.5005 |
| $V = +25$ mV | | |
| 7 | 0.8008 | 0.4899 |
| 8 | 0.9799 | 0.5180 |
| 9 | 0.9232 | 0.5331 |
| $V = +30$ mV | | |
| 3 | 0.8816 | 0.4970 |
| 4 | 0.8566 | 0.5468 |
| 7 | 0.9233 | 0.4937 |
| $V = -20$ mV | | |
| 2 | 0.9782 | 0.5734 |
| 4 | 0.8908 | 0.5467 |
| 6 | 0.9900 | 0.4712 |
| 19 | 0.8205 | 0.5239 |
| $V = -25$ mV | | |
| 2 | 0.7955 | 0.5534 |
| 3 | 0.8919 | 0.5305 |
| 5 | 0.9781 | 0.5238 |
| 17 | 0.9834 | 0.5445 |
| 19 | 0.9811 | 0.5002 |
| $V = -30$ mV | | |
| 5 | 0.7793 | 0.5038 |
| 9 | 0.9725 | 0.4912 |
| 13 | 0.8976 | 0.4867 |
| 14 | 0.9428 | 0.5101 |

b) Multifractal scaling exponent ($\tau(q)$) and Singularity spectrum: The values of $\tau(q)$ are estimated from $h(q)$ according to the equation 4.8 existence of the multifractality is further supported in fig. 4.7 wherein the scaling exponent, $\tau(q)$, is found to be not varying linearly with order q . The singularity spectrum, $f(\alpha)$ vs α , depicted in fig. 4.8 encodes the global scaling information of a set further supports the multifractal nature of the system (Glazier and Libchaber 1988).

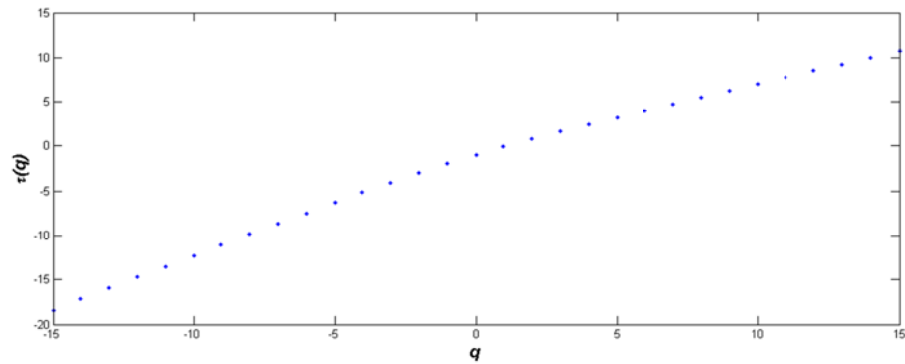


Fig. 4.7: The plot showing the q dependence of multifractal scaling exponent, $\tau(q)$, for the representative trace mentioned in the inset of fig. 4.3.

The observed multifractal nature could be a result of broad probability distribution of the data or inherent correlations in the system. In order to confirm the origin of the multifractality, the MF-DFA method was applied to surrogate time series generated according to the method detailed in section 4.2.3d. It may be mentioned here that any random dephasing of the time series would result in loss of any temporal correlation. Therefore, the singularity spectrum of such a reshuffled time series is expected to be of reduced width as also shown in fig. 4.8. Further, the MF-DFA when applied to the surrogate time series in all the cases considered here resulted in $h^{su}(2) \sim 0.5$ thus indicating a loss of intrinsic correlations.

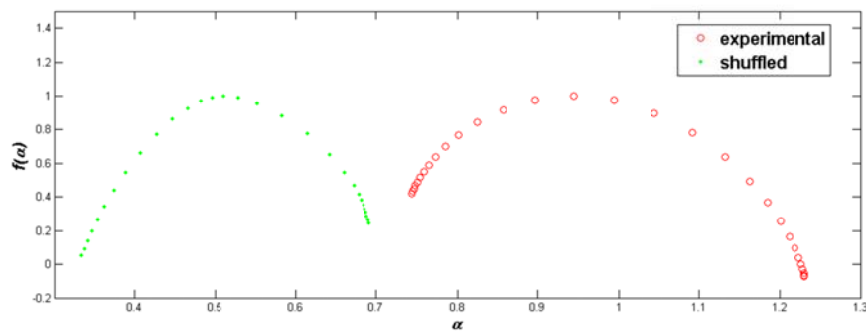


Fig. 4.8: Singularity spectra ($f(\alpha)$) of both the experimental and the shuffled time series for the representative trace mentioned in the inset of fig. 4.3.

The multifractal behaviour of the multichannel VDAC ensembles as evident from the temporal correlations and the singularity spectra could be explained by the spatial arrangement of the distributed VDAC clusters of varying size on the natural membranes (Goncalves, *et al.* 2007). The idea that the VDAC molecules are self-organized into clusters in multichannel membranes (Raschle, *et al.* 2009) and the short to long range interactions among VDAC molecules in the clusters could be the basis of the observed multifractal behaviour. It may be mentioned here that the auto-directed insertion capability of VDAC (Xu and Colombini 1997), is in agreement with the self-organization model proposed by Sieber *et al.*, (Sieber, *et al.* 2007) for the spatial organization of membrane proteins. In view of the fact that VDAC clusters of various sizes exist on the membrane, the conformational dynamics of VDAC molecules in the clusters are expected to be influenced by the neighboring molecules. Finer details provided by the high resolution X-ray crystallographic structure of mouse VDAC1 isoform suggests that hydrophobic thickness of VDAC is less than that of the membrane (Lomize, *et al.* 2006, Ujwal, *et al.* 2008). Therefore the VDAC is expected to cause local membrane deformations. The energetics of these membrane deformations could therefore induce membrane mediated protein-protein interactions ranging from submicron to micron spatial scales (Harroun, *et al.* 1999a, Harroun, *et al.* 1999b, Lague, *et al.* 2001, Lundbaek, *et al.*, Partenskii, *et al.* 2003, Ursell, *et al.* 2007). The afore-mentioned interactions may lead to channel-channel cooperativity, resulting in the observed correlations with $h(2) > 0.5$ (Table-4.2). The observed positive correlations indicate a positive cooperativity between the conformational dynamics of the VDAC molecules. The observed multifractal nature of the fluctuations in the current steps could thus be attributed to such inherent nonlinear interactions.

Recently, Ihlen *et al.*, demonstrated that width of the multifractal spectrum can be used to study the multiplicative interactions and the reduction in width of the multifractal spectrum for surrogate time series validates the same (Ihlen and Vereijken 2010). Figure 4.8 shows a similar kind of results in our case. Therefore, we suggest that cooperative interactions of VDAC multichannels in the membrane underlie the observed multifractal nature in the fluctuations of the macroscopic

current steps. Further, we propose MF-DFA as a tool to investigate the effect of various ligands and post-translational modifications on the collective behaviour of VDAC ensemble.

Conclusions

Conclusions:

In the present thesis some aspects of the biochemical modifications of Voltage Dependent Anion Channel (VDAC) have been studied. VDAC is a multifunctional membrane (channel) protein localized in the outer mitochondrial membrane. It forms a major conducting pathway between the mitochondrial sub-compartments and cytoplasm, and allows the passage of small metabolites, ions and nucleotides during physiological conditions. During pathological conditions, it is implicated in the formation of a non-specific, high conductance pore releasing the pro-apoptotic proteins like cytochrome c, Smac/DIABLO and apoptosis inducing factor (AIF) into the cytoplasm which are otherwise sequestered in the mitochondrial intermembrane space. VDAC has been shown to be the convergence point for a number of pathways involved in the mitochondrial cell death/survival signaling. Hence, the regulation of VDAC plays a pivotal role in the cell death/survival decisions. Biochemical modifications, e.g. nitration, phosphorylation etc. of VDAC do take place in cell, known as post-translational modifications. These are significant in the regulation of VDAC and the aforesaid physiological processes. Keeping this in view some structure-function studies (in vitro) were taken up on native as well as nitrated and phosphorylated VDAC.

VDAC has been shown to be regulated in different ways including mitochondrial membrane potential; interaction with other proteins; non-protein ligands; osmotic pressure and pH; variations in its isoform levels; biochemical modifications and its membrane organization. Sometimes a complex interplay between these factors also affects the VDAC activity. Of all these factors, biochemical modifications and alterations in membrane organization of VDAC have been identified to be the most commonly involved in the mitochondria mediated apoptosis. Hence, identification and characterization of such biochemical modifications and understanding their effect on functional activity of VDAC and its membrane organization is essential to get more insight into the molecular mechanisms of mitochondria mediated apoptosis. This was the main motivation of the present work.

In the first part of the work, we studied the functional effects of tyrosine nitration of VDAC, an oxidative stress induced biochemical modification identified in various tissues in disease conditions, *in vitro*. We found that one or more tyrosine residues of VDAC are nitrated by peroxynitrite. We report here that nitrated VDAC has approximately a 5 fold high conductance at positive holding potentials and the channel remains in the closed state at negative holding potentials. This kind of voltage dependent asymmetric behaviour might be involved in the regulation of VDAC which is further controlled by the transmembrane potential across the outer mitochondrial membrane. In other words, mitochondrial outer membrane potential might be playing a key role in the regulation of nitrated VDAC activity *in vivo* and thus the cell survival/death signaling.

Although oxidative stress is alone sufficient to induce mitochondria mediated apoptosis, in some cases it has been observed that oxidative stress also activate the cJun N-terminal kinase pathway (JNK) which further enhances the effects of oxidative stress through induction of mitochondrial permeability transition pore (mPTP) formation. However, the mitochondrial targets of JNK through which it regulates the mitochondrial permeability transition is not clear yet. As a putative component of permeability transition pore, we believe, VDAC could be a potential target for JNK. In the second part of the work, JNK mediated phosphorylation of VDAC has been verified. We found that JNK phosphorylates the VDAC isoforms. It phosphorylates VDAC1 and VDAC2 at different sites. Moreover, VDAC1 was found to be phosphorylated at three residues, Thr-19, Thr-116 and Ser-260. Evolutionary conservation scores calculated by conseq server suggested that the phosphorylatable residue on VDAC2 is not conserved even in mammals, whereas, the phosphorylatable sites on VDAC1 isoform were found to be identical. Further, Gaussian network modeling of VDAC1 3D-structure (PDB ID: 3EMN) suggested that one of the sites amenable to phosphorylation by JNK is very much important for the structural stability of the protein. Therefore, we anticipate that the JNK might phosphorylate the VDAC1 isoform *in vivo* and affect its membrane incorporation, thus regulate the mitochondria mediated death/survival signaling. However, taking into consideration, the rest of the two residues being phosphorylated by JNK, its effect on functional

modulation of VDAC1 could not be ruled out. The functional studies of JNK phosphorylation VDAC will throw some interesting features; this can be taken up as a future work.

Changes in membrane organization of VDAC have been proposed to be involved in the modulation of VDAC activity and also formation of permeability transition pore. Therefore, it is important to study the membrane organization of VDAC. Unfortunately, the functional implications of the spatial organization of VDAC are not understood well due to lack of precise methods to study them. In the last part of the work, we attempted to identify the nature of interactions between the native VDAC molecules through novel multifractal analysis of open channel fluctuations of macroscopic ionic current time series. We found the signature of multifractal behaviour in all the time series analyzed independent of the applied holding potential and the number of channels associated with the current steps. Further, we concluded that the channel-channel interaction gives rise to the VDAC multichannel dynamics. It may be mentioned here that the effects of the VDAC regulators, e.g. nitration, phosphorylation, on its membrane organization are of specific interest and these could be taken up for future investigations.

In conclusion, our findings are as follows:

- On bilayer lipid membrane nitrated VDAC has a ~5 fold high conductance at positive holding potentials whereas the channel remains in the closed state at negative holding potentials.
- JNK phosphorylates the VDAC isoforms.
- VDAC1 and VDAC2 are phosphorylated at different sites, VDAC1 was found to be phosphorylated at three residues, Thr-19, Thr-116 and Ser-260, whereas, only Ser-179 of VDAC2 was found to be phosphorylated.
- From the evolution point of view the phosphorylatable residue on VDAC2 is not conserved even in mammals, whereas, the phosphorylatable sites on VDAC1 isoform were found to be identical.

- VDAC multi-channels show Multifractal behaviour in all the current-time series at all the holding potentials applied across the bilayer lipid membrane with various number of channels incorporated.

We believe both the biochemical modifications nitration and JNK mediated phosphorylation might play an important role in modulation of mitochondrial cell death/survival signaling through modulation of VDAC *in vivo*. Further, interactions between the VDAC molecules *in vivo* might be involved in either the fine tuning of the effects of the biochemical modifications of VDAC.

A number of future investigation projects/ problems have evolved out of our present work. These are as follows:

- I. Functional studies of JNK Phosphorylation of VDAC, e.g. Bilayer electrophysiological studies.
- II. Cellular and physiological studies of JNK Phosphorylation and its link to (i).
- III. Simultaneous investigation of Nitration and Phosphorylation on VDAC.
- IV. Studies on channel-channel cooperativity with Nitration and Phosphorylation effects.

Summary

Summary:

Voltage dependent anion channel (VDAC), an abundant integral protein of the outer mitochondrial membrane (OMM) forms the interface between the cytoplasm and mitochondrial sub-compartments. In physiological conditions, it allows the exchange of the ions and metabolites across the OMM and thus regulates the cellular bioenergetics. In pathological conditions, VDAC acts as a convergence point for a wide variety of apoptotic signals and is involved in the OMM permeabilization and subsequent release of the pro-apoptotic proteins such as cytochrome c, Smac/DIABLO and apoptosis inducing factor (AIF). Further, biochemical modifications and/or oligomerization of VDAC have been shown to be associated with the OMM permeabilization. However, the exact molecular mechanisms, indicating how these biochemical modifications and/or alterations in the membrane organization cause the OMM permeabilization are not clear.

In the present work, we investigated the structure-function relations of two such novel biochemical modifications involved in the oxidative stress induced mitochondria mediated apoptosis *in vitro*. In the last part of the work, we made an attempt to understand the functional significance of supramolecular organization of VDAC through analysis of the macroscopic ionic current time series of reconstituted VDAC ensemble *in vitro*.

In the first part of the work, effect of the peroxynitrite on the VDAC purified from rat brain mitochondria was studied. Using immunological detection methods, we showed that one or more tyrosine residues are nitrated by peroxynitrite. Further, it was found that peroxynitrite mediated nitration of planar lipid bilayer reconstituted VDAC single channel results in an asymmetric gating behaviour. Nitrated VDAC has a ~5 fold high conductance at positive holding potentials and the channel remains in the closed state at negative holding potentials. Analysis of the rat VDAC sequence (Accession No. NP_112643) revealed the presence of 11 tyrosine residues in the primary structure. The reason for the observed asymmetric behaviour could be the asymmetric distribution of the nitrotyrosine residues in the three dimensional structure of VDAC. Since the rat VDAC sequence is identical to mouse VDAC sequence, the

crystal structure of mouse VDAC was analyzed to check the distribution of the 11 tyrosine residues in the three dimensional space. It was found that out of the eleven tyrosine residues, eight are located on one side of the pore orifice and one is located on the other side. The remaining two tyrosine residues are located on the N-terminal α -helix. This would definitely result in an asymmetric distribution of the nitrotyrosine residues and we assume that this asymmetric distribution might be responsible for the observed asymmetric conductance levels.

Apart from the direct effects of the oxidative stress mediators, oxidative stress has also been shown to induce the JNK pathway. The activated JNK was shown to induce the mitochondrial permeability transition (MPT) and subsequent release of pro-apoptotic proteins into the cytosol. The mechanisms involved in the JNK mediated activation of MPT are not clearly understood yet. In the present part of the work, we found that recombinant active JNK phosphorylates purified rat brain mitochondrial VDAC in an *in vitro* kinase reaction. Recombinant purified VDAC1 and VDAC2 isoforms expressed in *E.coli* were further used to check the specific sites amenable to JNK mediated phosphorylation. By using mass spectrometry, we identified that both the isoforms were differentially phosphorylated. Three phosphorylated sites threonine-19, threonine-116 and serine-260 were identified in case of VDAC1, whereas, only serine-179 was found to be phosphorylated in case of VDAC2 isoform. Further, the phosphorylated sites of alone VDAC1 isoform were found to be evolutionarily conserved. The importance of these three residues in the native VDAC1 structure was analyzed using Gaussian network modeling (GNM). GNM analysis suggested that serine-260 might play a key role in the structural stability of the VDAC1. Therefore, any kind of perturbation at this site would result in a structural changes and loss of function.

VDAC molecules exist and function in clusters on the membranes. Such supramolecular organization has also been evidenced in natural membranes using high resolution imaging techniques. Due to lack of proper analysis techniques, functional implications of the membrane organization of VDAC were not understood. In the last part of the work, the existence of inter-channel interactions between the

individual molecules in VDAC ensemble has been studied through multifractal analysis of fluctuations in the macroscopic ionic current time series of the VDAC multichannels. A common multifractal signature was found in open channel current fluctuations of all the current steps analyzed independent of the holding potential and the number of channels associated with each current step. The observed multifractality indicate inherent interactions between the VDAC molecules. We propose that the observed multifractal behaviour and inter-channel interactions could be membrane-mediated and are caused due to hydrophobic mismatch induced membrane deformations.

In conclusion, the biochemical modifications and membrane organization of VDAC might regulate its behaviour in both physiological and pathological conditions.

Bibliography

- Abu-Hamad, S., Arbel, N., Calo, D., Arzoine, L., Israelson, A., Keinan, N., Ben-Romano, R., Friedman, O. and Shoshan-Barmatz, V. (2009) The VDAC1 N-terminus is essential both for apoptosis and the protective effect of anti-apoptotic proteins. *J Cell Sci*, **122**, 1906-1916.
- Abu-Hamad, S., Sivan, S. and Shoshan-Barmatz, V. (2006) The expression level of the voltage-dependent anion channel controls life and death of the cell. *Proc Natl Acad Sci U S A*, **103**, 5787-5792.
- Adams, V., Griffin, L., Towbin, J., Gelb, B., Worley, K. and McCabe, E.R. (1991) Porin interaction with hexokinase and glycerol kinase: metabolic microcompartmentation at the outer mitochondrial membrane. *Biochem Med Metab Biol*, **45**, 271-291.
- Astashev, M.E., Kazachenko, V.N. and Grigoriev, P.A. (2007) Alamethicin Channel Kinetics: Studies Using Fluctuation Analysis and Multifractal Fluctuation Analysis. *Biochemistry (Moscow) Supplementary series A: Membrane and Cell Biology* **1**, 246-252.
- Baddeley, D., Jayasinghe, I.D., Lam, L., Rossberger, S., Cannell, M.B. and Soeller, C. (2009) Optical single-channel resolution imaging of the ryanodine receptor distribution in rat cardiac myocytes. *Proc Natl Acad Sci U S A*, **106**, 22275-22280.
- Bahar, I., Atilgan, A.R. and Erman, B. (1997) Direct evaluation of thermal fluctuations in proteins using a single-parameter harmonic potential. *Fold Des*, **2**, 173-181.
- Baines, C.P., Kaiser, R.A., Sheiko, T., Craigen, W.J. and Molkentin, J.D. (2007) Voltage-dependent anion channels are dispensable for mitochondrial-dependent cell death. *Nat Cell Biol*, **9**, 550-555.
- Baines, C.P., Song, C.X., Zheng, Y.T., Wang, G.W., Zhang, J., Wang, O.L., Guo, Y., Bolli, R., Cardwell, E.M. and Ping, P. (2003) Protein kinase Cepsilon interacts with and inhibits the permeability transition pore in cardiac mitochondria. *Circ Res*, **92**, 873-880.
- Baker, M.A., Lane, D.J., Ly, J.D., De Pinto, V. and Lawen, A. (2004) VDAC1 is a transplasma membrane NADH-ferricyanide reductase. *J Biol Chem*, **279**, 4811-4819.
- Balakirev, M., Khramtsov, V.V. and Zimmer, G. (1997) Modulation of the mitochondrial permeability transition by nitric oxide. *Eur J Biochem*, **246**, 710-718.
- Banerjee, J. and Ghosh, S. (2004) Bax increases the pore size of rat brain mitochondrial voltage-dependent anion channel in the presence of tBid. *Biochem Biophys Res Commun*, **323**, 310-314.
- Banerjee, J. and Ghosh, S. (2006) Phosphorylation of rat brain mitochondrial voltage-dependent anion as a potential tool to control leakage of cytochrome c. *J Neurochem*, **98**, 670-676.

- Bassingthwaighte, J.B., Liebovitch, L.S. and West, B.J. (1994) *Fractal Physiology: Methods in Physiology*. Oxford University Press, New York.
- Bathori, G., Parolini, I., Szabo, I., Tombola, F., Messina, A., Oliva, M., Sargiacomo, M., De Pinto, V. and Zoratti, M. (2000) Extramitochondrial porin: facts and hypotheses. *J Bioenerg Biomembr*, **32**, 79-89.
- Bathori, G., Szabo, I., Schmehl, I., Tombola, F., Messina, A., De Pinto, V. and Zoratti, M. (1998) Novel aspects of the electrophysiology of mitochondrial porin. *Biochem Biophys Res Commun*, **243**, 258-263.
- Bayrhuber, M., Meins, T., Habeck, M., Becker, S., Giller, K., Villinger, S., Vonrhein, C., Griesinger, C., Zweckstetter, M. and Zeth, K. (2008) Structure of the human voltage-dependent anion channel. *Proc Natl Acad Sci U S A*, **105**, 15370-15375.
- Benz, R. (1985) Porin from bacterial and mitochondrial outer membranes. *CRC Crit Rev Biochem*, **19**, 145-190.
- Benz, R. (1990) Biophysical properties of porin pores from mitochondrial outer membrane of eukaryotic cells. *Experientia*, **46**, 131-137.
- Benz, R. (1994) Permeation of hydrophilic solutes through mitochondrial outer membranes: review on mitochondrial porins. *Biochim Biophys Acta*, **1197**, 167-196.
- Benz, R., Janko, K. and Lauger, P. (1979) Ionic selectivity of pores formed by the matrix protein (porin) of *Escherichia coli*. *Biochim Biophys Acta*, **551**, 238-247.
- Bera, A.K. and Ghosh, S. (2001) Dual mode of gating of voltage-dependent anion channel as revealed by phosphorylation. *J Struct Biol*, **135**, 67-72.
- Bera, A.K., Ghosh, S. and Das, S. (1995) Mitochondrial VDAC can be phosphorylated by cyclic AMP-dependent protein kinase. *Biochem Biophys Res Commun*, **209**, 213-217.
- Blachly-Dyson, E., Peng, S., Colombini, M. and Forte, M. (1990) Selectivity changes in site-directed mutants of the VDAC ion channel: structural implications. *Science*, **247**, 1233-1236.
- Blachly-Dyson, E., Zambronicz, E.B., Yu, W.H., Adams, V., McCabe, E.R., Adelman, J., Colombini, M. and Forte, M. (1993) Cloning and functional expression in yeast of two human isoforms of the outer mitochondrial membrane channel, the voltage-dependent anion channel. *J Biol Chem*, **268**, 1835-1841.
- Bogoyevitch, M.A. and Kobe, B. (2006) Uses for JNK: the many and varied substrates of the c-Jun N-terminal kinases. *Microbiol Mol Biol Rev*, **70**, 1061-1095.
- Borutaite, V., Morkuniene, R. and Brown, G.C. (1999) Release of cytochrome c from heart mitochondria is induced by high Ca²⁺ and peroxynitrite and is responsible for Ca(2+)-induced inhibition of substrate oxidation. *Biochim Biophys Acta*, **1453**, 41-48.

- Bowen, K.A., Tam, K. and Colombini, M. (1985) Evidence for titratable gating charges controlling the voltage dependence of the outer mitochondrial membrane channel, VDAC. *J Membr Biol*, **86**, 51-59.
- Brdiczka, D. (1990) Interaction of mitochondrial porin with cytosolic proteins. *Experientia*, **46**, 161-167.
- Brdiczka, D. (1991) Contact sites between mitochondrial envelope membranes. Structure and function in energy- and protein-transfer. *Biochim Biophys Acta*, **1071**, 291-312.
- Brdiczka, D., Kaldis, P. and Wallimann, T. (1994) In vitro complex formation between the octamer of mitochondrial creatine kinase and porin. *J Biol Chem*, **269**, 27640-27644.
- Brookes, P.S. and Darley-Usmar, V.M. (2004) Role of calcium and superoxide dismutase in sensitizing mitochondria to peroxynitrite-induced permeability transition. *Am J Physiol Heart Circ Physiol*, **286**, H39-H46.
- Brookes, P.S., Salinas, E.P., Darley-Usmar, K., Eiserich, J.P., Freeman, B.A., Darley-Usmar, V.M. and Anderson, P.G. (2000) Concentration-dependent effects of nitric oxide on mitochondrial permeability transition and cytochrome c release. *J. Biol. Chem.*, **275**, 20474-20479.
- Brown, G.C. (2001) Regulation of mitochondrial respiration by nitric oxide inhibition of cytochrome c oxidase. *Biochim Biophys Acta*, **1504**, 46-57.
- Castro, L., Demicheli, V., Tortora, V. and Radi, R. (2011) Mitochondrial protein tyrosine nitration. *Free Radic Res*, **45**, 37-52.
- Chandarajan, J. and Klein, L. (1975) Lowry assay of dilute protein solutions containing high concentrations of Triton X-100. *Anal Biochem*, **69**, 632-636.
- Cheng, E.H., Sheiko, T.V., Fisher, J.K., Craigen, W.J. and Korsmeyer, S.J. (2003) VDAC2 inhibits BAK activation and mitochondrial apoptosis. *Science*, **301**, 513-517.
- Cheng, Q., Sedlic, F., Pravdic, D., Bosnjak, Z.J. and Kwok, W.M. (2010) Biphasic effect of nitric oxide on the cardiac voltage-dependent anion channel. *FEBS Lett*, **585**, 328-334.
- Coffey, E.T., Hongisto, V., Dickens, M., Davis, R.J. and Courtney, M.J. (2000) Dual roles for c-Jun N-terminal kinase in developmental and stress responses in cerebellar granule neurons. *J Neurosci*, **20**, 7602-7613.
- Colombini, M. (1979) A candidate for the permeability pathway of the outer mitochondrial membrane. *Nature*, **279**, 643-645.

- Colombini, M. (1980) Structure and mode of action of a voltage dependent anion-selective channel (VDAC) located in the outer mitochondrial membrane. *Ann N Y Acad Sci*, **341**, 552-563.
- Colombini, M., Yeung, C.L., Tung, J. and Konig, T. (1987) The mitochondrial outer membrane channel, VDAC, is regulated by a synthetic polyanion. *Biochim Biophys Acta*, **905**, 279-286.
- Condo, I., Ventura, N., Malisan, F., Tomassini, B. and Testi, R. (2006) A pool of extramitochondrial frataxin that promotes cell survival. *J Biol Chem*, **281**, 16750-16756.
- Danial, N.N. and Korsmeyer, S.J. (2004) Cell death: critical control points. *Cell*, **116**, 205-219.
- De Pinto, V., Guarino, F., Guarnera, A., Messina, A., Reina, S., Tomasello, F.M., Palermo, V. and Mazzoni, C. (2010a) Characterization of human VDAC isoforms: a peculiar function for VDAC3? *Biochim Biophys Acta*, **1797**, 1268-1275.
- De Pinto, V., Ludwig, O., Krause, J., Benz, R. and Palmieri, F. (1987a) Porin pores of mitochondrial outer membranes from high and low eukaryotic cells: biochemical and biophysical characterization. *Biochim Biophys Acta*, **894**, 109-119.
- De Pinto, V., Messina, A., Lane, D.J. and Lawen, A. (2010b) Voltage-dependent anion-selective channel (VDAC) in the plasma membrane. *FEBS Lett*, **584**, 1793-1799.
- De Pinto, V., Prezioso, G. and Palmieri, F. (1987b) A simple and rapid method for the purification of the mitochondrial porin from mammalian tissues. *Biochim Biophys Acta*, **905**, 499-502.
- Diniz, A., Wijnants, M.L., Torre, K., Barreiros, J., Crato, N., Bosman, A.M., Hasselman, F., Cox, R.F., Van Orden, G.C. and Delignieres, D. (2010) Contemporary theories of 1/f noise in motor control. *Hum Mov Sci*, (article in press).
- Distler, A.M., Kerner, J. and Hoppel, C.L. (2007) Post-translational modifications of rat liver mitochondrial outer membrane proteins identified by mass spectrometry. *Biochim Biophys Acta*, **1774**, 628-636.
- Dolan, K.T. and Spano, M.L. (2001) Surrogate for nonlinear time series analysis. *Phys Rev E Stat Nonlin Soft Matter Phys*, **64**, 046128.
- Dolder, M., Zeth, K., Tittmann, P., Gross, H., Welte, W. and Wallimann, T. (1999) Crystallization of the human, mitochondrial voltage-dependent anion-selective channel in the presence of phospholipids. *J Struct Biol*, **127**, 64-71.
- Elmore, S. (2007) Apoptosis: a review of programmed cell death. *Toxicol Pathol*, **35**, 495-516.

- Eminel, S., Klettner, A., Roemer, L., Herdegen, T. and Waetzig, V. (2005) JNK2 translocates to the mitochondria and mediates cytochrome c release in PC12 cells in response to 6-hydroxydopamine. *J Biol Chem*, **279**, 55385-55392.
- Forte, M., Guy, H.R. and Mannella, C.A. (1987) Molecular genetics of the VDAC ion channel: structural model and sequence analysis. *J Bioenerg Biomembr*, **19**, 341-350.
- Gakh, O., Park, S., Liu, G., Macomber, L., Imlay, J.A., Ferreira, G.C. and Isaya, G. (2006) Mitochondrial iron detoxification is a primary function of frataxin that limits oxidative damage and preserves cell longevity. *Hum Mol Genet*, **15**, 467-479.
- Gincel, D. and Shoshan-Barmatz, V. (2004) Glutamate interacts with VDAC and modulates opening of the mitochondrial permeability transition pore. *J Bioenerg Biomembr*, **36**, 179-186.
- Gincel, D., Silberberg, S.D. and Shoshan-Barmatz, V. (2000) Modulation of the voltage-dependent anion channel (VDAC) by glutamate. *J Bioenerg Biomembr*, **32**, 571-583.
- Gincel, D., Zaid, H. and Shoshan-Barmatz, V. (2001) Calcium binding and translocation by the voltage-dependent anion channel: a possible regulatory mechanism in mitochondrial function. *Biochem J*, **358**, 147-155.
- Glazier, J.A. and Libchaber, A. (1988) Quasiperiodicity and dynamical systems: An experimentalist's view. *IEEE Transactions on circuits and systems*, 35.
- Goldberger, A.L., Amaral, L.A., Hausdorff, J.M., Ivanov, P., Peng, C.K. and Stanley, H.E. (2002) Fractal dynamics in physiology: alterations with disease and aging. *Proc Natl Acad Sci U S A*, **99 Suppl 1**, 2466-2472.
- Goncalves, R.P., Buzhynskyy, N., Prima, V., Sturgis, J.N. and Scheuring, S. (2007) Supramolecular assembly of VDAC in native mitochondrial outer membranes. *J Mol Biol*, **369**, 413-418.
- Goncalves, R.P., Buzhynskyy, N. and Scheuring, S. (2008) Mini review on the structure and supramolecular assembly of VDAC. *J Bioenerg Biomembr*, **40**, 133-138.
- Gonzalez-Gronow, M., Kalfa, T., Johnson, C.E., Gawdi, G. and Pizzo, S.V. (2003) The voltage-dependent anion channel is a receptor for plasminogen kringle 5 on human endothelial cells. *J Biol Chem*, **278**, 27312-27318.
- Grage, S.L., Keleshian, A.M., Turdeladze, T., Battle, A.R., Tay, W.C., May, R.P., Holt, S.A., Contera, S.A., Haertlein, M., Moulin, M., Pal, P., Rohde, P.R., Forsyth, V.T., Watts, A., Huang, K.C., Ulrich, A.S. and Martinac, B. Bilayer-mediated clustering and functional interaction of MscL channels. *Biophys J*, **100**, 1252-1260.
- Green, D.R. (2000) Apoptotic pathways: paper wraps stone blunts scissors. *Cell*, **102**, 1-4.

- Grinevich, A.A., Astashev, M. E. and Kazachenko, V. N. (2007) Model of Multifractal Gating of Single Ionic Channels in Biological Membranes. *Biochemistry (Moscow) Supplementary series A: Membrane and Cell Biology*, **1**, 253-269.
- Gupta, S., Barrett, T., Whitmarsh, A.J., Cavanagh, J., Sluss, H.K., Derijard, B. and Davis, R.J. (1996) Selective interaction of JNK protein kinase isoforms with transcription factors. *EMBO J*, **15**, 2760-2770.
- Han, D., Antunes, F., Canali, R., Rettori, D. and Cadenas, E. (2003) Voltage-dependent anion channels control the release of the superoxide anion from mitochondria to cytosol. *J Biol Chem*, **278**, 5557-5563.
- Harroun, T.A., Heller, W.T., Weiss, T.M., Yang, L. and Huang, H.W. (1999a) Experimental evidence for hydrophobic matching and membrane-mediated interactions in lipid bilayers containing gramicidin. *Biophys J*, **76**, 937-945.
- Harroun, T.A., Heller, W.T., Weiss, T.M., Yang, L. and Huang, H.W. (1999b) Theoretical analysis of hydrophobic matching and membrane-mediated interactions in lipid bilayers containing gramicidin. *Biophys J*, **76**, 3176-3185.
- Hausdorff, J.M., Purdon, P.L., Peng, C.K., Ladin, Z., Wei, J.Y. and Goldberger, A.L. (1996) Fractal dynamics of human gait: stability of long-range correlations in stride interval fluctuations. *J Appl Physiol*, **80**, 1448-1457.
- Hiller, S., Garces, R.G., Malia, T.J., Orekhov, V.Y., Colombini, M. and Wagner, G. (2008) Solution structure of the integral human membrane protein VDAC-1 in detergent micelles. *Science*, **321**, 1206-1210.
- Hiller, S. and Wagner, G. (2009) The role of solution NMR in the structure determinations of VDAC-1 and other membrane proteins. *Curr Opin Struct Biol*, **19**, 396-401.
- Hodge, T. and Colombini, M. (1997) Regulation of metabolite flux through voltage-gating of VDAC channels. *J Membr Biol*, **157**, 271-279.
- Holden, M.J. and Colombini, M. (1988) The mitochondrial outer membrane channel, VDAC, is modulated by a soluble protein. *FEBS Lett*, **241**, 105-109.
- Hoogenboom, B.W., Suda, K., Engel, A. and Fotiadis, D. (2007) The supramolecular assemblies of voltage-dependent anion channels in the native membrane. *J Mol Biol*, **370**, 246-255.
- Ignarro, L.J. (1990) Nitric oxide. A novel signal transduction mechanism for transcellular communication. *Hypertension*, **16**, 477-483.
- Ihlen, E.A.F. and Vereijken, B. (2010) Interaction-Dominant Dynamics in Human Cognition: Beyond 1/f Fluctuation. *Journal of Experimental Psychology*, **139**, 436-463.

- Ivanov, P.C., Nunes Amaral, L.A., Goldberger, A.L., Havlin, S., Rosenblum, M.G., Stanley, H.E. and Struzik, Z.R. (2001) From 1/f noise to multifractal cascades in heartbeat dynamics. *Chaos*, **11**, 641-652.
- Kantelhardt, J.W., Zschiegner, S.A., Koscielny-Bunde, E., Havlin, S., Bunde, A. and Stanley, H.E. (2002) Multifractal detrended fluctuation analysis of nonstationary time series. *Physica A*, **316**, 87-114.
- Kayser, H., Kratzin, H.D., Thinner, F.P., Gotz, H., Schmidt, W.E., Eckart, K. and Hilschmann, N. (1989) Identification of human porins. II. Characterization and primary structure of a 31-kDa porin from human B lymphocytes (Porin 31H1). *Biol. Chem. Hoppe Seyler*, **370**, 1265-1278.
- Kazachenko, V.N., Astashev, M.E. and Grinevich, A.A. (2007) Multifractal analysis of K⁺ channel activity. *Biochemistry (Moscow) Supplementary series A: Membrane and Cell Biology*, **1**, 169-175.
- Keinan, N., Tyomkin, D. and Shoshan-Barmatz, V. (2010) Oligomerization of the mitochondrial protein voltage-dependent anion channel is coupled to the induction of apoptosis. *Mol Cell Biol*, **30**, 5698-5709.
- Keleshian, A.M., Edeson, R.O., Liu, G.J. and Madsen, B.W. (2000) Evidence for cooperativity between nicotinic acetylcholine receptors in patch clamp records. *Biophys J*, **78**, 1-12.
- Kenyon, J.L. and Bauer, R.J. (2000) Amplitude histograms can identify positively but not negatively coupled channels. *J Neurosci Methods*, **96**, 105-111.
- Kerr, J.F., Wyllie, A.H. and Currie, A.R. (1972) Apoptosis: a basic biological phenomenon with wide-ranging implications in tissue kinetics. *Br J Cancer*, **26**, 239-257.
- Kim, Y.M., Bombeck, C.A. and Billiar, T.R. (1999) Nitric oxide as a bifunctional regulator of apoptosis. *Circ Res*, **84**, 253-256.
- Kroemer, G., Galluzzi, L. and Brenner, C. (2007) Mitochondrial membrane permeabilization in cell death. *Physiol Rev*, **87**, 99-163.
- Kruman, I., Bruce-Keller, A.J., Bredesen, D., Waeg, G. and Mattson, M.P. (1997) Evidence that 4-hydroxynonenal mediates oxidative stress-induced neuronal apoptosis. *J Neurosci*, **17**, 5089-5100.
- Laemmli, U.K. (1970) Cleavage of Structural Proteins during the Assembly of the Head of Bacteriophage T4. *Nature*, **227**, 680-685.
- Lague, P., Zuckermann, M.J. and Roux, B. (2001) Lipid-mediated interactions between intrinsic membrane proteins: dependence on protein size and lipid composition. *Biophys J*, **81**, 276-284.

- Le Mellay, V., Troppmair, J., Benz, R. and Rapp, U.R. (2002) Negative regulation of mitochondrial VDAC channels by C-Raf kinase. *BMC Cell Biol*, **3**, 14.
- Li, J., Bombeck, C.A., Yang, S., Kim, Y.M. and Billiar, T.R. (1999) Nitric oxide suppresses apoptosis via interrupting caspase activation and mitochondrial dysfunction in cultured hepatocytes. *J Biol Chem*, **274**, 17325-17333.
- Li, X.X. and Colombini, M. (2002) Catalyzed insertion of proteins into phospholipid membranes: specificity of the process. *Biophys J*, **83**, 2550-2559.
- Liberatori, S., Canas, B., Tani, C., Bini, L., Buonocore, G., Godovac-zimmermann, J., Mishra, O.P., Delivoria-papadopoulos, M., Bracci, R. and Pallini, V. (2004) Proteomic approach to the identification of voltage-dependent anion channel protein isoforms in guinea pig brain synaptosomes. *Proteomics*, **4**, 125-129.
- Liebovitch, L.S., Fischbarg, J., Koniarek, J.P., Todorova, I. and Wang, M. (1987) Fractal model of ion-channel kinetics. *Biochim Biophys Acta*, **896**, 173-180.
- Linden, M., Gellerfors, P. and Nelson, B.D. (1982) Pore protein and the hexokinase-binding protein from the outer membrane of rat liver mitochondria are identical. *FEBS Lett*, **141**, 189-192.
- Lomize, M.A., Lomize, A.L., Pogozheva, I.D. and Mosberg, H.I. (2006) OPM: orientations of proteins in membranes database. *Bioinformatics*, **22**, 623-625.
- Lopes, R. and Betrouni, N. (2009) Fractal and multifractal analysis: a review. *Med Image Anal*, **13**, 634-649.
- Lowen, S.B., Liebovitch, L.S. and White, J.A. (1999) Fractal ion-channel behavior generates fractal firing patterns in neuronal models. *Phys Rev E Stat Phys Plasmas Fluids Relat Interdiscip Topics*, **59**, 5970-5980.
- Lu, A.J., Dong, C.W., Du, C.S. and Zhang, Q.Y. (2007) Characterization and expression analysis of *Paralichthys olivaceus* voltage-dependent anion channel (VDAC) gene in response to virus infection. *Fish Shellfish Immunol*, **23**, 601-613.
- Lundbaek, J.A., Collingwood, S.A., Ingolfsson, H.I., Kapoor, R. and Andersen, O.S. Lipid bilayer regulation of membrane protein function: gramicidin channels as molecular force probes. *J R Soc Interface*, **7**, 373-395.
- Madesh, M. and Hajnoczky, G. (2001) VDAC-dependent permeabilization of the outer mitochondrial membrane by superoxide induces rapid and massive cytochrome c release. *J Cell Biol*, **155**, 1003-1015.
- Mandelbrot, B.B. (1977) *Fractals: Form, chance and dimension*. W.H. Freeman & Co.,.
- Mandelbrot, B.B. (1982) *The Fractal Geometry of Nature*. W.H. Freeman & Co.,.

- Manna, S., Banerjee, J. and Ghosh, S. (2007) Breathing of voltage dependent anion channel as revealed by fractal property of its gating. *Physica A*, **386**, 573-580.
- Mannella, C.A. (1982) Structure of the outer mitochondrial membrane: ordered arrays of porelike subunits in outer-membrane fractions from *Neurospora crassa* mitochondria. *J Cell Biol*, **94**, 680-687.
- Mannella, C.A. (1987) Electron microscopy and image analysis of the mitochondrial outer membrane channel, VDAC. *J Bioenerg Biomembr*, **19**, 329-340.
- Mannella, C.A. (1998) Conformational changes in the mitochondrial channel protein, VDAC, and their functional implications. *J Struct Biol*, **121**, 207-218.
- Marin, R., Ramirez, C.M., Gonzalez, M., Gonzalez-Munoz, E., Zorzano, A., Camps, M., Alonso, R. and Diaz, M. (2007) Voltage-dependent anion channel (VDAC) participates in amyloid beta-induced toxicity and interacts with plasma membrane estrogen receptor alpha in septal and hippocampal neurons. *Mol Membr Biol*, **24**, 148-160.
- Markwell, M.A., Haas, S.M., Bieber, L.L. and Tolbert, N.E. (1978) A modification of the Lowry procedure to simplify protein determination in membrane and lipoprotein samples. *Anal Biochem*, **87**, 206-210.
- Marques, E.J., Carneiro, C.M., Silva, A.S. and Krasilnikov, O.V. (2004) Does VDAC insert into membranes in random orientation? *Biochim Biophys Acta*, **1661**, 68-77.
- Marx, S.O., Ondrias, K. and Marks, A.R. (1998) Coupled gating between individual skeletal muscle Ca²⁺ release channels (ryanodine receptors). *Science*, **281**, 818-821.
- Mathupala, S.P., Ko, Y.H. and Pedersen, P.L. (2006) Hexokinase II: cancer's double-edged sword acting as both facilitator and gatekeeper of malignancy when bound to mitochondria. *Oncogene*, **25**, 4777-4786.
- Mohit, A.A., Martin, J.H. and Miller, C.A. (1995) p493F12 kinase: a novel MAP kinase expressed in a subset of neurons in the human nervous system. *Neuron*, **14**, 67-78.
- Molina, M.L., Barrera, F.N., Fernandez, A.M., Poveda, J.A., Renart, M.L., Encinar, J.A., Riquelme, G. and Gonzalez-Ros, J.M. (2006) Clustering and coupled gating modulate the activity in KcsA, a potassium channel model. *J Biol Chem*, **281**, 18837-18848.
- Moon, J.I., Jung, Y.W., Ko, B.H., De Pinto, V., Jin, I. and Moon, I.S. (1999) Presence of a voltage-dependent anion channel 1 in the rat postsynaptic density fraction. *Neuroreport*, **10**, 443-447.
- Moran, O., Sciancalepore, M., Sandri, G., Panfili, E., Bassi, R., Ballarin, C. and Sorgato, M.C. (1992) Ionic permeability of the mitochondrial outer membrane. *Eur Biophys J*, **20**, 311-319.

- Mueller, P., Rudin, D.O., Tien, H.T. and Westcott, W.C. (1963) Methods for the formation of single bimolecular lipid membranes in aqueous solution. *J Phys Chem*, **67**, 534-535.
- Pacher, P., Beckman, J.S. and Liaudet, L. (2007) Nitric oxide and peroxynitrite in health and disease. *Physiol Rev*, **87**, 315-424.
- Parsons, D.F., Bonner Jr., W.D. and Verboon, J.G. (1965) Electron microscopy of isolated plant mitochondria and plastids using both the thin-section and negative-staining techniques. *Canadian Journal of Botany*, **43**, 647-655.
- Partenskii, M.B., Miloshevsky, G.V. and Jordan, P.C. (2003) Membrane inclusions as coupled harmonic oscillators: Effects due to anisotropic membrane slope relaxation. *Journal of Chemical Physics*, **118**, 7183-7193.
- Pastorino, J.G. and Hoek, J.B. (2008) Regulation of hexokinase binding to VDAC. *J Bioenerg Biomembr*, **40**, 171-182.
- Pavlov, E., Grigoriev, S.M., Dejean, L.M., Zweihorn, C.L., Mannella, C.A. and Kinnally, K.W. (2005) The mitochondrial channel VDAC has a cation-selective open state. *Biochim Biophys Acta*, **1710**, 96-102.
- Peng, S., Blachly-Dyson, E., Colombini, M. and Forte, M. (1992a) Determination of the number of polypeptide subunits in a functional VDAC channel from *Saccharomyces cerevisiae*. *J Bioenerg Biomembr*, **24**, 27-31.
- Peng, S., Blachly-Dyson, E., Forte, M. and Colombini, M. (1992b) Large scale rearrangement of protein domains is associated with voltage gating of the VDAC channel. *Biophys J*, **62**, 123-131; discussion 131-125.
- Poleti, M.D., Tesch, A.C., Crepaldi, C.R., Souza, G.H., Eberlin, M.N. and de Cerqueira Cesar, M. Relationship between expression of voltage-dependent anion channel (VDAC) isoforms and type of hexokinase binding sites on brain mitochondria. *J Mol Neurosci*, **41**, 48-54.
- Putcha, G.V., Harris, C.A., Moulder, K.L., Easton, R.M., Thompson, C.B. and Johnson, E.M., Jr. (2002) Intrinsic and extrinsic pathway signaling during neuronal apoptosis: lessons from the analysis of mutant mice. *J Cell Biol*, **157**, 441-453.
- Putcha, G.V., Le, S., Frank, S., Besirli, C.G., Clark, K., Chu, B., Alix, S., Youle, R.J., LaMarche, A., Maroney, A.C. and Johnson, E.M., Jr. (2003) JNK-mediated BIM phosphorylation potentiates BAX-dependent apoptosis. *Neuron*, **38**, 899-914.
- Rader, A.J., Chennubhotla, C., Yang, L.-W. and Bahar, I. (2006) *The gaussian network model: theory and applications: Normal Mode Analysis. Theory and Applications to Biological and Chemical Systems*. Taylor and Francis Group, New York

- Raschle, T., Hiller, S., Yu, T.Y., Rice, A.J., Walz, T. and Wagner, G. (2009) Structural and functional characterization of the integral membrane protein VDAC-1 in lipid bilayer nanodiscs. *J Am Chem Soc*, **131**, 17777-17779.
- Robinson, K.M. and Beckman, J.S. (2005) Synthesis of peroxynitrite from nitrite and hydrogen peroxide. *Methods Enzymol*, **396**, 207-214.
- Roman, I., Figys, J., Steurs, G. and Zizi, M. (2006a) Direct measurement of VDAC-actin interaction by surface plasmon resonance. *Biochim Biophys Acta*, **1758**, 479-486.
- Roman, I., Figys, J., Steurs, G. and Zizi, M. (2006b) Hunting interactomes of a membrane protein: obtaining the largest set of voltage-dependent anion channel-interacting protein epitopes. *Mol Cell Proteomics*, **5**, 1667-1680.
- Rostovtseva, T. and Colombini, M. (1997) VDAC channels mediate and gate the flow of ATP: implications for the regulation of mitochondrial function. *Biophys J*, **72**, 1954-1962.
- Rostovtseva, T.K., Sheldon, K.L., Hassanzadeh, E., Monge, C., Saks, V., Bezrukov, S.M. and Sackett, D.L. (2008) Tubulin binding blocks mitochondrial voltage-dependent anion channel and regulates respiration. *Proc Natl Acad Sci U S A*, **105**, 18746-18751.
- Sabirov, R.Z. and Okada, Y. (2009) The maxi-anion channel: a classical channel playing novel roles through an unidentified molecular entity. *J Physiol Sci*, **59**, 3-21.
- Saccone, C., Caggese, C., D'Erchia, A.M., Lanave, C., Oliva, M. and Pesole, G. (2003) Molecular clock and gene function. *J Mol Evol*, **57 Suppl 1**, S277-285.
- Saks, V.A., Vasil'eva, E., Belikova Yu, O., Kuznetsov, A.V., Lyapina, S., Petrova, L. and Perov, N.A. (1993) Retarded diffusion of ADP in cardiomyocytes: possible role of mitochondrial outer membrane and creatine kinase in cellular regulation of oxidative phosphorylation. *Biochim Biophys Acta*, **1144**, 134-148.
- Sambrook, J. and Rusel, D.W. (2000) *Molecular Cloning: A laboratory manual*. Cold Spring Harbor Laboratory Press, Cold Spring Harbor, NY.
- Scarlett, J.L., Packer, M.A., Porteous, C.M. and Murphy, M.P. (1996) Alterations to glutathione and nicotinamide nucleotides during the mitochondrial permeability transition induced by peroxynitrite. *Biochem Pharmacol*, **52**, 1047-1055.
- Schein, S.J., Colombini, M. and Finkelstein, A. (1976) Reconstitution in planar lipid bilayers of a voltage-dependent anion-selective channel obtained from paramecium mitochondria. *J Membr Biol*, **30**, 99-120.
- Schlattner, U., Dolder, M., Wallimann, T. and Tokarska-Schlattner, M. (2001) Mitochondrial creatine kinase and mitochondrial outer membrane porin show a direct interaction that is modulated by calcium. *J Biol Chem*, **276**, 48027-48030.

- Schroeter, H., Boyd, C.S., Ahmed, R., Spencer, J.P., Duncan, R.F., Rice-Evans, C. and Cadenas, E. (2003) c-Jun N-terminal kinase (JNK)-mediated modulation of brain mitochondria function: new target proteins for JNK signalling in mitochondrion-dependent apoptosis. *Biochem J*, **372**, 359-369.
- Shen, H. and Liu, Z. (2006) JNK signaling pathway is a key modulator in cell death mediated by reactive oxygen and nitrogen species. *Free rad. biol. med.*, **40**, 928-939.
- Shi, Y., Jiang, C., Chen, Q. and Tang, H. (2003) One-step on-column affinity refolding purification and functional analysis of recombinant human VDAC1. *Biochem Biophys Res Commun*, **303**, 475-482.
- Shimizu, S., Narita, M. and Tsujimoto, Y. (1999) Bcl-2 family proteins regulate the release of apoptogenic cytochrome c by the mitochondrial channel VDAC. *Nature*, **399**, 483-487.
- Shimizu, S. and Tsujimoto, Y. (2000) Proapoptotic BH3-only Bcl-2 family members induce cytochrome c release, but not mitochondrial membrane potential loss, and do not directly modulate voltage-dependent anion channel activity. *Proc Natl Acad Sci U S A*, **97**, 577-582.
- Shoshan-Barmatz, V. and Ben-Hail, D. (2011) VDAC, a multi-functional mitochondrial protein as a pharmacological target. *Mitochondrion*, (article in press).
- Shoshan-Barmatz, V., De Pinto, V., Zweckstetter, M., Raviv, Z., Keinan, N. and Arbel, N. (2010a) VDAC, a multi-functional mitochondrial protein regulating cell life and death. *Mol Aspects Med*, **31**, 227-285.
- Shoshan-Barmatz, V., Hadad, N., Feng, W., Shafir, I., Orr, I., Varsanyi, M. and Heilmeyer, L.M. (1996) VDAC/porin is present in sarcoplasmic reticulum from skeletal muscle. *FEBS Lett*, **386**, 205-210.
- Shoshan-Barmatz, V., Keinan, N. and Zaid, H. (2008) Uncovering the role of VDAC in the regulation of cell life and death. *J Bioenerg Biomembr*, **40**, 183-191.
- Shoshan-Barmatz, V., Keinan, N., Abu-Hamad, S., Tyomkin, D. and Aram, L. (2010b) Apoptosis is regulated by the VDAC1 N-terminal region and by VDAC oligomerization: release of cytochrome c, AIF and Smac/Diablo. *Biochim Biophys Acta*, **1797**, 1281-1291.
- Sieber, J.J., Willig, K.I., Kutzner, C., Gerding-Reimers, C., Harke, B., Donnert, G., Rammner, B., Eggeling, C., Hell, S.W., Grubmuller, H. and Lang, T. (2007) Anatomy and dynamics of a supramolecular membrane protein cluster. *Science*, **317**, 1072-1076.
- Song, J. and Colombini, M. (1996) Indications of a common folding pattern for VDAC channels from all sources. *J Bioenerg Biomembr*, **28**, 153-161.

- Stahl, W.L., Smith, J.C., Napolitano, L.M. and Basford, R.E. (1963) Brain Mitochondria. I. Isolation of Bovine Brain Mitochondria. *J Cell Biol*, **19**, 293-307.
- Sultana, R., Poon, H.F., Cai, J., Pierce, W.M., Merchant, M., Klein, J.B., Markesbery, W.R. and Butterfield, D.A. (2006) Identification of nitrated proteins in Alzheimer's disease brain using a redox proteomics approach. *Neurobiol Dis*, **22**, 76-87.
- Sun, J. and Liao, J.K. (2002) Functional interaction of endothelial nitric oxide synthase with a voltage-dependent anion channel. *Proc Natl Acad Sci U S A*, **99**, 13108-13113.
- Tararuk, T., Ostman, N., Li, W., Bjorkblom, B., Padzik, A., Zdrojewska, J., Hongisto, V., Herdegen, T., Konopka, W., Courtney, M.J. and Coffey, E.T. (2006) JNK1 phosphorylation of SCG10 determines microtubule dynamics and axodendritic length. *J Cell Biol*, **173**, 265-277.
- Tedeschi, H., Mannella, C.A. and Bowman, C.L. (1987) Patch clamping the outer mitochondrial membrane. *J Membr Biol*, **97**, 21-29.
- Towbin, H., Staehelin, T. and Gordon, J. (1979) Electrophoretic transfer of proteins from polyacrylamide gels to nitrocellulose sheets: procedure and some applications. *Proc Natl Acad Sci U S A*, **76**, 4350-4354.
- Ujwal, R., Cascio, D., Colletier, J.P., Faham, S., Zhang, J., Toro, L., Ping, P. and Abramson, J. (2008) The crystal structure of mouse VDAC1 at 2.3 Å resolution reveals mechanistic insights into metabolite gating. *Proc Natl Acad Sci U S A*, **105**, 17742-17747.
- Ursell, T., Huang, K.C., Peterson, E. and Phillips, R. (2007) Cooperative gating and spatial organization of membrane proteins through elastic interactions. *PLoS Comput Biol*, **3**, e81.
- Vander Heiden, M.G., Chandel, N.S., Li, X.X., Schumacker, P.T., Colombini, M. and Thompson, C.B. (2000) Outer mitochondrial membrane permeability can regulate coupled respiration and cell survival. *Proc Natl Acad Sci U S A*, **97**, 4666-4671.
- Vander Heiden, M.G., Li, X.X., Gottlieb, E., Hill, R.B., Thompson, C.B. and Colombini, M. (2001) Bcl-xL promotes the open configuration of the voltage-dependent anion channel and metabolite passage through the outer mitochondrial membrane. *J Biol Chem*, **276**, 19414-19419.
- Veenman, L., Shandalov, Y. and Gavish, M. (2008) VDAC activation by the 18 kDa translocator protein (TSPO), implications for apoptosis. *J Bioenerg Biomembr*, **40**, 199-205.
- Vieira, H.L., Belzacq, A.S., Haouzi, D., Bernassola, F., Cohen, I., Jacotot, E., Ferri, K.F., El Hamel, C., Bartle, L.M., Melino, G., Brenner, C., Goldmacher, V. and Kroemer, G. (2001) The adenine nucleotide translocator: a target of nitric oxide, peroxynitrite, and 4-hydroxynonenal. *Oncogene*, **20**, 4305-4316.

- Villinger, S., Briones, R., Giller, K., Zachariae, U., Lange, A., de Groot, B.L., Griesinger, C., Becker, S. and Zweckstetter, M. (2010) Functional dynamics in the voltage-dependent anion channel. *Proc Natl Acad Sci U S A*, **107**, 22546-22551.
- Wink, A.M., Bullmore, E., Barnes, A., Bernard, F. and Suckling, J. (2008) Monofractal and multifractal dynamics of low frequency endogenous brain oscillations in functional MRI. *Hum Brain Mapp*, **29**, 791-801.
- Xu, X. and Colombini, M. (1997) Autodirected insertion: preinserted VDAC channels greatly shorten the delay to the insertion of new channels. *Biophys J*, **72**, 2129-2136.
- Xu, X., Decker, W., Sampson, M.J., Craigen, W.J. and Colombini, M. (1999) Mouse VDAC isoforms expressed in yeast: channel properties and their roles in mitochondrial outer membrane permeability. *J Membr Biol*, **170**, 89-102.
- Xu, X., Forbes, J.G. and Colombini, M. (2001) Actin modulates the gating of *Neurospora crassa* VDAC. *J Membr Biol*, **180**, 73-81.
- Yamamoto, T., Yamada, A., Watanabe, M., Yoshimura, Y., Yamazaki, N., Yamauchi, T., Kataoka, M., Nagata, T., Terada, H. and Shinohara, Y. (2006) VDAC1, having a shorter N-terminus than VDAC2 but showing the same migration in an SDS-polyacrylamide gel, is the predominant form expressed in mitochondria of various tissues. *J Proteome Res*, **5**, 3336-3344.
- Yeramian, E., Trautmann, A. and Claverie, P. (1986) Acetylcholine receptors are not functionally independent. *Biophys J*, **50**, 253-263.
- Yu, W.H., Wolfgang, W. and Forte, M. (1995) Subcellular localization of human voltage-dependent anion channel isoforms. *J Biol Chem*, **270**, 13998-14006.
- Yuan, S., Fu, Y., Wang, X., Shi, H., Huang, Y., Song, X., Li, L., Song, N. and Luo, Y. (2008) Voltage-dependent anion channel 1 is involved in endostatin-induced endothelial cell apoptosis. *FASEB J*, **22**, 2809-2820.
- Zalk, R., Israelson, A., Garty, E.S., Azoulay-Zohar, H. and Shoshan-Barmatz, V. (2005) Oligomeric states of the voltage-dependent anion channel and cytochrome c release from mitochondria. *Biochem J*, **386**, 73-83.
- Zeth, K. (2010) Structure and evolution of mitochondrial outer membrane proteins of beta-barrel topology. *Biochim Biophys Acta*, **1797**, 1292-1299.
- Zhao, Y. and Herdegen, T. (2009) Cerebral ischemia provokes a profound exchange of activated JNK isoforms in brain mitochondria. *Mol Cell Neurosci*, **41**, 186-195.
- Zhou, Q., Lam, P.Y., Han, D. and Cadenas, E. (2008) c-Jun N-terminal kinase regulates mitochondrial bioenergetics by modulating pyruvate dehydrogenase activity in primary cortical neurons. *J Neurochem*, **104**, 325-335.

Zhou, Q., Lam, P.Y., Han, D. and Cadenas, E. (2009) Activation of c-Jun-N-terminal kinase and decline of mitochondrial pyruvate dehydrogenase activity during brain aging. *FEBS Lett*, **583**, 1132-1140.

Zimmerberg, J. and Parsegian, V.A. (1986) Polymer inaccessible volume changes during opening and closing of a voltage-dependent ionic channel. *Nature*, **323**, 36-39.

Zizi, M., Forte, M., Blachly-Dyson, E. and Colombini, M. (1994) NADH regulates the gating of VDAC, the mitochondrial outer membrane channel. *J Biol Chem*, **269**, 1614-1616.

Zizi, M., Thomas, L., Blachly-Dyson, E., Forte, M. and Colombini, M. (1995) Oriented channel insertion reveals the motion of a transmembrane beta strand during voltage gating of VDAC. *J Membr Biol*, **144**, 121-129.

Zweier, J.L., Wang, P., Samouilov, A. and Kuppusamy, P. (1995) Enzyme-independent formation of nitric oxide in biological tissues. *Nat Med*, **1**, 804-809.

Appendix-I

Experimental materials used in the present work were procured from diverse sources as shown in the **Table-A1**. Other fine chemicals, kits, and enzymes are mentioned along with their sources as and where needed in the text.

Table-A1 List of materials used in this study

| MATERIALS | SOURCE |
|---|---|
| Chemicals and materials used for peroxynitrite synthesis | SRL, India; Himedia, India; Dispovan, India. |
| Chemicals used for purification of VDAC and bilayer lipid membrane electrophysiology | Avanti polar lipids, USA; Sigma Aldrich, USA; BioRad, USA. |
| γP^{32} ATP | BRIT, India |
| Recombinant active JNK3 | BIOMOL international, USA |
| Chemicals and enzymes used for recombinant expression of VDAC1 and VDAC2 isoforms | Diverse sources that include Sigma Aldrich, USA; Merck, Germany; Thermo Scientific Corp, USA; Invitrogen, USA; Himedia, India; Fermentas, Germany, Biotools, Spain; Taurus Scientific, USA; Applied Biosystems, USA, etc. |
| Primers <i>VDAC1</i> <i>VDAC2</i> | Eurofins genomics, India |
| Plasmid pASK-43 | IBA BioTAGnologies, Germany |
| Bacterial Strains <i>Escherichia coli</i> BL21 CodonPlus | MVR Lab, UDSC, New Delhi |
| Softwares Primer3 BLAST MATLAB 7.0 Origin 6.0 pCLAMP 10 PyMOL 1.1 eval Microsoft Office Package | SourceForge, USA NCBI, USA Mathworks, USA Microcal Origin, USA Molecular Devices inc., USA The PyMOL molecular graphics system, Schrödinger, LLC Microsoft Inc., USA |

Appendix-II

Protein Estimation (Modified Lowry's method):

Protein estimations carried out according to Lowry's method modified by Markwell et al (1981). Following reagents were prepared for protein estimation.

Reagent A:

(2% Na₂CO₃, 0.4% NaOH, 0.16% Sodium tartarate, 1%SDS)

Reagent B:

(4% CuSO₄,5 H₂O)

Reagent C:

100 parts of reagent A was mixed with 1 part of reagent B to form alkaline copper reagent. It was made freshly before protein estimation.

Reagent D:

Folin-Ciocalteu 2N phenol reagent was diluted (1:1 v/v) with double distilled water. It was made freshly before protein estimation.

Reagent E:

Crystalline Bovine Serum Albumin (BSA) was dissolved at 0.1 mg/ml in double distilled water and stored at -20°C.

SDS-PAGE Buffer Compositions:***Resolving gel composition for mini-gel:***

| Stock solution | 10% | 12% |
|------------------------|------------|------------|
| Double distilled water | 1.9 ml | 2.35 ml |
| Lower Tris (pH-8.8) | 1.3 ml | 1.75 ml |
| Acrylamide | 1.7 ml | 3.0 ml |
| 10% APS | 50 μ l | 50 μ l |
| TEMED | 10 μ l | 10 μ l |

Stacking gel composition for mini-gel:

| Stock solution | 4% |
|------------------------|-------------|
| Double distilled water | 1.44 ml |
| Upper Tris (pH-6.8) | 625 μ l |
| Acrylamide | 400 μ l |
| 10% APS | 25 μ l |
| TEMED | 10 μ l |

Western Blotting:***Towbin Buffer (pH: 8.1-8.5):***

| Chemical | Final concentration |
|-----------------|----------------------------|
| Tris base | 25 mM |
| Glycine | 192 mM |
| Methanol | 20 % |

Tris Buffered Saline (TBS) (pH- 7.4):

| Chemical | Final concentration |
|-----------------|----------------------------|
| Tris base | 10 mM |
| NaCl | 150 mM |

Blocking buffer: TBS + 3% BSA